Naval
Oceanographic and
Atmospheric
Research
Laboratory

Stennis Space Center,
MS 39529-5004

AEAS Document 92-004
January 1992

Environmental Assessment for Selected Regions in the Mediterranean Sea

Mark J. Null
Paul J. Bucca
Bruce R. Gomes

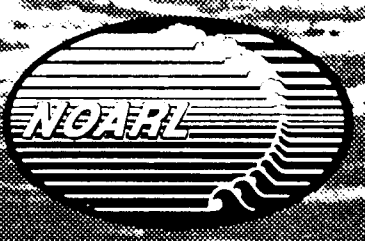

Approved for public release, distribution is unlimited

Acknowledgments

The tasking support provided by Dr. P Feden, Director, ASW Environmental Acoustic Support (AEAS) project office (Program Element 0603785N), is greatly appreciated.

The author wishes to thank Dr. George Heburn, NOARL's Ocean Dynamics and Prediction Branch, and his staff for supplying the numerous Layered Circulation Model abyssal current predictions contained in this document. The extensive literature searches and the interlibrary loans of numerous documents were possible only with the cooperation and assistance of the personnel of the Naval Oceanographic Office's technical library.

Finally, the assistance of Dr. Budd Adams, NOARL, in technically reviewing this document is appreciated.

Contents

Summary

Physiography and Geology

The most predominant physiographic feature of the Cretan and Levantine Seas is the Mediterranean Rise, an elongated submarine mountain range that generally trends from east to west. The subbottom seismic signature associated with this feature is weak and is underlain by a strong smooth reflector of evaporites (salt deposits). The Ionian Sea, which contains the greatest reported depth in the Mediterranean Sea, has a diverse physiography. This central Mediterranean Basin is characterized by the broad Libyan continental shelf and by the large abyssal Ionian Plain, which contains a thin layer of unconsolidated sediments that overlie the same highly reflective evaporite sequence found to the east.

The high variable physiography characteristic of the Strait of Sicily is composed of three elongate troughs (Linosa, Malta, and Pantellaria) and extensive flat-topped plateaus and banks—most notably, the Skerki Bank on the western end of the strait and the Medina Bank on the eastern approaches. The troughs are generally composed of sand and mud, and the banks contain large amounts of coarse calcareous sands.

In contrast, the Balearic Basin, located between the Alboran Sea and western Corsica, is flat, featureless abyssal plain characterized by thick sedimentary sequences. The western Alboran Basin has an almost uniform narrow shelf along both the African and Spanish coastlines. The slopes are deeply dissected with canyons and ravines, and the Alboran Ridge divides the basin into eastern and western sections. Because currents are so dynamic in the Strait of Gibraltar, this area contains both depositional and erosional sedimentary features. However, the peripheral canyon areas are protected from currents by outcrops and contain silty muds and gravel.

Oceanography

The oceanography over large portions of the Eastern Mediterranean Sea, as reflected in the results of the 1979–1988 multinational exercise, Physical Oceanography of the Eastern Mediterranean (POEM) is quite different from the "definitive" descriptions of researchers of four generations ago. The existence of Levantine Surface Water, the relatively fresh and thin underlying Atlantic Water lens, and the Levantine Deep Water mass were identified prior to the POEM exercise. However, the formative areas of these water masses and the circulation of the eastern basins are much more precisely defined. Perhaps the most revolutionary finding of recent years lies in the delineation of numerous permanent and semipermanent gyres in the Levantine and Cretan Seas. The thermal signatures of the dissimilar waters within and outside these features can exceed 2°C. Since these gyres are temporally variable in shape and

position, it is questionable whether existing historical data bases can adequately resolve the sound speed variability contained within them.

Since POEM data were basically confined to the northern Ionian Basin, an update of the oceanography in the southern Ionian Sea is limited. However, abundant documentation describes frontal zones that separate the eastward-flowing Atlantic water from the indigenous Ionian surface waters. The most prominent of these zones, the Maltese Front, located between 16° and 18°E on the flanks of the continental slope, can have thermal gradients as great as 5.2°C over a distance of 2 km.

The circulation in the Strait of Sicily is characterized by the eastward surface flow of the Atlantic water and the westward bottom flow of the Levantine Water formed in the evaporative basin of the Levantine Sea. Recent research performed in the Strait of Sicily indicates that the flow of the Atlantic water through the strait is seasonally and geographically bimodal. During the winter this water mass is strongest and exhibits a well-defined, low-salinity core against the coast of Africa; during the summer, the mass transport of Atlantic water is at a minimum and is generally distributed laterally across the entire strait. In addition, there is often a strong water mass contrast between the Atlantic water and the Sicilian coastal upwelling.

Water masses in the Strait of Sardinia are essentially the same as those in the Strait of Sicily. In this strait, eastward-flowing Atlantic water is entrained at the surface along the coast of Africa while the Levantine Intermediate Water undergoes a major bifurcation to the north after exiting the northern Sicilian Strait and, by one account, greatly reduces its net transport through the Strait of Sardinia.

The western Alboran Basin is the first basin encountered by the inflowing Atlantic water and is the last basin occupied by the outflowing Mediterranean water. The Alboran Front, formed by the mixing of the Atlantic water and Atlantic water modified by resident Mediterranean water, is probably the strongest frontal feature in the Mediterranean. Another prominent feature in this area is the Atlantic jet, which flows along the southern coast of Spain and forms the northern boundary of the Alboran Front.

The Strait of Gibraltar is one of the most oceanographically dynamic areas in the world. Over long time scales, the near-surface waters of Atlantic origin flow into the Alboran Basin, while the Levantine intermediate water flows westward along the floor of the strait into the Atlantic Ocean. Over a time frame commensurate with the tidal frequencies, the strait is subjected to currents as great as 4 kt, intense current shear and internal wave activity, and large temperature differences (as great as 2.5°C in 15 minutes).

Sound Speed

A subset of the Master Oceanographic Observation Data Set was analyzed to obtain a seasonal sound speed description of selected areas of the Mediterranean Sea. The areas were examined for near-surface layer changes, which dictated seasonal profile groups and overall profile gradient changes, that determined province grouping. The sound speed structures of the Levantine and Cretan Seas are similar in both shape and magnitude during similar seasons. Specifically, a relatively deep sonic layer is present in the winter and a well-developed negative gradient is present in the summer. The major sound speed difference between these basins and the Ionian Basin is in the characteristic positive gradient from the surface to the seafloor during the Ionian winter. Year-to-year variability in the oceanography of the Strait of Sicily resulted in temporal smearing of the data base. The smearing precluded the delineation of sound speed provinces that contained profiles indicative of Atlantic, Levantine, and coastal upwelled waters. The presence of the Alboran Front required that the western Alboran Sea be divided into northern and southern sections. Lower sound speed values and a shallower deep sound channel axis in the northern section characterize the primary differences in the two sections.

Currents

Currents are depicted using literature-cited measurements where available. In lieu of measurements, geostrophic calculations based on the temperature and salinity field are described. Where these parameters or measurements are unavailable, the Naval Oceanographic and Atmospheric Research Laboratory's Layered Circulation Model is used. The strongest currents in the Levantine and Cretan Seas are associated with the mid-Mediterranean jet, where speeds of 20 to 40 cm/sec have been documented. Currents in several straits, which connect the Levantine and the Aegean Seas, can attain similar velocities.

Numerous current measurements have been taken in the Strait of Sicily. The magnitude of both the Levantine and Atlantic waters in the strait exhibit considerable temporal variability and attain their highest velocities in the winter season. In addition, Atlantic water is geographically variable because it is entrained against the African coast during the winter, but during the summer, this water mass spreads across the entire Sicilian channel. Time series measurements in this area demonstrate considerable short-term variability and speeds as great as 2.95 kt in the Atlantic water layer.

Geostrophically derived current calculations in the Strait of Sardinia indicate that the highest speeds also reside in the near-surface Atlantic water layer and decay rapidly below 200 m. The highest currents in the near-surface layers of the western Alboran Sea reside within the temporally and spatially variable Atlantic jet where speeds have been documented as great as 96 cm/sec. Perhaps the most comprehensive update on the circulation in this area is in the documentation of the abyssal currents

Sound Speed

A subset of the Master Oceanographic Observation Data Set was analyzed to obtain a seasonal sound speed description of selected areas of the Mediterranean Sea. The areas were examined for near-surface layer changes, which dictated seasonal profile groups and overall profile gradient changes, that determined province grouping. The sound speed structures of the Levantine and Cretan Seas are similar in both shape and magnitude during similar seasons. Specifically, a relatively deep sonic layer is present in the winter and a well-developed negative gradient is present in the summer. The major sound speed difference between these basins and the Ionian Basin is in the characteristic positive gradient from the surface to the seafloor during the Ionian winter. Year-to-year variability in the oceanography of the Strait of Sicily resulted in temporal smearing of the data base. The smearing precluded the delineation of sound speed provinces that contained profiles indicative of Atlantic, Levantine, and coastal upwelled waters. The presence of the Alboran Front required that the western Alboran Sea be divided into northern and southern sections. Lower sound speed values and a shallower deep sound channel axis in the northern section characterize the primary differences in the two sections.

Currents

Currents are depicted using literature-cited measurements where available. In lieu of measurements, geostrophic calculations based on the temperature and salinity field are described. Where these parameters or measurements are unavailable, the Naval Oceanographic and Atmospheric Research Laboratory's Layered Circulation Model is used. The strongest currents in the Levantine and Cretan Seas are associated with the mid-Mediterranean jet, where speeds of 20 to 40 cm/sec have been documented. Currents in several straits, which connect the Levantine and the Aegean Seas, can attain similar velocities.

Numerous current measurements have been taken in the Strait of Sicily. The magnitude of both the Levantine and Atlantic waters in the strait exhibit considerable temporal variability and attain their highest velocities in the winter season. In addition, Atlantic water is geographically variable because it is entrained against the African coast during the winter, but during the summer, this water mass spreads across the entire Sicilian channel. Time series measurements in this area demonstrate considerable short-term variability and speeds as great as 2.95 kt in the Atlantic water layer.

Geostrophically derived current calculations in the Strait of Sardinia indicate that the highest speeds also reside in the near-surface Atlantic water layer and decay rapidly below 200 m. The highest currents in the near-surface layers of the western Alboran Sea reside within the temporally and spatially variable Atlantic jet where speeds have been documented as great as 96 cm/sec. Perhaps the most comprehensive update on the circulation in this area is in the documentation of the abyssal currents

Environmental Assessment for Selected Regions in the Mediterranean Sea

1.0 Physiography and Geology of the Mediterranean Sea

The Mediterranean Sea is one of the more geologically and geophysically complex regions in the world. Its origin and evolution have long been a topic of debate by researchers. The objective of this section, however, is not to dwell on the Mediterranean's complicated geologic history but to introduce factors that may be pertinent to future operational planning and system performance predictions.

In general, the Mediterranean Sea can be subdivided into three distinct physiographic provinces: (1) the eastern Mediterranean province, which is dominated by the presence of an arcuate submarine mountain chain, the Mediterranean Ridge; (2) the back-arc basins of the central Mediterranean, which are dotted with numerous seamounts and active volcanos; and (3) the western Mediterranean Sea, which is characterized by an abyssal plain almost devoid of relief. Factors that will be addressed in this section include physiography, sediment thickness, depositional processes, volcanism, and seismicity of the region.

1.1 Levantine Sea and Easternmost Mediterranean

The Levantine Sea is bordered on the north by Crete, the Dodecanese Islands, and Turkey (Fig. 1.1.1). On the east, the sea is bordered by Syria and Lebanon, and on the south by Egypt and Libya. The Levantine Sea covers approximately 320,000 km^2, and the maximum depth is 4384 m (Carter et al., 1972). The predominant topographic feature of this region is the Mediterranean Rise. In general, sediment sequences are thick throughout the eastern Mediterranean region. The thickest accumulations of sedimentary material occur along the Nile Fan (16 km), the Mediterranean Ridge (12-14 km), and the Herodotus Basin (12–14 km). Surficial sediments consist primarily of calcareous ooze in the deeper regions of the sea. Amounts of calcareous silt and clay vary near the shore. Near the mouth of the Nile, surface sediments consist of terrigenous silts and clays. Figure 1.1.2 outlines surficial sediment distribution for the Mediterranean Sea.

The continental shelf along the Levantine Sea is absent in many places or marginally apparent, particularly on the sea's northern margin, and is irregular along the sea's southern boundary. The broadest shelf regions occur near the mouth of the Nile, where the width is approximately 70 km. On this portion of the shelf, the shelf break is found at depths of about 260 m. Westward from the Nile Fan to a point

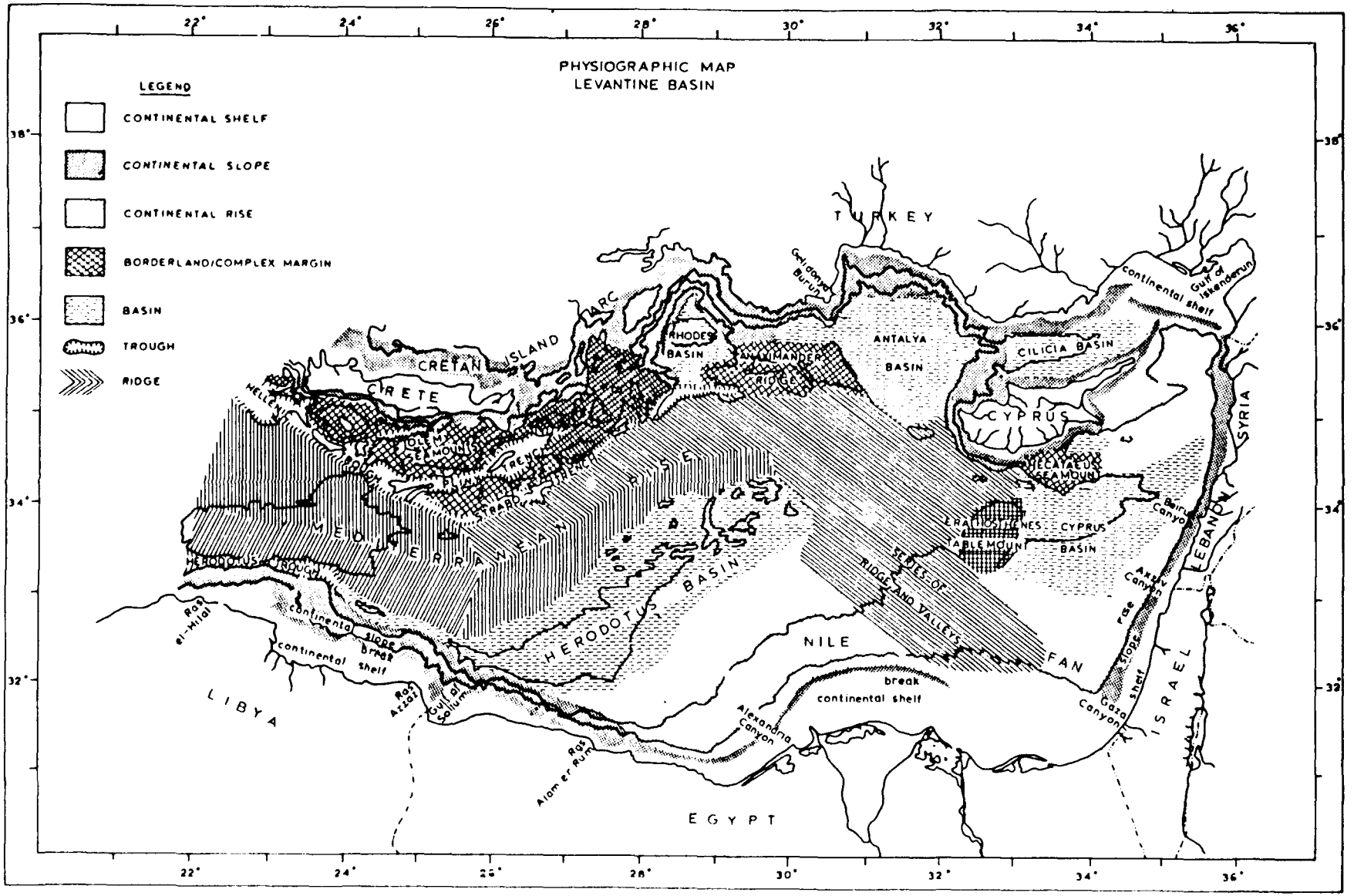

Fig. 1.1.1 Physiographic map of the Levantine Sea (After Carter et al., 1972)

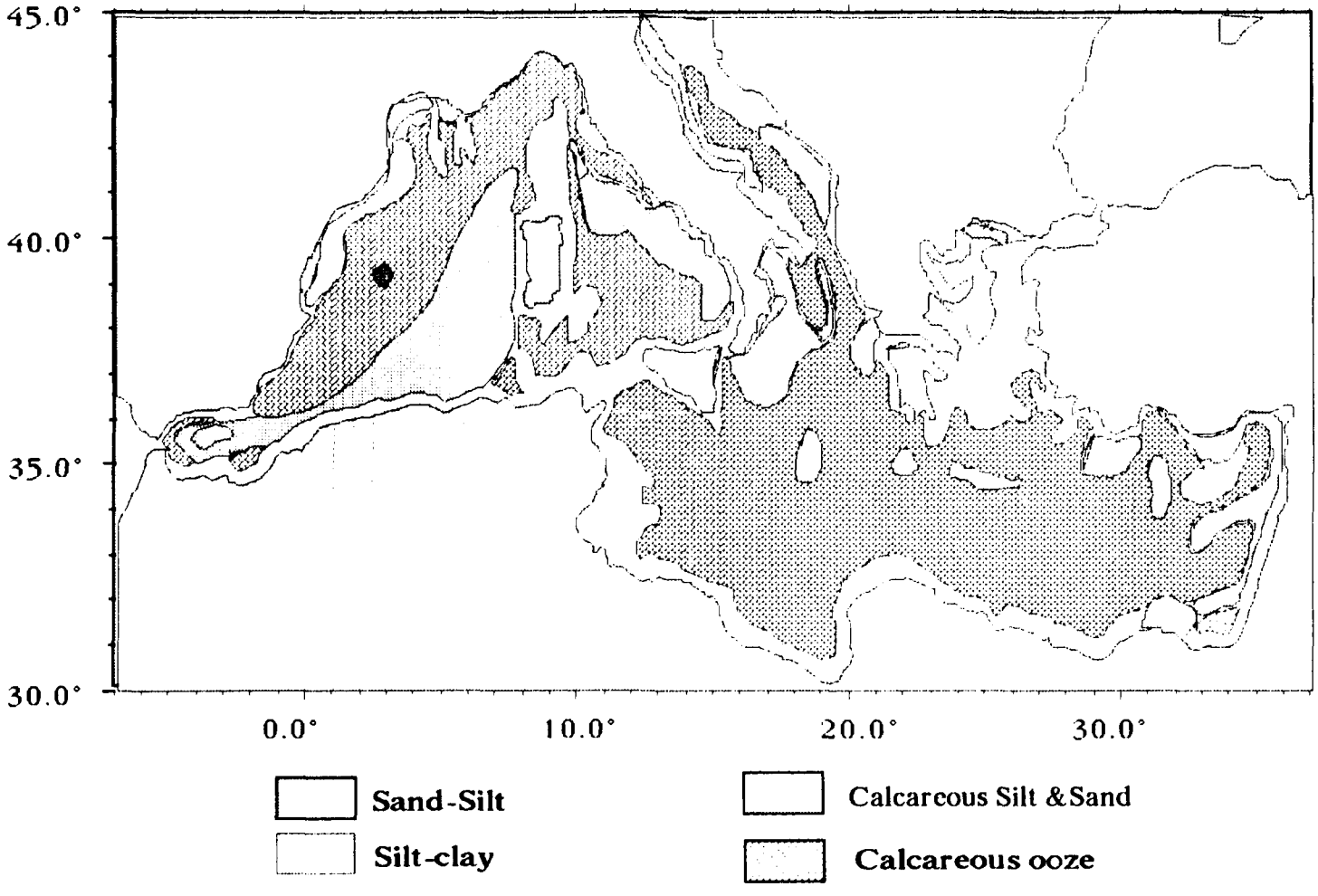

Fig. 1.1.2 Generalized surficial sediment distribution in the Mediterranean Sea (after Keller and Lambert, 1972)

midway between Ras 'Alam er Rum, Egypt, and the Gulf of Sollum, the irregular continental shelf has an average width of about 7 km and extends about 80 m into the sea. West of this point to Ras Azzaz the shelf widens to about 25 km. This increase in width is accompanied by an increase in depth of the shelf break from 80 to 240 m. The continental shelf off Ras el-Hilal, Libya, extends about 4 km into the sea with a depth of 110 m. There is no significant shelf along the coasts of Crete. On the southern coast of Cyprus, the shelf width averages 2 km wide with a shelf break at 30 m.

The continental margin along the Egyptian coastline is occupied almost exclusively by the Nile Fan. The fan is approximately 320 km wide and extends approximately 160 m from the continental shelf to depths of 2800 m on the western end and 1600 m on the eastern end. The gradient of the continental slope off the Egyptian and Libyan coasts ranges from 1:10 near the Nile Fan to 1:35 to the west of the fan. The slope off the Cretan Island Arc is complex because of numerous bisecting depressions (Carter et al., 1972).

The most dominant physiographic feature in the Eastern Mediterranean is the Mediterranean Rise. This arcuate submarine mountain chain spans the Ionian and Levantine Seas and extends approximately 2000 km from Sicily to Cyprus. The undulating topography of the ridge is attributed primarily to recent uplifting and folding of the abyssal plain (Vanney and Gennesseaux, 1985). Seismic response along the rise is generally poor due to a rough seafloor surface and a high reflection coefficient at the water-bottom interface. Echo soundings along the ridge exhibit an irregular seafloor with acoustical nonstratified to weakly stratified sediments overlying a strong, smooth reflector, the evaporite sequence. The crest of the rise is about 700 m above the abyssal plains and trenches that border it. In general, the many minor knolls and small depressions create a rough topography.

1.2 Eastern Mediterranean

The Ionian Sea is located in the central portion of the Mediterranean Sea. It extends north to Sicily, Italy, and Greece, connecting the Adriatic Sea by the Strait of Otranto; east to a line from Akra Kios south to 34°N, and then southwest to Ras Aamer; south to Libya and Tunisia; and west, including the Strait of Sicily (Carter et al., 1972). The area approximately 616,000 km^2 and maximum depth is 5093 m, which is the greatest reported depth in the Mediterranean Sea (Hersey, 1965).

The physiography of the Ionian Sea is diverse, as shown in Figure 1.2.1; the sea contains extensive and broad continental rises, deep oceanic basins, and an arcuate submarine mountain range—the Mediterranean Rise. The Ionian Sea is composed of several structural units. The central abyssal Ionian plain is bounded on the north by the deeply dissected Messina Cone with its abundant gravitational slides, on the east

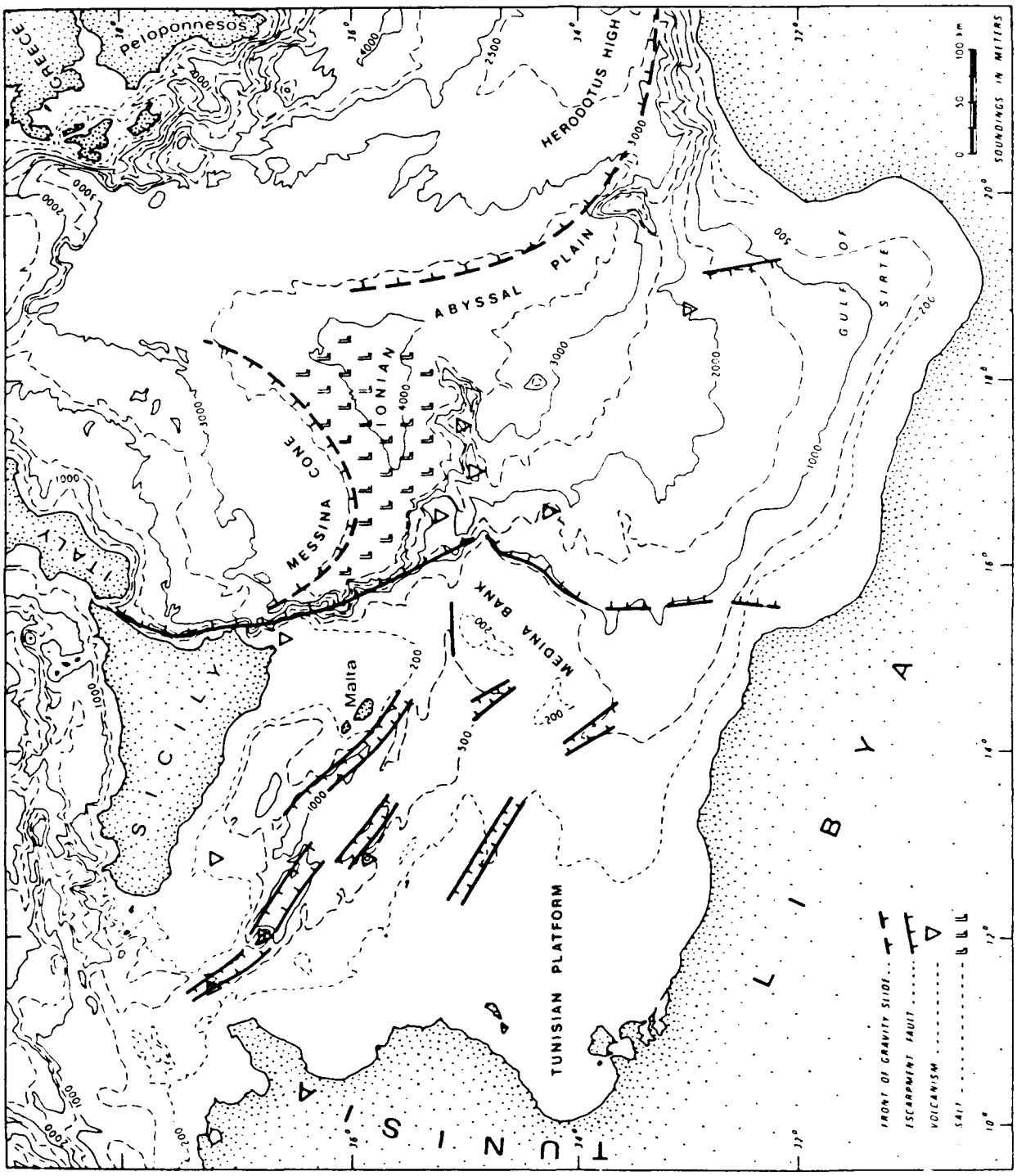

Fig. 1.2.1 Physiographic map of the Ionian Sea (After Burollet et al., 1978)

by the western end of the Mediterranean Ridge, on the south by the Gulf of Sidra, and on the west by the Pelagian (Tunesian) margin. The abyssal plain is characteristically flat and contains a thin layer of unconsolidated sediments that overlie a thick evaporitic (halite) sequence (Burollet et al., 1978). Seismic records from the western Ionian Sea reveal thick, well-stratified, and highly reflecting sedimentary layers that are continuous for hundreds of kilometers. Between the Strait of Sicily and the Ionian Sea (Fig. 1.2.2) is a series of vertical to subvertical faults lowering to the Ionian side (Finetti and Morelli, 1972).

Unlike the western Mediterranean, the continental shelf along the Libyan coast is broad. The gradient at the shelf break is on the order of 1:40 at a depth ranging from 250 to 300 m. Between Tripoli and Bengasi the shelf region is narrower; depths reach 80–110 m at the shelf break. The extremely narrow continental shelf off southern Italy varies from 2 to 7 km wide and from 30 to 130 m deep (Carter et al., 1972). Since river input in the region is almost nonexistent, sedimentation rates along the shelf and upper part of the rise are constrained. Sediments recently deposited on the shelf and rise consist mainly of clay-sized volcanic mud. The deep-sea or abyssal sedimentary deposits are chiefly calcareous oozes.

1.3 Central Mediterranean—Straits of Sicily and Sardinia-Tunisia

The straits among Sicily, Sardinia, and the African coast divide the western Mediterranean from the eastern Mediterranean, as well as into two regions of geologic and geophysical diversity. In terms of bathymetry, the northwest/southeast-trending straits form an epicontinental bridge between Sicily and Africa. The bridge is bounded on the east by the north/south-trending Malta Escarpment and on the west by the Balearic Basin (Lort, 1977). From a physiographic point of view, the seafloor of the Straits of Sicily and Sardinia–Tunisia represents a topographic high separating deeper basins to the west and east (Fig. 1.3.1). Over half the surface area in the region is dominated by water depths of about 200 m or less. Three elongate, steep-walled troughs—the Linosa (1600 m), Malta (1700 m), and Pantelleria (1300 m) Troughs—are situated within the central portion of the Strait of Sicily.

The region is characterized by extensive flat-topped plateaus and banks, including the Malta, Adventure, and Tunisian Banks. Of particular importance are two shallow banks at both ends of the strait: Skeri Bank on the west and Medina Bank on the east. These elongate topographic highs serve as barriers to water masses that flow across the platform of the strait (Maldonado, 1976).

Sedimentation in the straits region is diverse among the physiographic environments. Seismic records indicate thick accumulations of flat-lying Tertiary-Mesozoic age (136–65 mya) sediments broken by vertical and subvertical faults that form horst and graben features (Figs. 1.3.2, 1.3.3, and 1.3.4). Some of these fault

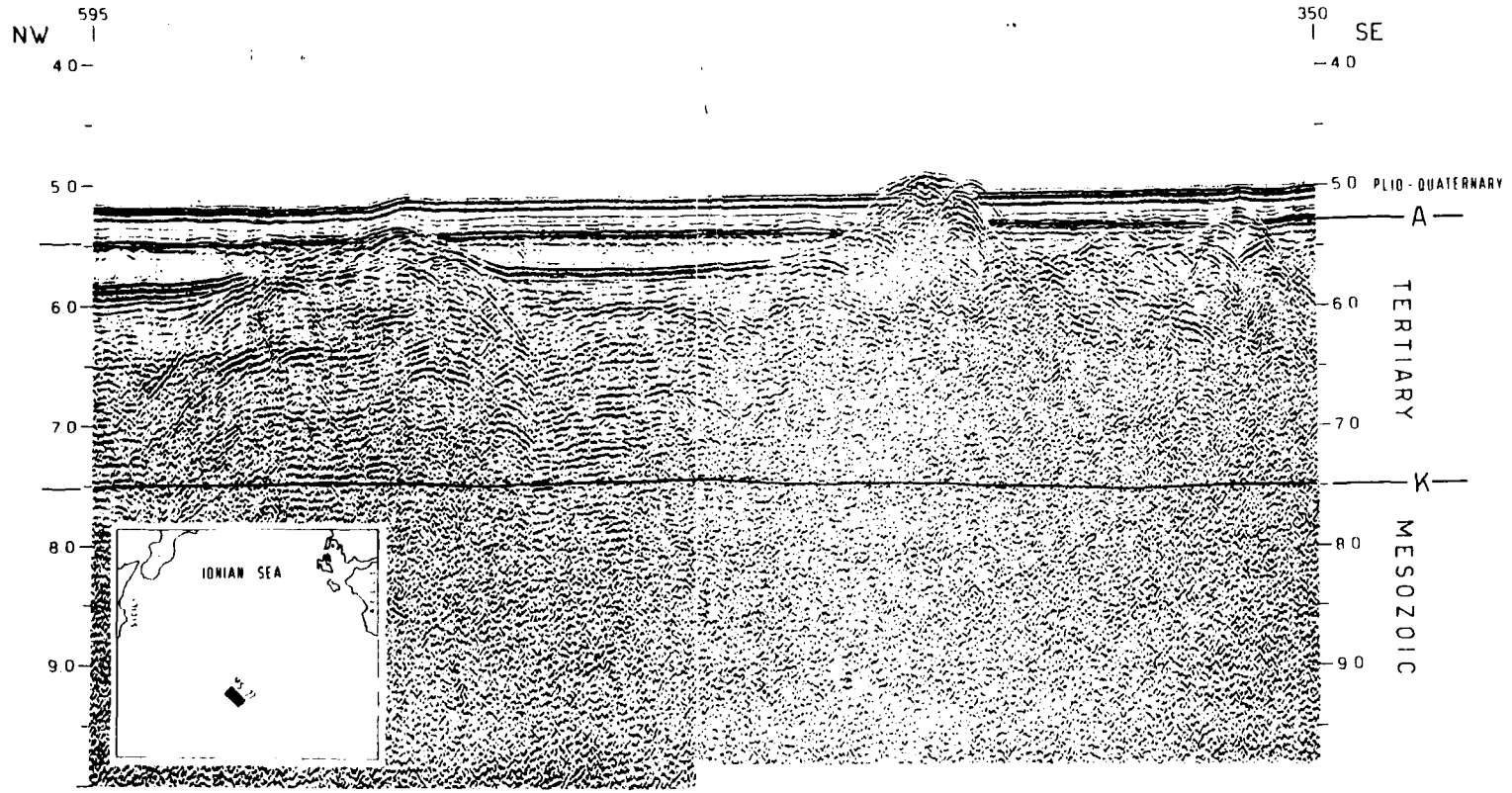

Fig. 1.2.2 Example of seismic reflection profile in the Ionian Sea. Presence of thick Mesozoic-Tertiary age sediments with diapiric structures. (After Finetti and Morelli, 1973)

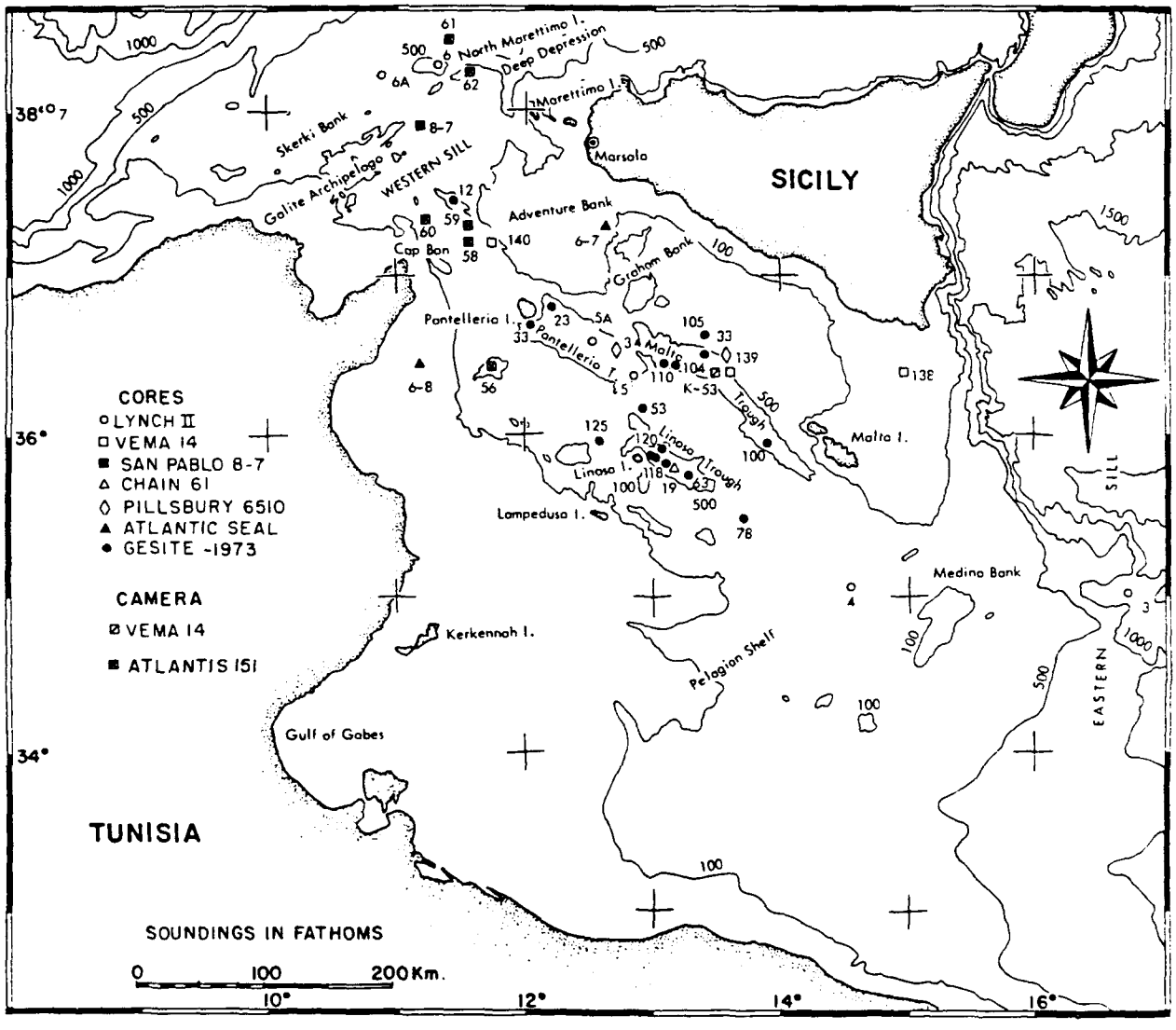

Fig. 1.3.1 Physiographic map of the of the Straits of Sicily and Sardinia-Tunisia (after Stanley, 1972).

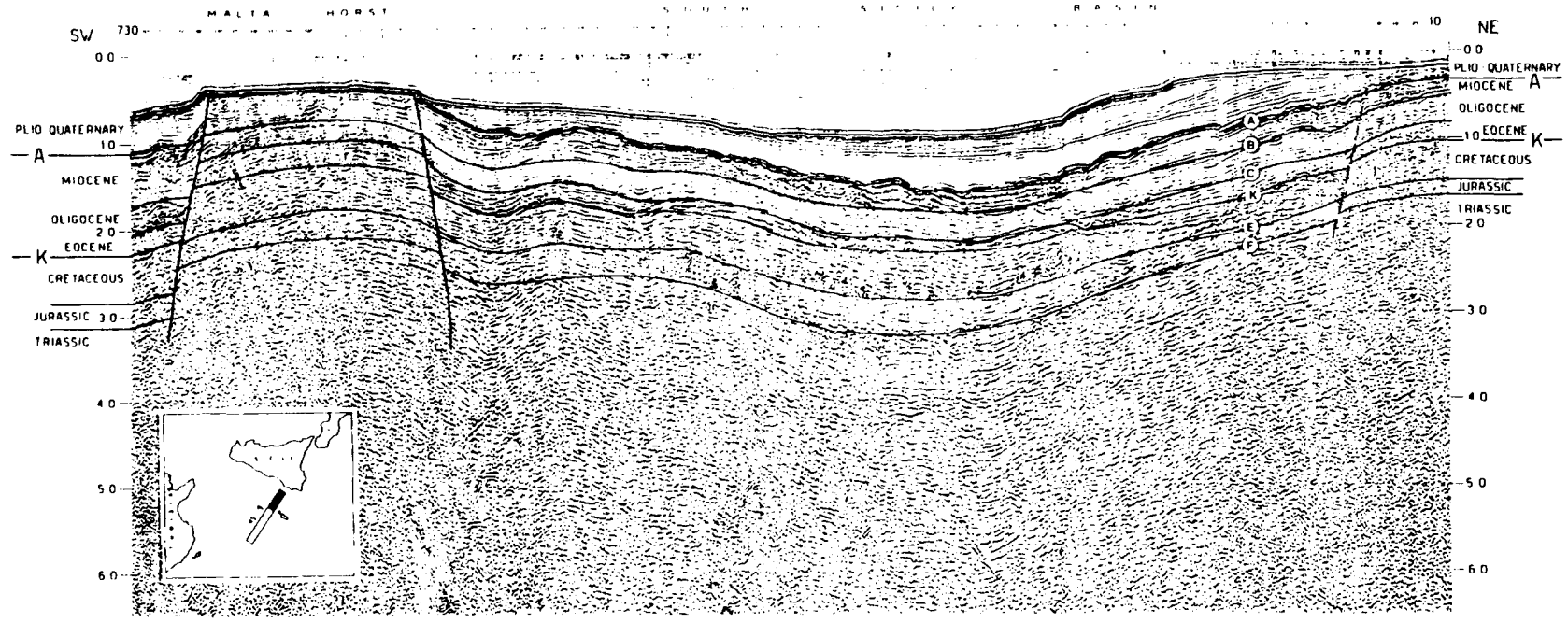

Fig. 1.3.2 Example of aseismic reflection profile in the Strait of Sicily. The dominant features in the figure are the South Sicily Basin and the Malta Horst. (After Finetti and Morelli, 1973)

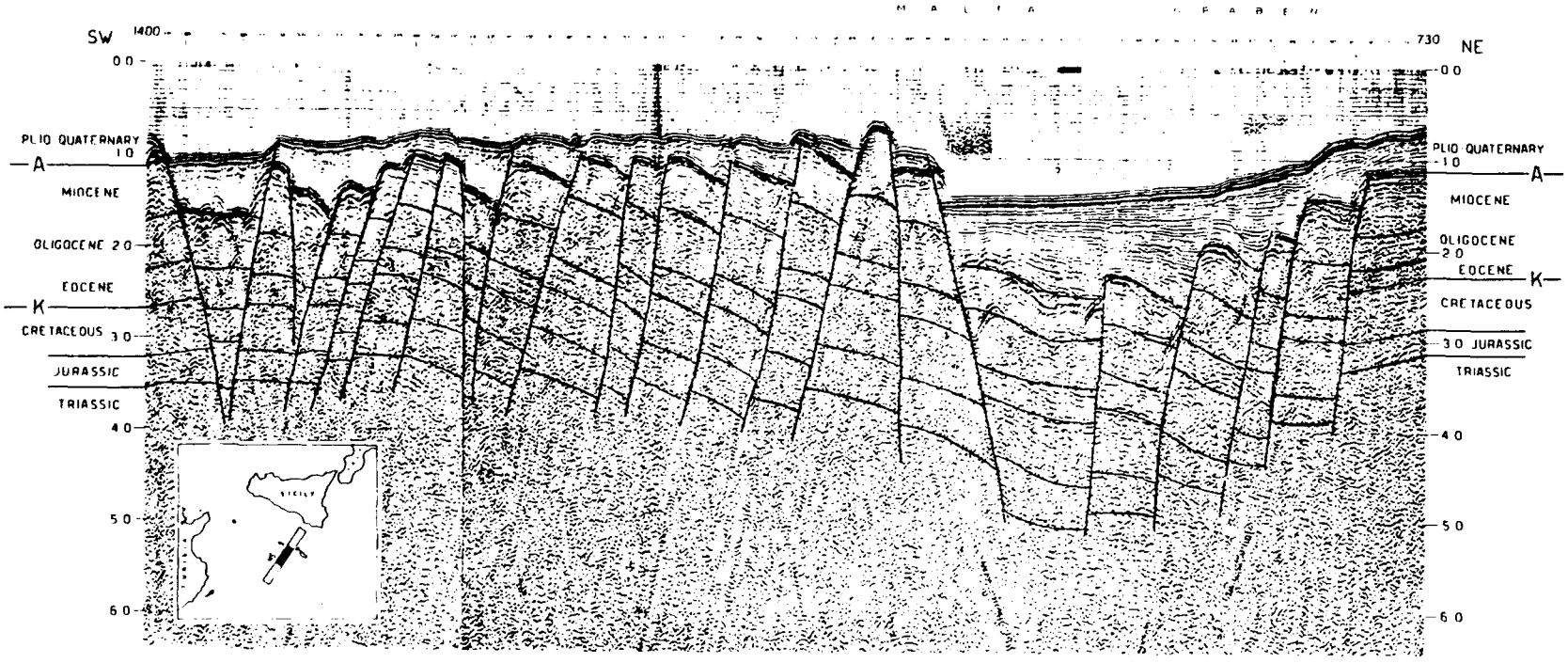

Fig. 1.3.3 Continuation of seismic reflection profile presented in Figure 1.2.2. Note the intensive tensional faulting that has deformed the upper Plio-Quaternary sediments which implies that rifting is continuing at present. (After Finetti and Morelli, 1973)

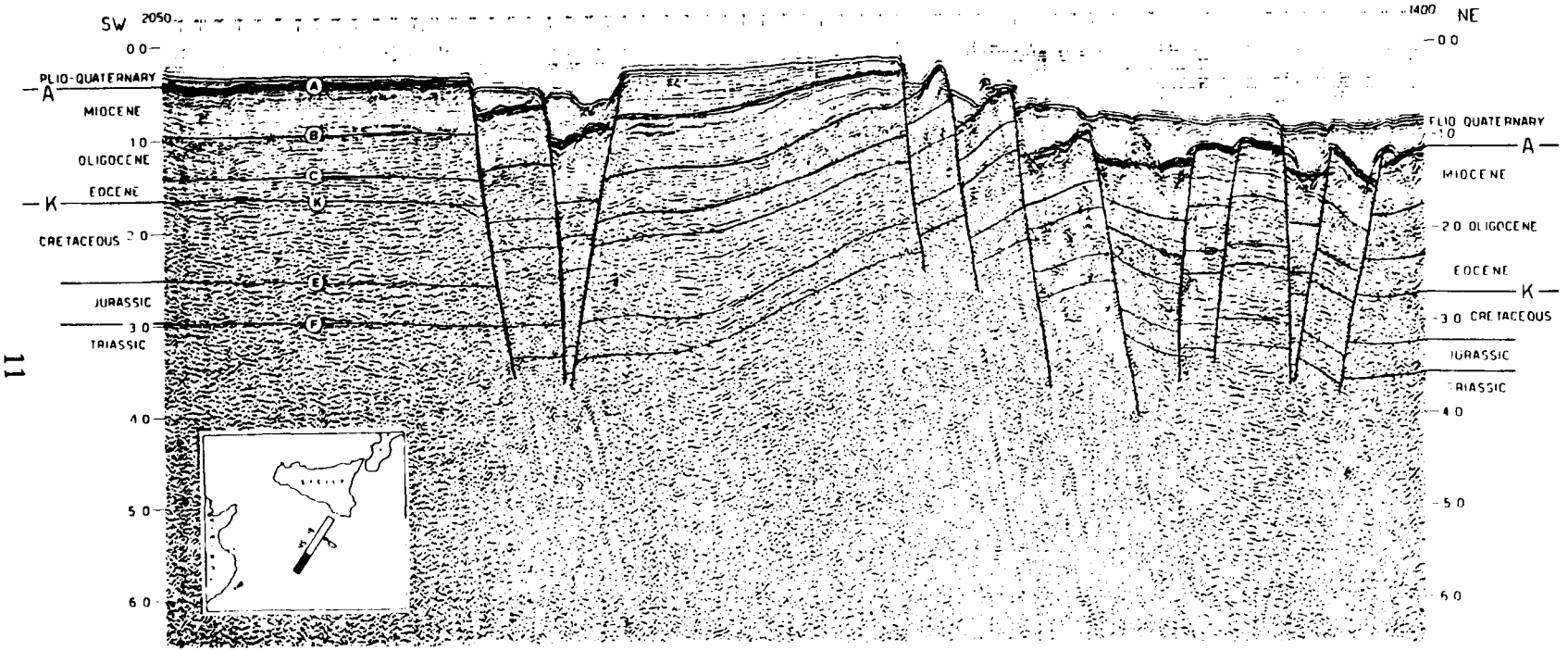

Fig. 1.3.4 Southwestward continuation of the seismic line presented in figures 1.2.2 and 1.2.3. (After Finetti and Morelli, 1973)

systems have remained active through recent times, as evidenced by disruptions of Quaternary (recent age) sediments. The three narrow troughs or basins—the Linosa, Malta, and Pantelleria Troughs—have thick sequences (in excess of 1000 m) of unconsolidated sediments. In general, the sediment type in the troughs is limited to moderate to well-stratified sand and mud units that were derived from gravity and turbidity flows and include ash layers interbedded with hemipelagic mud. Sedimentation rates in these regions are on the order of 20 to 25 cm/1000 years (Maldonado, 1976). The bank surfaces are characterized by gentle slopes composed of coarse calcareous sands, interrupted by occasional mounts and depressions. Seismic profiles indicate considerably less unconsolidated sediment than encountered in the troughs. Sediments consist primarily of coarse, calcareous sand layers interbedded with mud and sandy clay (Fig. 1.3.5). Sedimentation rates in these shallow-water environments are high, approximately 52 cm/year (Maldonado, 1976).

1.4 Western Mediterranean

The Strait of Gibraltar represents the westernmost boundary of the Mediterranean Sea. This narrow, relatively shallow, east/west-trending passage is about 14 km in minimum width, 730 m in depth, and 50 km in length and occupies about 1200 km^2. Bottom photographs and grab samples combined with echo soundings (Fig. 1.4.1) generally indicate that the channel floor of the strait consists of coarse sand and gravel, with frequent rock outcrops, especially on the northern branch of the strait channel. Depositional and erosional sedimentary features are abundant in the strait proper due to the strong westward-moving bottom currents. In contrast, the shallow inner zones of Gibraltar Canyon and Ceuta Canyon, where bottom currents are not significant, are covered by silty muds with occasional outcrops of rock and associated gravel (Kelling and Stanley, 1972).

The Alboran Sea is located in the westernmost region of the Mediterranean Sea between the Strait of Gibraltar on the west and the Balearic Sea on the east. It occupies approximately 54,000 km^2, and the maximum depth is slightly less than 1500 m. The continental shelf along the Alboran is divided into an upper shelf out to the first shelf break and a lower shelf that extends to the continental slope. From the Strait of Gibraltar northeastward along the Spanish coast, the shelf varies from a maximum width of 10 km off Malaga to a minimum of 2 km off Cape Sacratif. Along the coast of North Africa to Point Busicur, Morocco, the shelf is uniformly narrow and averages about 6 km in width. The shelf varies substantially to the east (Fig. 1.4.2) from a minimum width of 3 km to a maximum of 18 km (Carter et al., 1972). The lower shelf region off the North African coastline contains an extensive area of elongate gently sloping plateaus and ridges. This step-like nature of the continental slope and shelf is attributed primarily to normal faults that trend toward the northeast.

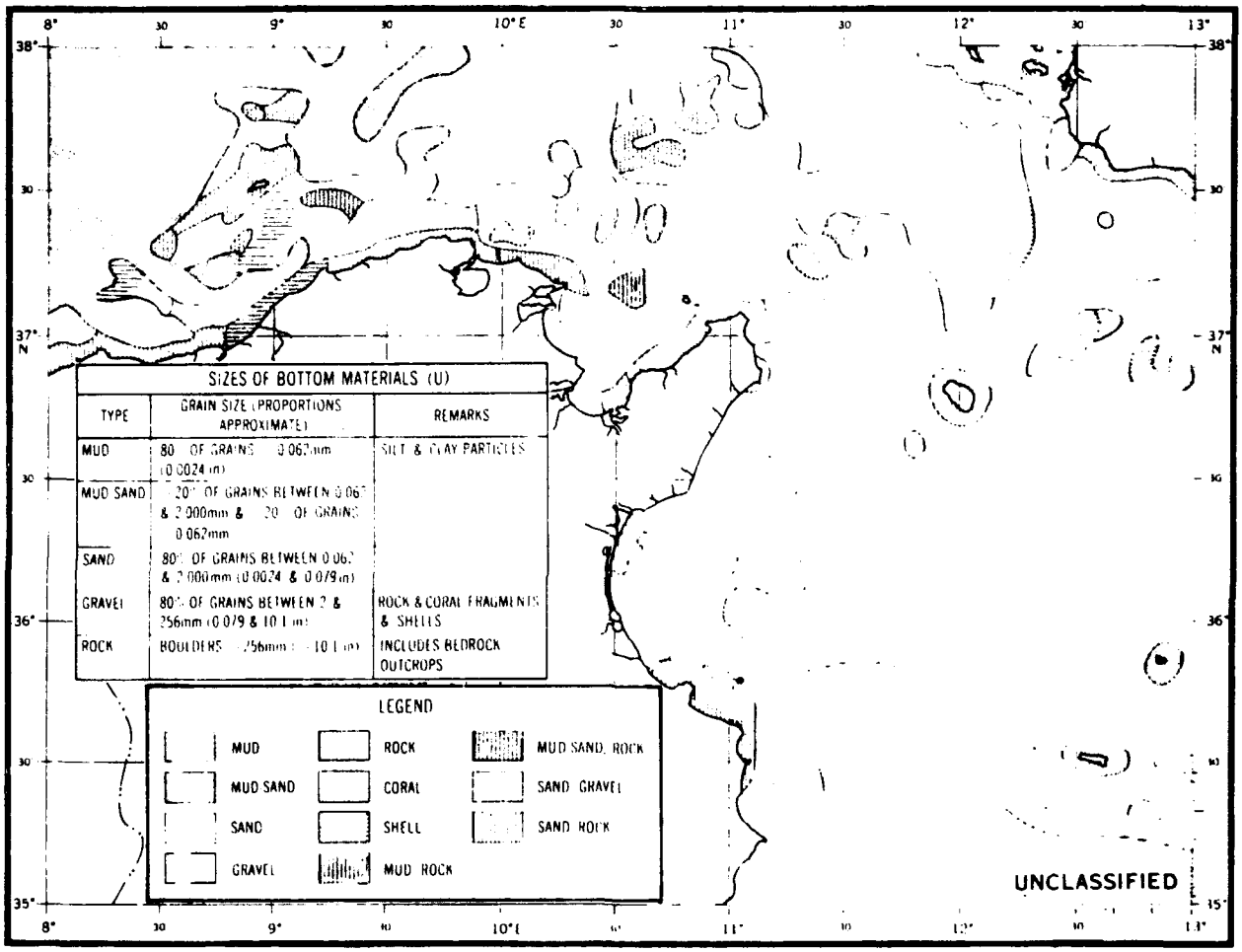

Fig. 1.3.5 Surficial sediment distribution in the Strait of Sicily (NAVOCEANO, 1970)

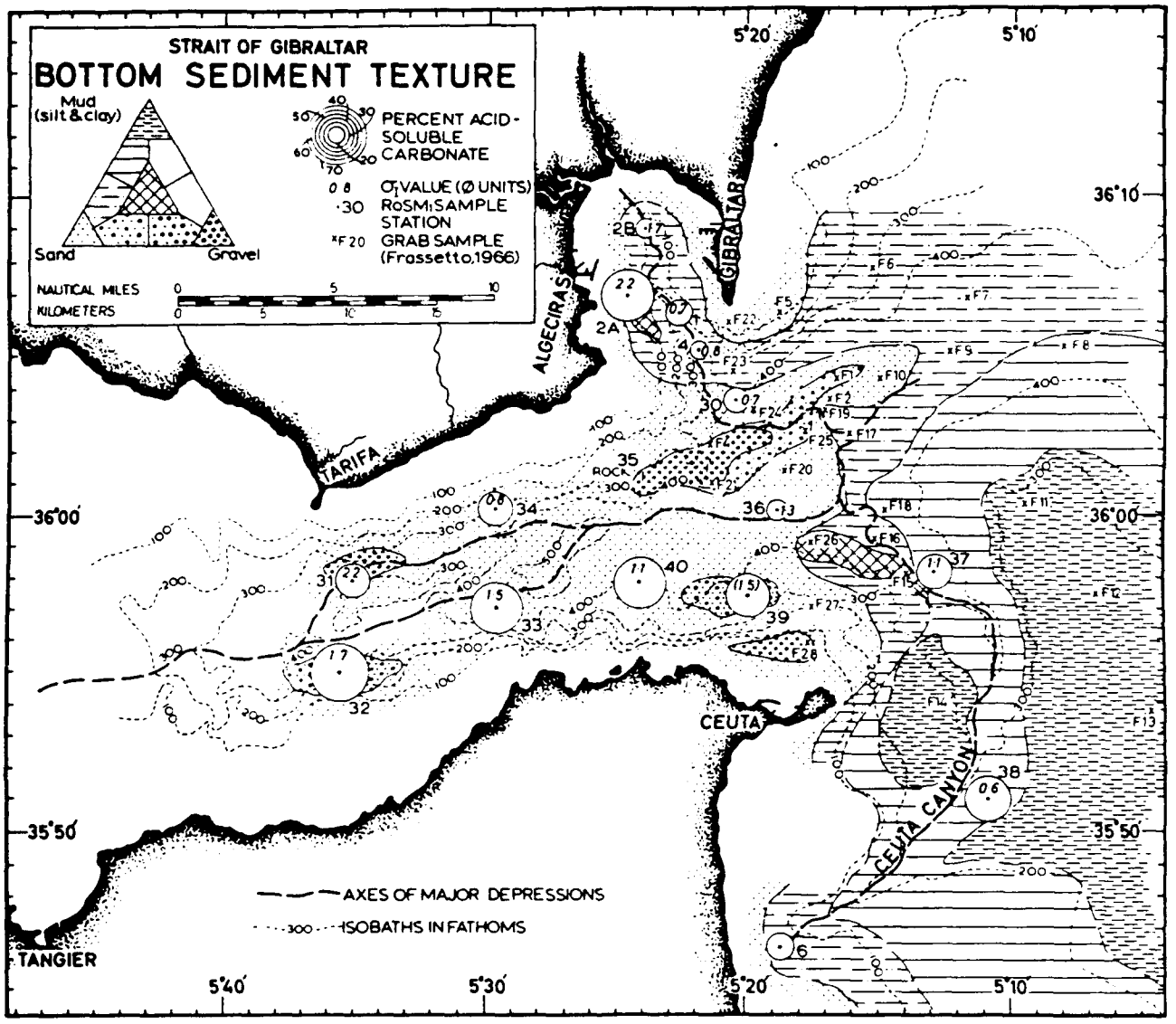

Fig. 1.4.1 Distribution of surficial sediments in the Straits of Gibraltar (after Kelling and Stanely, 1972).

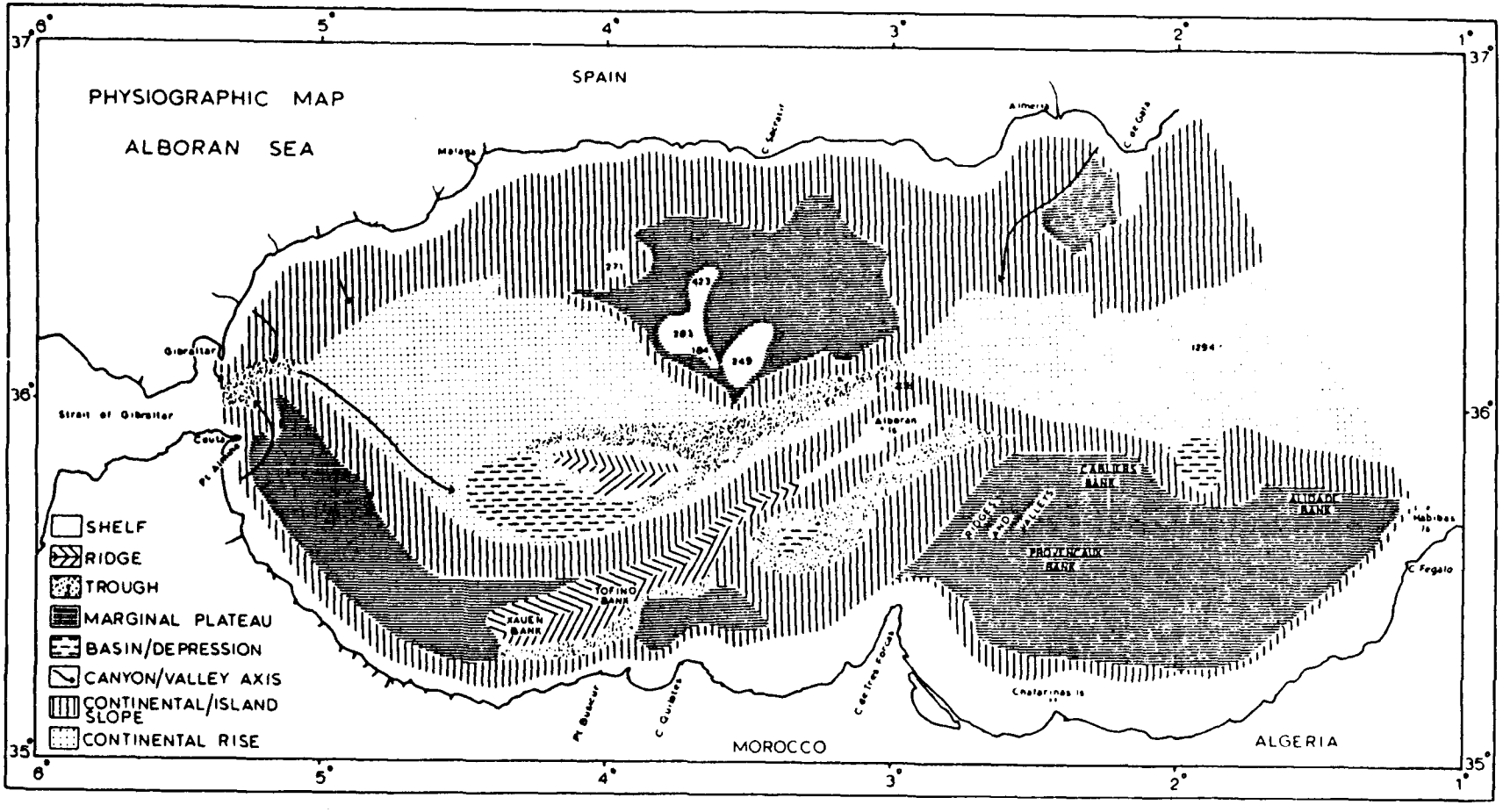

Fig. 1.4.2 Physiographic map of the Alboran Sea and the westernmost Mediterranean (After Carter et al., 1972).

As with the shelf widths, the continental slope in the Alboran varies greatly. Overall, the continental slopes along the Alboran are steep and are deeply dissected with canyons and ravines. The gradient of the slope off Spain is consistently about 1:30, but off the North African coast the gradient varies from about 1:15 north of Xauen Bank to 1:9 north of Alidade Bank. An anomalously steep slope east of Calipers Bank leads from the bank to a submerged collapsed volcano. In areas west of Corsica and Sardinia the slope gradient is typically less than the norm; however, there is no apparent continental rise but, rather, an abrupt transition from basin to slope.

A volcanic submarine ridge, comprised of the Alboran Ridge and Alboran Island, divides the Alboran Sea into two basins: the Western Alboran Basin and the Eastern Alboran Basin. The western basin is the larger of the two and is generally defined by the 1400-m isobath. Results from Deep Sea Drilling Project (DSDP) site 121 in the Alboran Sea reveal thick sequences of sediments in excess of 1000 m overlying basement material. The uppermost 300 m of the core consist primarily of mud and calcareous ooze. Surficial sediments in the basinal regions consist primarily of calcareous sands and silts. Seismic profiles indicate that thick, fine-grained sedimentary sequences cover the basinal regions of the sea except for isolated seamounts where geologic basement material is exposed.

The Balearic Basin (frequently referred to the Algéro-Provençal Basin), is the most distinctive physiographic feature in the western Mediterranean (Figure 1.4.3). This long (>800 km), almost featureless basin extends without interruption from the Alboran Sea to western Corsica with depths of 2600 to 2800 m (Vanney and Gennessaux, 1985). The bottom gradient of the basin is on the order of 1:3000 (Carter et al., 1972). A thick (1000–2000 m) upper sequence of unconsolidated sediments consists primarily of turbidites and hemipelagics and overlies a thick series of evaporites. The extent of these evaporitic regimes has been thoroughly documented by Finetti and Morelli (1973). Greater accumulations of sediment (3000–4000 m) occur toward the northeast portion of the basin near the mouth of the Rhône River where slumping and other mass transport mechanisms have predominated (Stanley, 1977). Overall, hemipelagics and mud turbidites (attributed to downslope processes and deposition from circulating water masses) account for the bulk of the sedimentary sequences on the slopes and basins over the recent geologic past (Stanley, 1977).

The complete reflecting sequence in the western Mediterranean Sea (from seafloor to acoustic basement) can often be recognized from multichannel seismic records (Figure 1.4.4). By convention of previous studies (Finetti and Morelli, 1973), Horizon A on seismic records is attributed to the base of Quaternary-Tertiary (2.5 mya) age unconsolidated sediments (about 600 m thick). Horizon B is the thick upper Miocene age (7 mya) evaporitic interval (about 1800–1900 m thick) overlaying a 1200- to 1400-m-thick preevaporitic sediments of upper Mesozoic age (65 mya). Acoustic basement (Horizon S), when present, appears as a weak coherent reflector

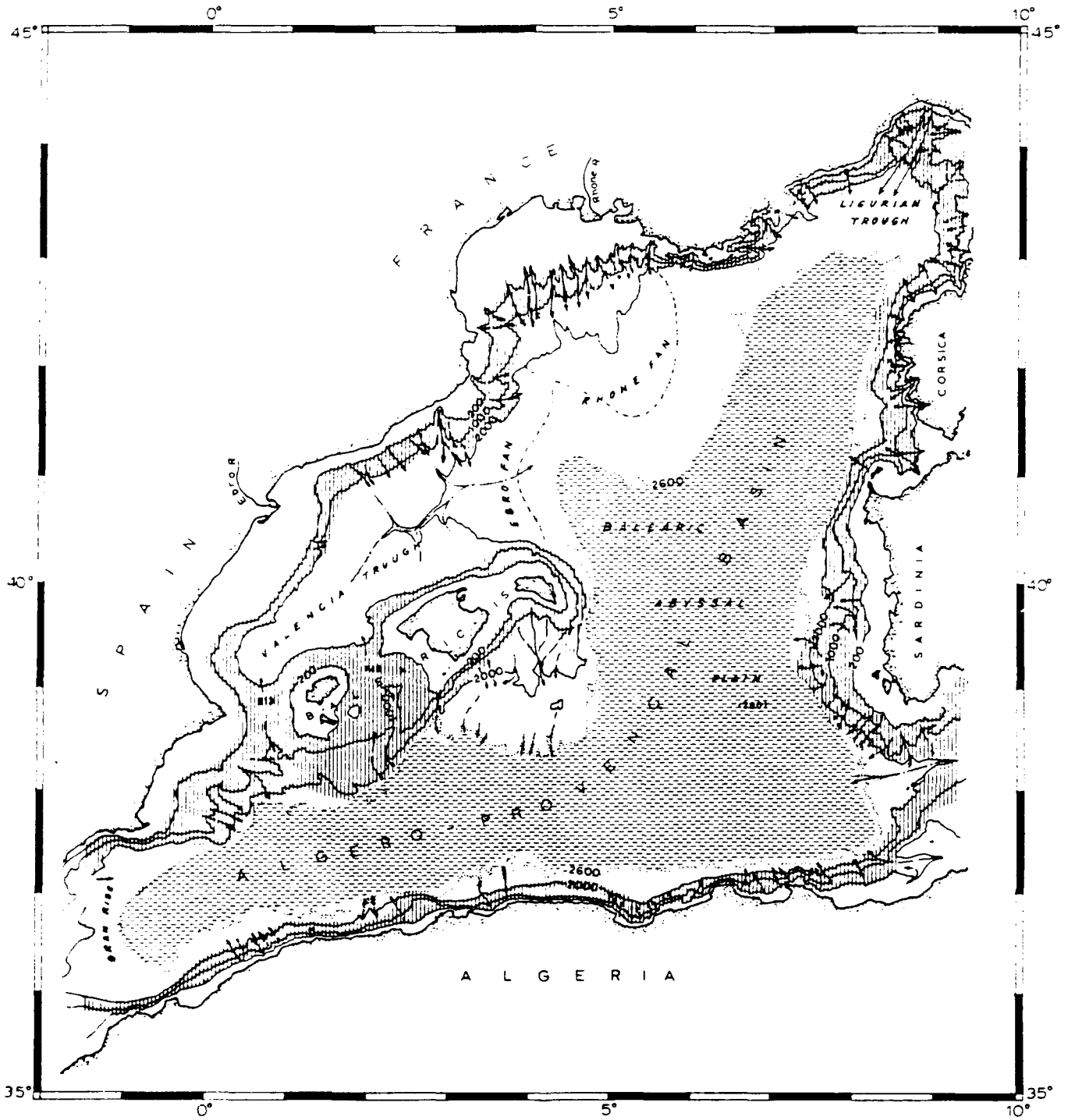

Fig. 1.4.3 Physiographic map of the Balearic Sea and Algerian Basin (after Carter et al., 1972).

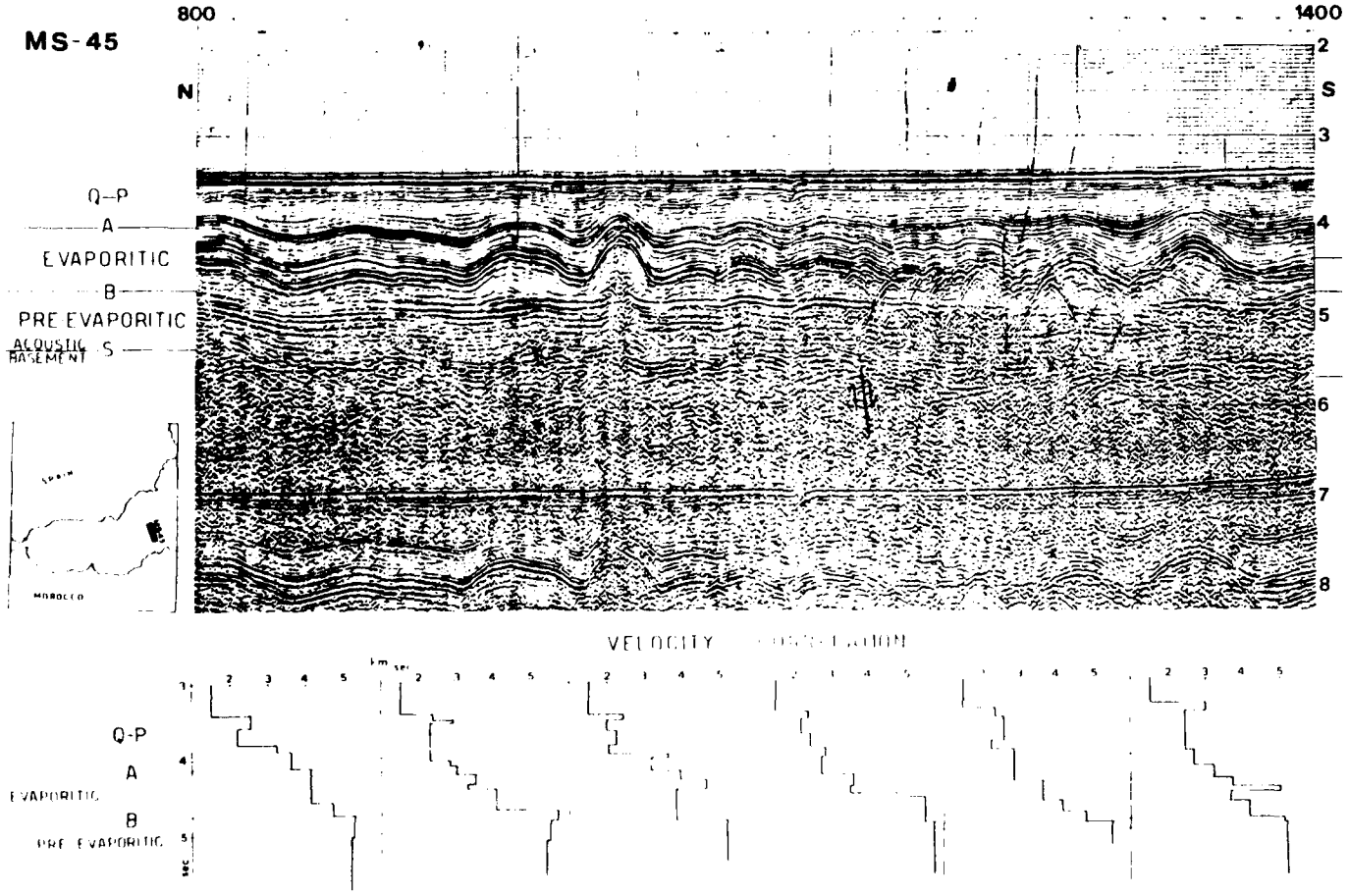

Fig. 1.4.4 Example of seismic reflection line in the Alboran Sea. The undulating layers, associated with the upper Miocene evaporitic interval, are related to diapiric structures. Typical interval velocity functions for the region are also shown. (After Finetti and Morelli, 1973)

that exhibits a rough upper boundary; however, the horizon is usually masked on seismic records by the first bottom multiple.

1.5 Seismicity and Volcanism

Geological evidence suggests that the vast majority of tectonic activity associated with the Mediterranean Sea involves strike-slip displacements. Entrances to the Mediterranean were greatly modified, even opened and closed by tectonic activity and eustatic changes in sea level. Active orogeny (mountain building) associated with overthrusting, subduction, and trench development has been limited in the Mediterranean Sea to the Hellenic Arc, south of Crete. Volcanism, during the Quaternary (2.5 mya) was widespread throughout the Mediterranean region but is now present mainly in the Aegean Sea (Lort, 1977). Lava flows and volcanic material from Mt. Ætna, Sicily, significantly affected the morphology of the Central Mediterranean. Current seismic activity as delineated in Figures 1.5.1 and 1.5.2, is chiefly restricted to the central and eastern Mediterranean—specifically, Italy, Sicily, Crete, Greece, and Turkey.

The term, intermediate focus earthquakes, generally implies earthquakes with focal points 70–300 km below the seafloor, whereas deep focus earthquakes occur at depths greater than 300 km below the seafloor. The concentration of shallow earthquakes (focal points less than 40 km below the seafloor) generally marks the boundary between the European and African plates. From the Strait of Gibraltar, the boundary extends along the northern coast of Morocco, Algeria, and Tunisia. From this point, the boundary trends northward along the Italian peninsula to the Alps and then southward along the coast of Yugoslavia and northern Greece, where it bends toward the east through the Hellenic Arc south of Crete and onward through the Cyprus Arc (Udias, 1985). The ambient noise (frequency spectrum) for a typical earthquake can range from a few hertz to several megahertz. Due to the attenuating nature of the earth, the higher frequencies tend to drop off rapidly with distance from the focal point.

2.0 Oceanographic Descriptions of Mediterranean Study Areas

2.1 Levantine Basin and Sea of Crete

Water masses in the Levantine Basin include warm, saline Levantine surface water in the near-surface layers, which overlie a relatively fresh and thin Atlantic Water lens. Below this layer the warm, saline, Levantine intermediate water is present. The majority of the water column in the deep basins consists of very stable Mediterranean deep water. The depths at which each water mass is present is

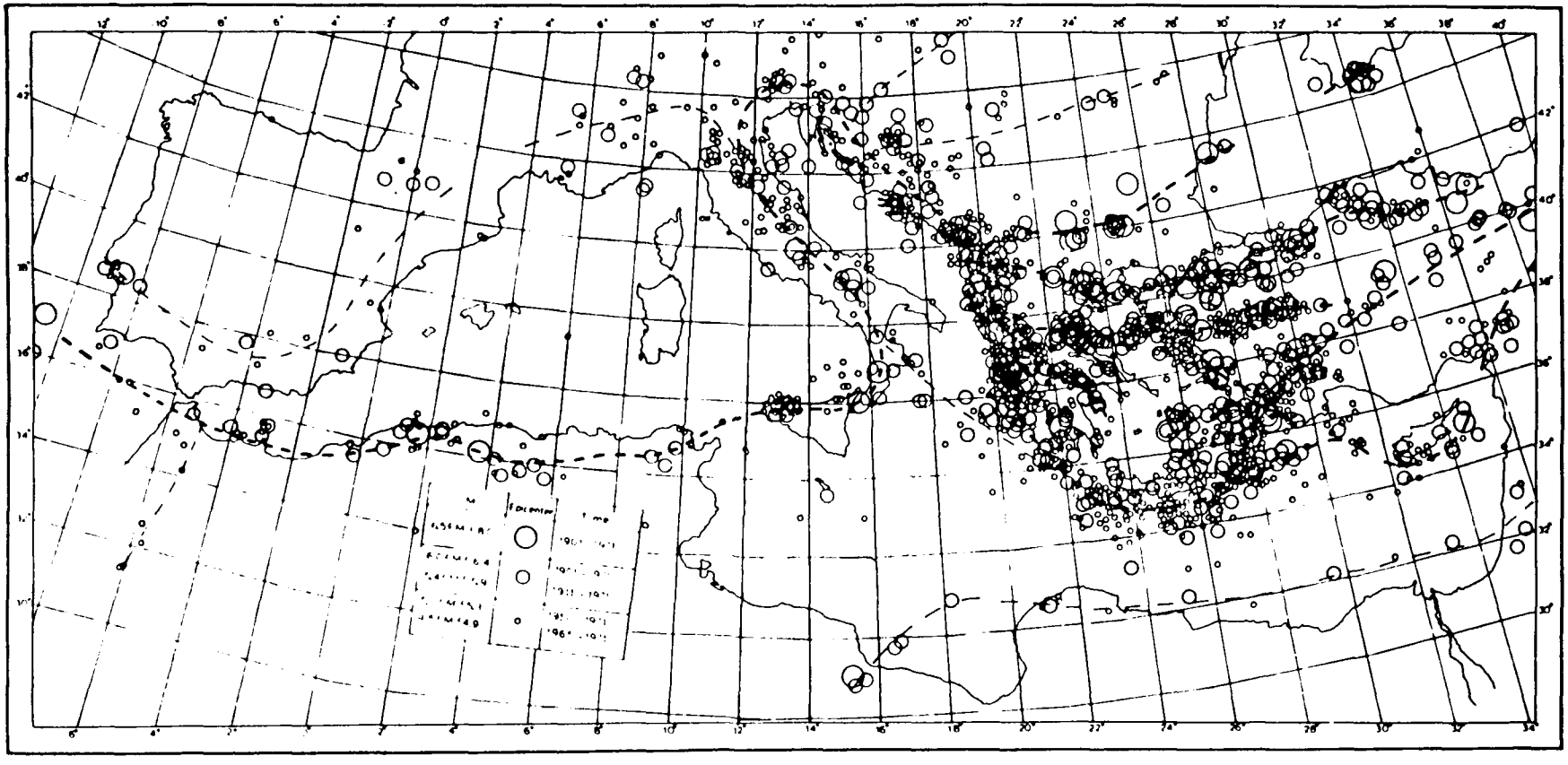

Fig. 1.5.1 Location of shallow focus earthquake epicenters for the period 1901-1971
(After Lort, 1977)

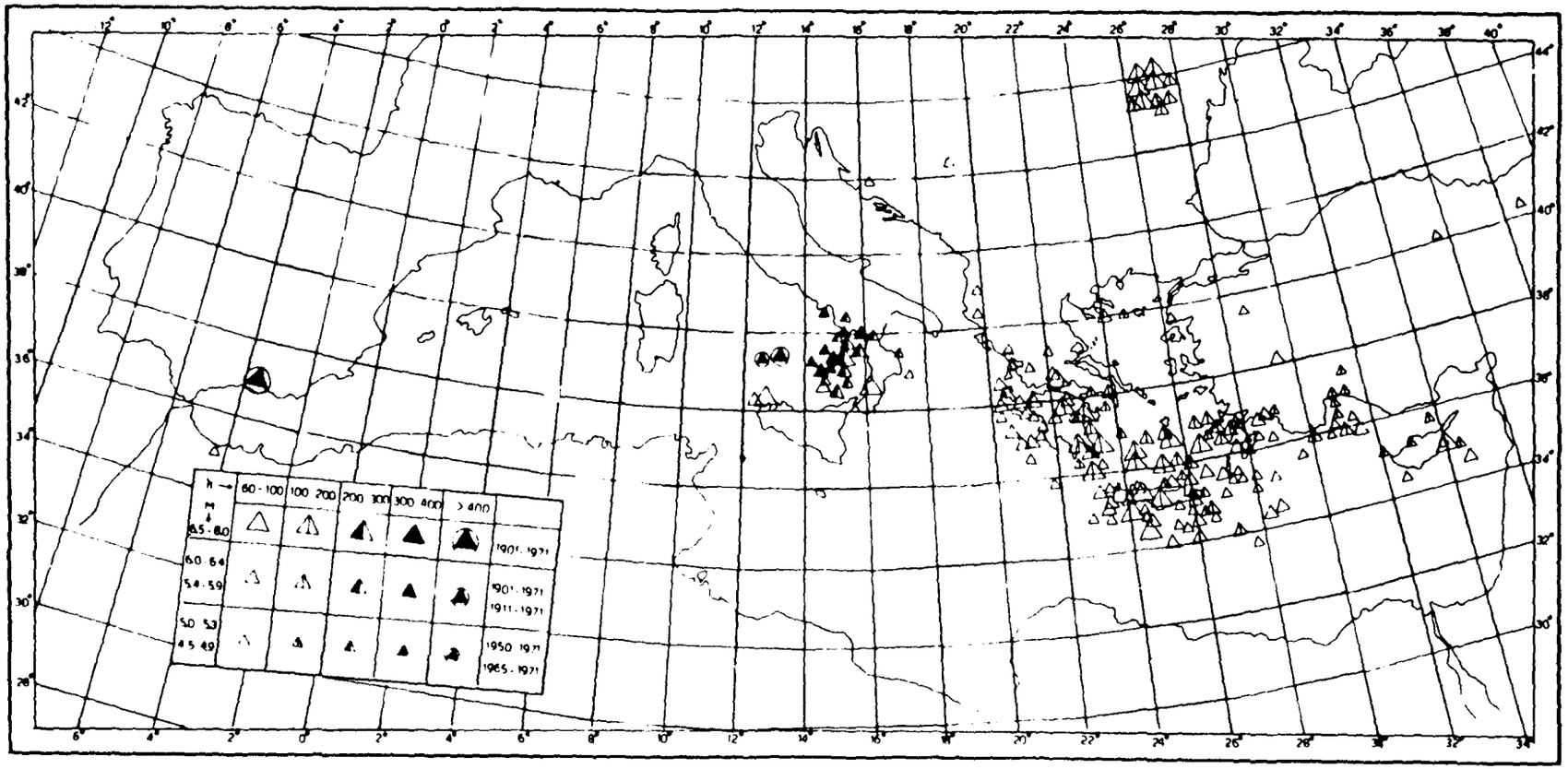

Fig. 1.5.2 Location of intermediate to deep earthquake epicenters for the period 1901-1971 (After Lort, 1977).

seasonally dependent; hence, average depth ranges are depicted in the following descriptions.

Levantine surface water is formed during the summer by intense evaporation and heat exchanges with the atmosphere and extends from the surface to 40 m. Below this layer is Atlantic water, which has advected into this area from the western Mediterranean. This water mass, which has undergone substantial modification upon its entry through the Strait of Gibraltar, has an average depth in the Levantine Basin between 65 and 95 m. Levantine intermediate water is formed in this basin at the surface when the highly saline surface waters become dense and sink to form the Levantine intermediate water mass. The average depth range of this water mass is from 200 to 310 m. The abundance of both the Levantine surface and intermediate waters apparently has no correlation with season. The stable Levantine deep water, an admixture of Adriatic, Cretan Sea and ambient Levantine water (in that relative proportion) (Ahmed et al., 1986), is present at depths greater than 685 m.

Prior to the advent of the Physical Oceanography of the Eastern Mediterranean (POEM) research program, which took place from 1979-1988, only fragmentary data sets were available to determine the hydrography and circulation of the Levantine Basin. The results of this series of cruises led to numerous papers that present a much more coherent description of the dynamics of this region. The previous depiction of the eastern Mediterranean as having a relatively simple circulation pattern has evolved to a picture of numerous transient and permanent eddies, which often have dissimilar water masses entrained into them. The first indication of this basin's complex circulation was documented by Hecht et al. (1988), who used early POEM data (1979–1984) and later by Robinson et al. (1991) and Ozoy et al. (1991), who analyzed data from this series of expeditions from 1985 to 1988.

Figure 2.1.1 is a schematic of the general circulation of the Levantine basin (after Robinson et al., 1991). All eddies depicted are either permanent (solid line) or recurrent (dashed line); the recurrent features have a time scale persistence between 6 months to 1 year. The shapes, strengths, and sizes of the eddies are temporally variable and are relatively stationary in position. In most cases, Levantine intermediate water is found in patches trapped inside clockwise eddies. The POEM data indicate that the temperature signature of even the most intense eddies appears to be less than 2°C. The mid-Mediterranean jet, which circulates Atlantic water in this basin, meanders and bifurcates several times to contribute to the flows around the main gyres. The position of this jet varies temporally in response to the varying sizes and shapes of the eddies. The use of various forcing factors in modeling studies indicates that thermohaline fluxes are the primary mechanisms that drive the circulation in the Levantine Basin (Malanotte-Rizzoli and Bergamasco, 1991).

Surface and deep-water masses in the Sea of Crete are similar to the waters in the Levantine Basin. The waters of the Sea of Crete are saline and have high

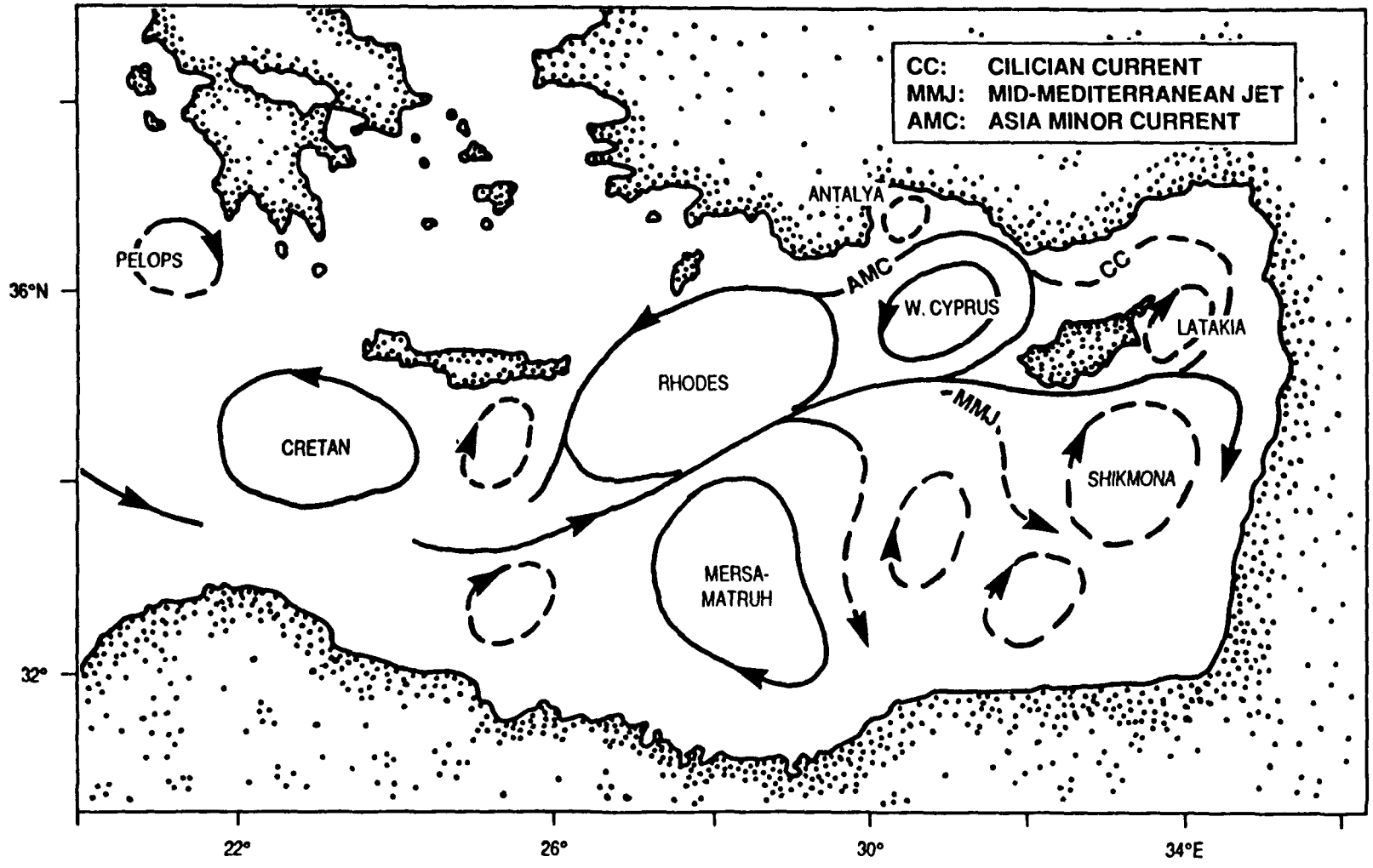

Figure 2.1.1 General surface circulation of the Levantine Basin and the Cretan Basin.

temperature characteristics. The deep-water masses in both areas are dominated by waters of the Adriatic and that produced locally in the Cretan Sea. The major circulation features in the Sea of Crete are the mid-Mediterranean jet (which represents the main forcing factor in the circulation of this basin) and the permanent, counterclockwise Cretan Sea gyre. The mid-Mediterranean jet, which circulates water of Atlantic origin, is topographically guided through this area by the mid-Mediterranean ridge. Despite our increased knowledge of the eddy dynamics in the Levantine and Cretan Basins, their impact on the acoustic significance of the sound speed structure of this region could be large. Thermal changes of 1.5 to 2°C through the strongest gyres in this region were documented in the POEM data; however, Levine and White (1972) documented thermal variability in the Levantine Basin as great as 4.4°C over 2 km. Such thermal variability can produce sound speed differences greater than 10 m/sec, an acoustically significant sound speed change. Specifically, this variability can result in acoustic phase errors and can impact on matched field processing techniques. The actual importance of sound speed variability of this magnitude is dependent on the inflections in the profile and the acoustic frequencies of interest. Unfortunately, it is questionable whether the existing oceanographic data bases can resolve this sound speed variability. Since the GDEM data base is gridded, both temporal and spatial smearing will occur, and only the latest POEM data must be extracted from MOODS to resolve gyre variability.

Variability resulting from the decay and formation of the thermocline caused by seasonal changes exerts the greatest impact on the sound speed variability in this area. The analysis of 5 years of measurements (Hecht et al., 1988) indicated that seasonal variability extends to depths no greater than 170 m.

2.2 Ionian Sea

The detail to which the Levantine Basin and the Cretan Sea can be described oceanographically is largely attributed to the POEM research program. Similarly, an in-depth knowledge of the western Mediterranean Sea was made possible by the Western Mediterranean Circulation Experiment (WMCE). Although the POEM V effort addressed the northern Ionian Basin (north of approximately 36°N), we must rely on uncoordinated sets of measurements to define the circulation, currents, and oceanographic characteristics of the central basin east of the Strait of Sicily.

Like the surface waters of the Levantine Basin, the warm, saline characteristics of the Ionian Sea's surface waters result from excessive evaporation over precipitation. The circulation in the southern portion of this basin is dominated by the eastward-flowing Atlantic water that emanates from the Strait of Sicily. Although detailed documentation of this current is not available, the northward meandering and subsequent southeastward flow of Atlantic water is indicated in the POEM V

measurements from the south (Robinson et al., 1991) and in the circulation models of Malanotte-Rizzoli and Bergamasco (1991).

This strong meandering of the Atlantic jet adjacent to the Strait of Sicily precipitates the existence of the north-to-south-oriented fronts, which separate the Atlantic waters from the Ionian surface waters. More accurately, these fronts may be result from a series of eddies where two dissimilar water masses mix. The Maltese Front, located between 16° and 18°E on the flanks of the continental slope south of Malta, is well documented by several investigators. The thermal intensity of this front (approximately 1.5°C) is weak. However, Levine and White (1972) report several thermal gradients in this region, some as great as 5.2°C over 2 km; hence, acoustically important sound speed variability may be present in this area. Sound speed provincing using historical data may smear the existence of these features both in space and in time, since it is not certain whether the thermal variability is seasonally dependent. The summer POEM V survey in the northern Ionian Basin indicates that the clockwise circulation is generally weak.

Wüst (1961) documented a well-defined core flow path of the Levantine intermediate water (formed at the surface in the Levantine Basin) that extends westward across the southern Ionian Sea into the Strait of Sicily at a depth of about 250 m. This Levantine core has a strong salinity signature; however, its thermal characteristics are acoustically insignificant. The stable bottom waters of the Ionian Basin are composed of large quantities of northern Adriatic winter waters, which cooled and sank, and were transported south through the Strait of Otranto into this basin.

2.3 Straits of Sicily and Sardinia

The Strait of Sicily separates the western Mediterranean basins from those of the eastern Mediterranean. Through this strait, relatively low-salinity Atlantic water flows into the eastern Mediterranean in the near-surface layers, and saline Levantine intermediate water flows into the western basins near the seafloor. The bathymetric constriction associated with the Strait of Sicily causes these dissimilar water masses to come into close contact with one another. In addition, the strait is sufficiently shallow to preclude the exchange of deep waters from the eastern Mediterranean with those of the western Mediterranean.

Oceanographic measurements taken during the early 1970s describe the preferential flow paths of these water masses through the Strait of Sicily; however, the seasonality and eddy dynamics within the strait have only recently been elucidated. Specifically, the flow of the near-surface Atlantic water through the strait is seasonally and geographically bimodal. During the winter, this water mass is strongest and exhibits a well-defined, low-salinity core against the coast of Africa; during the

summer, the mass transport of Atlantic water is at a minimum and is generally laterally distributed across the entire strait. For example, current speeds associated with this layer average 5 cm/sec in the summer and 15 cm/sec in the winter. Similarly, the transport of Levantine water in the deeper layers of the strait demonstrates a twofold increase in the winter.

The areas immediately to the south of Sicily are subject to upwelling phenomena associated with the prevalent westerly winds. Figure 2.3.1, a recent satellite thermal image, shows an elongate area of upwelling (the area of cool temperatures) along the Sicilian coast. The interaction of the Atlantic water and the coastal upwelling precipitates fronts in this region. In the southern portion of the strait immediately to the south of Malta, satellite imagery shows the existence of meanders, rings, and tongues of warm water. Figure 2.3.1 shows one such feature to the southwest of Malta. It is not certain whether these features within the strait are permanent features of the circulation, but we can infer that during summer, when the Atlantic water is less active, fewer eddies are probably formed.

The salinity signature of the various water masses and circulation features in the Strait of Sicily is certainly larger than the temperature variability. During the summer, upper water column stratification, which results from intense warming, dominates the thermal characteristics of waters in the strait. In the winter the axis of the strait lies along a preferential westerly wind stress region, which results from low-pressure systems over the Tyrrhenian Sea. This condition results in vertical mixing to the seafloor in all but the deepest areas of the strait. Hence, the sound speed structure in the strait exhibits more seasonal than geographical variability. The only exceptions may lie in the undocumented variability associated with localized upwelling near the Sicilian coast and in the gyres observed in the southern strait.

Water masses in the Strait of Sardinia are essentially the same as those in the Strait of Sicily. Easterly flowing Atlantic water is concentrated along the coast of Africa, shown in Figure 2.3.1 by the warm surface flow along the Tunisian coast. After exiting the northern Strait of Sicily, the Levantine Intermediate water bifurcates; a branch flows to the north into the Tyrrhenian Sea and one to the west in a well-defined maximum salinity core extending to approximately 400 m. Manzella et al. (1988a, 1988b) provide evidence that the northern flow may, at times, be stronger than the western flow. Upon entering the Sardinia Strait, large quantities of Levantine intermediate water flow to the north along the western side of Sardinia and circulate into the northern basins. The remainder is entrained into seaward (northward) shed eddies of the Algerian current (an eastward-flowing current along the coast of Africa) and flows toward the Alboran Sea.

Two separate oceanographic data sets indicate the existence of a clockwise eddy in the southern part of the strait (37°57'N, 8°20'E) and a smaller counterclockwise eddy in the northern reaches of the strait. The clockwise eddy is a much larger feature

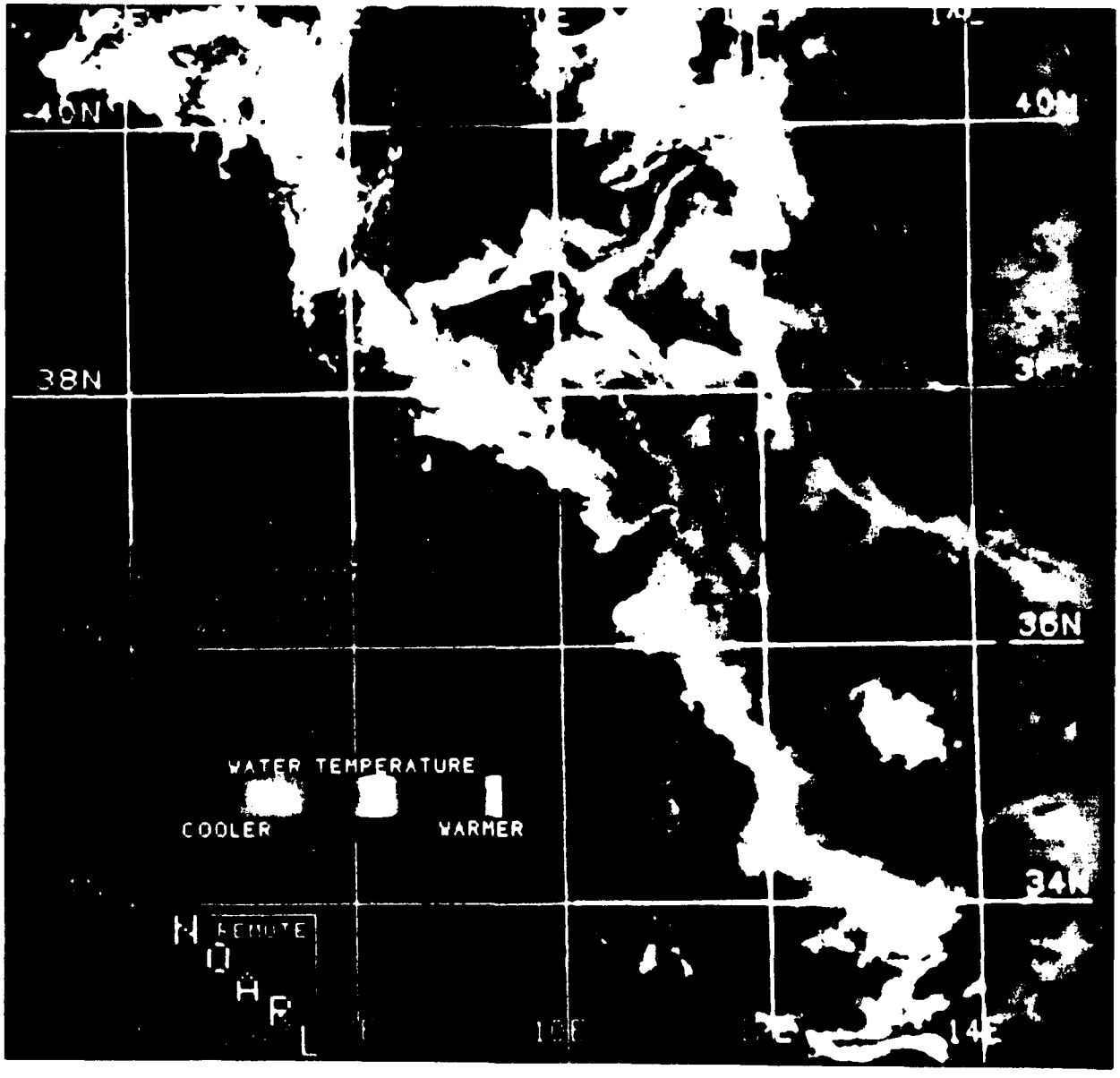

Figure 2.3.1. Satellite Thermal Image of the Straits of Sicily and Sardinia

than the eddy to the north and contains low-salinity water. This eddy, which extends to at least 400 m, effectively causes a bifurcation of the Levantine water mass. The temporal amplitude and position of the eddies have yet to be determined. However, other oceanographic sections in this area indicate that this eddy may be only semipermanent.

2.4 Western Alboran Sea

The Alboran Sea and adjacent Strait of Gibraltar are probably the two most oceanographically studied areas in the world. The western Alboran Sea is the first basin encountered by the inflowing Atlantic water and is the last basin occupied by the outflowing Mediterranean water. Atlantic water, which enters this basin through the Strait of Gibraltar, occupies the upper nearly isohaline layer and varies in depth from 150 m in the central western Alboran Basin to less than 50 m near the Spanish coast. The surface circulation pattern in the western Alboran Basin is dominated by the western Alboran gyre, a large, permanent clockwise feature centered approximately in the central basin (Fig. 2.4.1). This gyre is accompanied by the eastern Alboran gyre, another clockwise feature to the east of our area of interest. The western Alboran gyre can undergo large changes in shape and can change position as much as 50 km. Changes in the direction of inflow of the Atlantic water jet to the east or the southeast can completely obliterate the surface characterization of the gyre (Heburn and La Violette, 1990); however, its subsurface characteristics remain intact (Bucca and Kinder, 1984).

The incoming Atlantic water from the Strait of Gibraltar, characterized by a vein of relatively cooler water in the summer and warmer in the winter, forms a high-speed jet that flows to the northeast along the coast of Spain. The Alboran front, formed by the contrasting temperature and salinity properties of this relatively unmixed Atlantic flow and modified Atlantic waters to the south in the gyre, is probably the strongest frontal feature in the Mediterranean Sea. This front wraps around the northern outer edge of the gyre, is approximately 30 km wide, and is confined to the upper 200 m. The Alboran front is shown in Figure 2.4.1) as the interface between the blue area along the Spanish coast and the yellow region within the gyre. Total changes in temperature across the front in summer are on the order of 4 °C (> 11 m/sec in sound speed). Nonlinear internal waves, which emanate from the strait, propagate eastward about 50 km into the basin cause short time scale (on the order of hours) in this area (Kinder, 1984).

Beneath the Atlantic water is a transition zone approximately 100 m thick which separates this water mass from the more saline Levantine intermediate water formed in the far eastern Mediterranean. Embedded in this transition zone is a minor water mass, the winter intermediate water (Salat and Font, 1987), formed off the coast of Spain and France in the northern Mediterranean and typified by a salinity minimum.

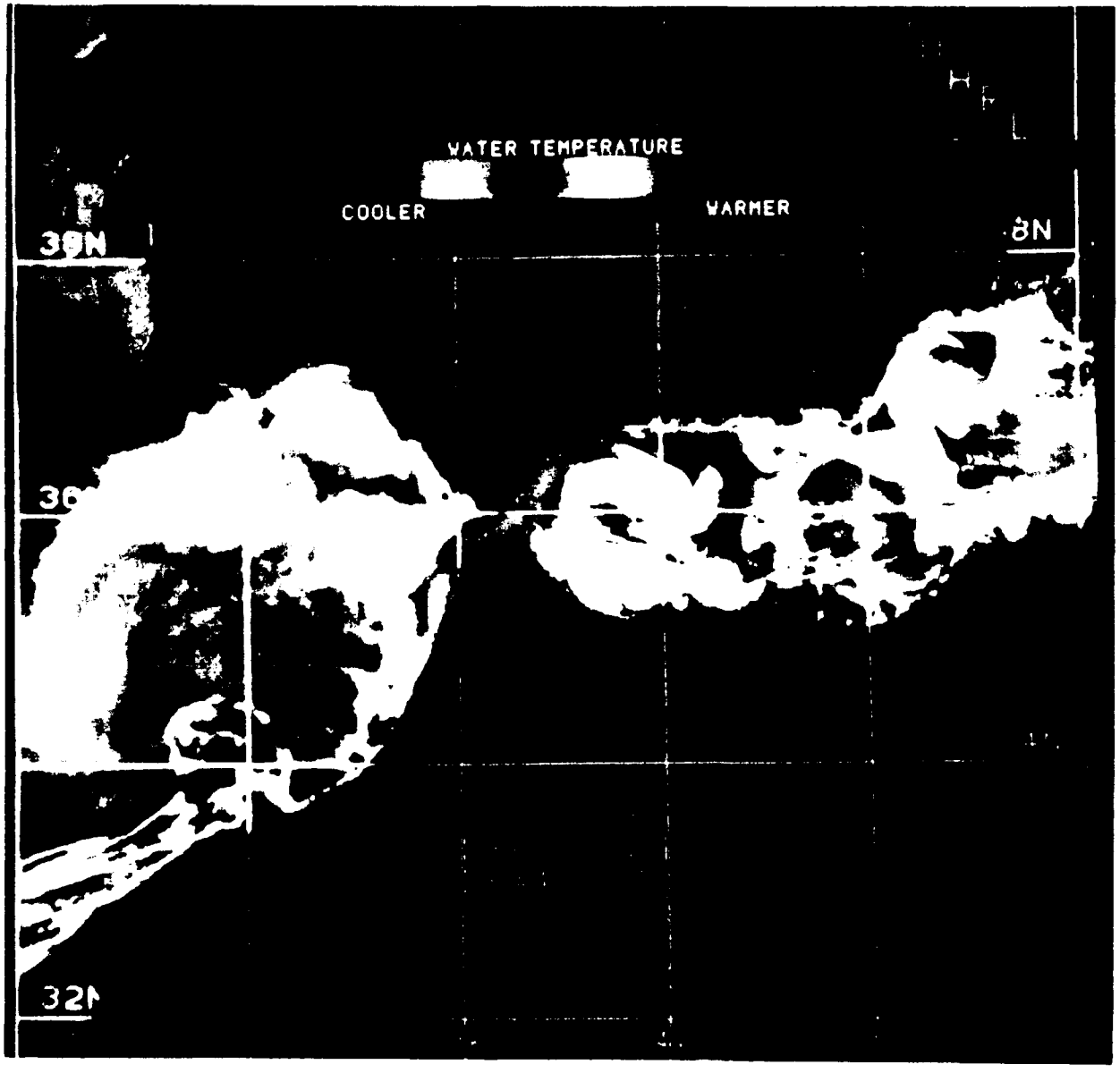

Figure 2.4.1. Satellite Thermal Image of the Alboran Sea and Atlantic Ocean Approaches.

The depth interval between 200 and 600 m is occupied by the Levantine intermediate water identifiable by a salinity maximum. Over long time scales, this water mass flows westward mainly along the northern half of the basin in a cell-like distribution.

Below this water mass lies the abyssal Mediterranean deep water, which is formed in the northwestern Mediterranean Sea south of France during winter. The depth of the deep water rises from east to west and from north to south. Hence, the shoalest area of this water mass is off the southwest coast of Africa adjacent to the Strait of Gibraltar. A well-defined abyssal (from ≈600 m to the seafloor) boundary current along the Moroccan continental slope extends from Alboran Island at ≈3°W to the strait entrance. The shoal areas in the southwest Alboran basin, coupled with the westward-flowing boundary current, are probably responsible for the passage of deep water through the Strait of Gibraltar. Just to the north of this flow is evidence of an eastward-flowing abyssal current. North of this current in the center of the basin is a weak, counterclockwise flow that exhibits substantial periods of stagnation.

2.5 Strait of Gibraltar

The Strait of Gibraltar is the channel through which water between the Atlantic Ocean and the basins of the Mediterranean Sea is exchanged. Over large time scales (greater than the tidal cycle), the flow through the strait at the surface layer is dominated by the influx of Atlantic water, and the deeper channels provide egress for Levantine intermediate (and, to a lesser extent, Mediterranean deep) water masses (see the discussion on currents for details on the topography and flow dynamics in the Strait of Gibraltar). Between these two opposing flows is an interface where intense current shear takes place. This interface is deeper in the western approaches and attains its minimum depth near the sill. The effects of the Coriolis force have caused a mean traverse slope where the interface is shallower at the northern portion of strait and deeper in the southern region. In fact, the interface may reach the surface near the northern coast of Spain.

The interface between the Atlantic and Levantine intermediate water masses is extremely dynamic over tidal frequency time frames. Superimposed on this mean flow regime is the semidiurnal tidal cycle which, with the variable topography of the strait, generates large internal waves. These internal waves are primarily created at the shallow sill and travel eastward along the interface between the dissimilar water masses at a speed of 3 to 4 kt. Temperature differences on the order of 2.5°C (≈7 m/sec in sound speed) over a 15-minute period are common along the interface generated by these internal waves. To the east of the sill where the internal waves broach the sea surface, temperatures drop more than 3°C (>9 m/sec in sound speed) in 45 minutes. The amplitude of the internal waves is larger in the eastern and southern portions of the strait.

Because the largest temperature (and, hence, sound speed) variations take place over periods that correspond to a tidal cycle, only the use of data sets taken within this time frame can be used to adequately quantify the variability present in this dynamic region. The use of any gridded or historical observational oceanographic data base to determine the variability in this area will result in both temporal and geographical smearing and therefore produce misleading results.

3.0 Sound Velocity Structure for the Mediterranean Sea

3.1 Levantine Basin

A Master Oceanographic Observation Data Set (MOODS) extraction was obtained for each month for an area covering 31.5-35°N, 031-034°E. Profiles were grouped into seasons based on obvious changes observed in sound speed gradients. Seasonal profile groups were edited to remove those with less than five data points, duplicates, and those that did not begin at the surface or extend beyond 50 m in depth. The edited seasonal profiles were interpolated to standard ocean depths and were statistically analyzed to obtain a mean value at each depth. The routine selects the real profile that is closest to the mean and produces a model profile, which is this same profile extended beyond its maximum depth with mean values. Model profiles were visually evaluated to determine if they were representative of their season. Minimum and maximum observed values and the standard deviation at each standard depth are also provided with each model profile.

In the winter (January-March), the Levantine Basin profiles exhibited a weak negative sound speed gradient from the surface to approximately 1000 m with some exceptions (Fig. 3.1.1). This sound speed minimum results from the vertical advection of the cooled, high-salinity surface waters during frontal passages with the formation of new Levantine intermediate water. The maximum standard deviation was 2.2 m/sec at a 50-m water depth (Table 3.1.1).

Spring (April and May) was deemed to begin when profiles exhibited a reasonably strong seasonal thermocline resulting from surface warming (Fig. 3.1.1). The maximum standard deviation was 3.0 m/sec at the surface (Table 3.1.2).

The summer (June-October) profiles exhibited a strong seasonal thermocline (Fig. 3.1.2). The summer season duration increased toward the southeast section of the Mediterranean Sea. Maximum standard deviation was 6.4 m/sec at 30 m (Table 3.1.3).

The autumn (November and December) profiles were selected based on the formation of a significant surface mixed layer resulting from increasing periods of high winds (Fig. 3.1.2). The maximum standard deviation was 3.5 m/sec at the surface (Table 3.1.4).

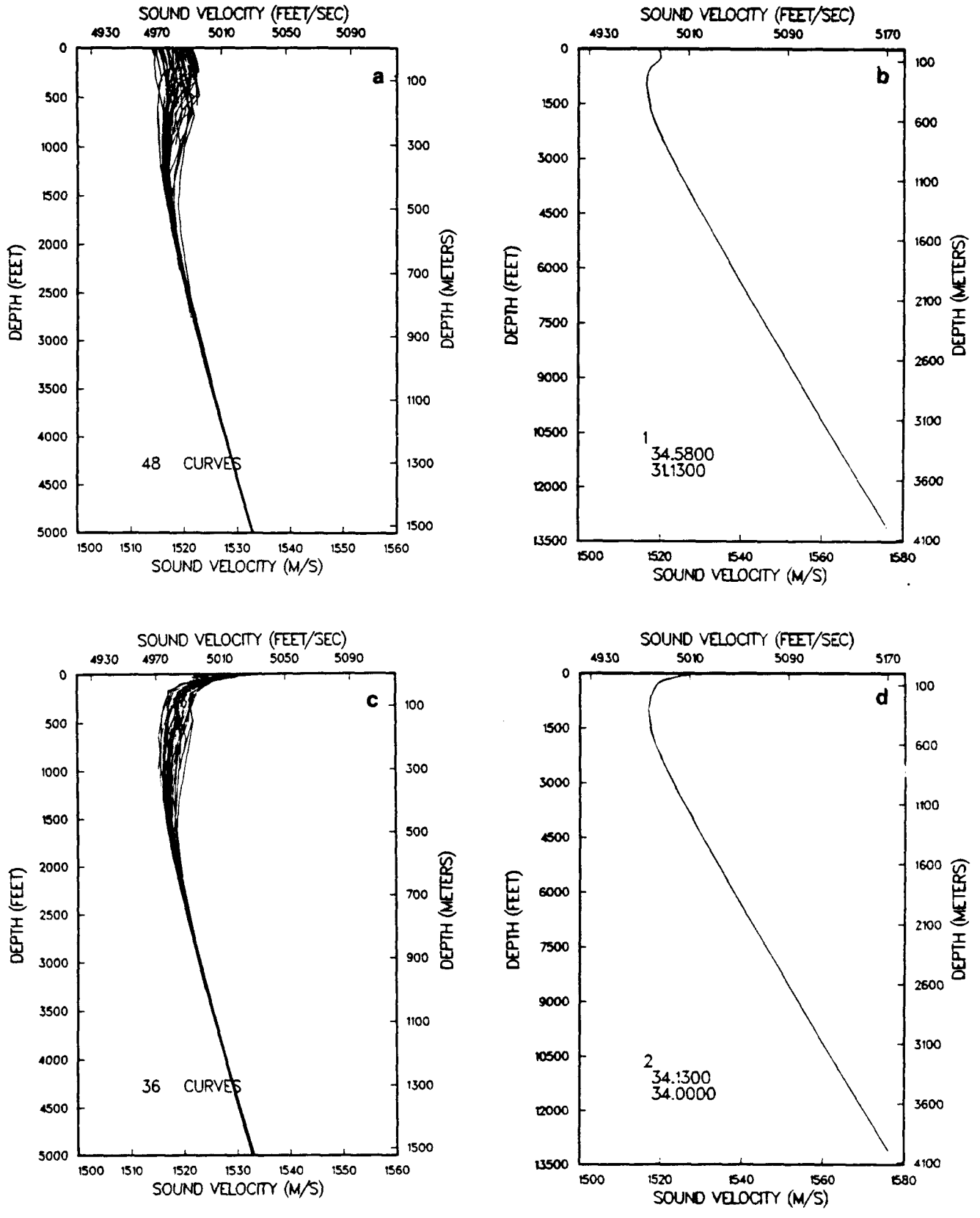

Figure 3.1.1. Levantine Basin: (a) winter profiles (January-March), (b) winter model profile, (c) spring profiles (April-May, (d) spring model profile.

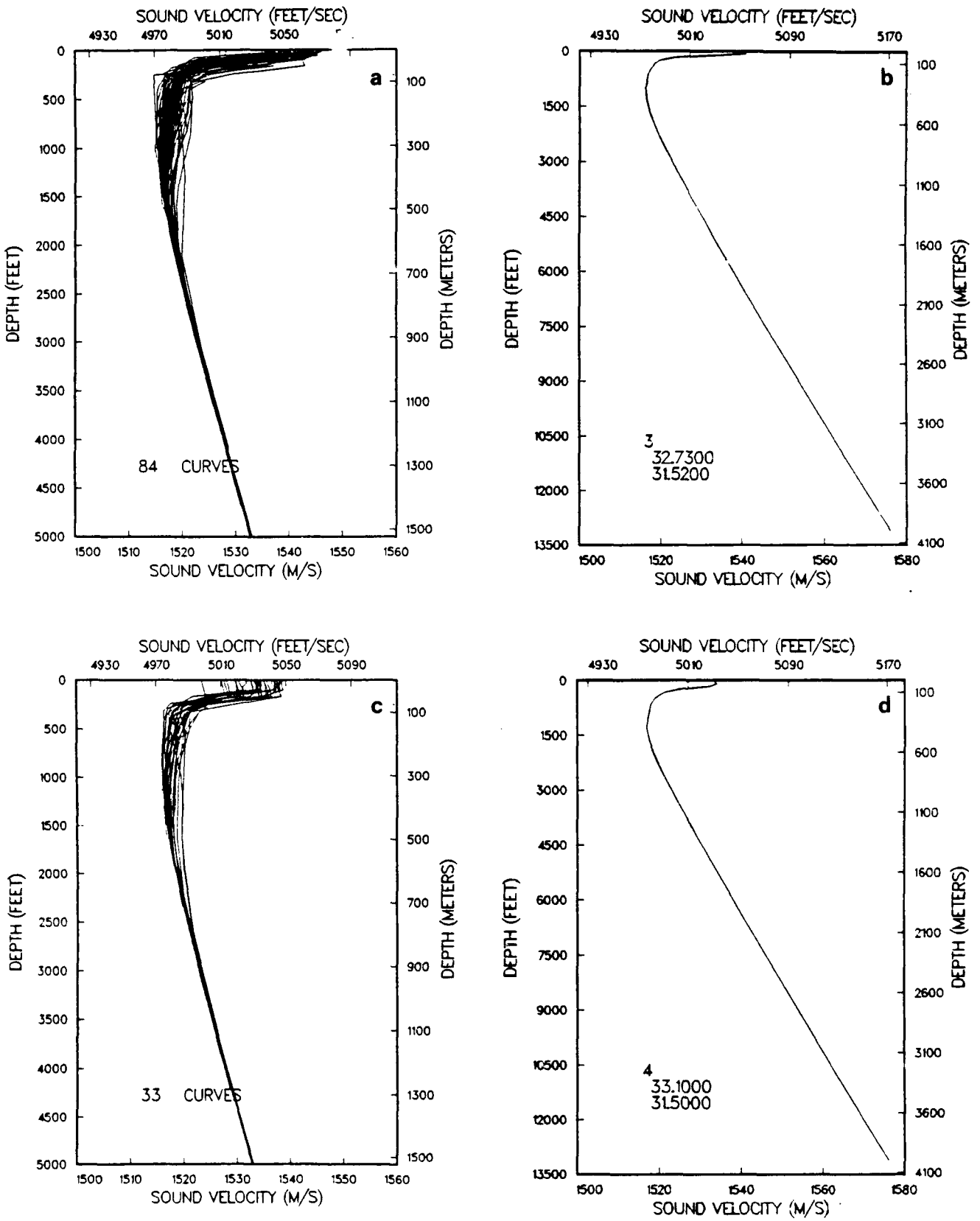

Figure 3.1.2. Levantine Basin:(a) summer profiles (June-October), (b) summer model profile, (c) autumn profiles (November-December), (d) autumn model profile

Table 3.1.1. Levantine Basin winter model profile, envelope values, and variability. Sound speeds for model, mean, minimum, and maximum are given in meters per second.

Depth (m)	Model	Mean	Min.	Max.	Std. Dev.	# of Obs.
0	1519.8	1518.8	1514.1	1521.7	1.9	47
10	1519.6	1518.9	1514.2	1521.9	2.0	47
20	1519.7	1519.0	1514.4	1522.1	2.0	47
30	1519.9	1519.2	1514.6	1522.3	2.1	47
50	1520.0	1519.3	1514.5	1522.6	2.2	47
75	1520.1	1519.5	1514.6	1522.8	2.0	47
100	1519.5	1519.2	1514.8	1522.5	1.8	45
125	1518.6	1519.0	1515.2	1522.7	1.8	45
150	1517.7	1518.7	1515.2	1522.8	2.1	44
200	1516.9	1517.9	1515.0	1521.9	1.8	42
250	1516.7	1517.4	1515.1	1521.2	1.5	42
300	1516.6	1517.1	1515.3	1520.2	1.1	41
400	1517.0	1516.9	1515.8	1519.3	1.3	35
500	1517.5	1517.4	1516.8	1519.0	0.6	35
600	1518.5	1518.4	1518.0	1519.7	0.5	35
700	1519.8	1519.8	1519.3	1520.6	0.6	33
800	1521.2	1521.1	1520.7	1521.6	0.8	31
900	1522.7	1522.7	1522.3	1523.1	0.7	28
1000	1524.2	1524.2	1523.9	1524.6	0.9	27
1100	1525.8	1525.8	1525.5	1526.0	0.9	27
1200	1527.4	1527.4	1527.2	1527.6	0.9	22
1300	1529.1	1529.1	1528.9	1529.2	0.8	20
1400	1530.8	1530.7	1530.5	1530.9	0.5	16
1500	1532.5	1532.4	1532.2	1532.6	0.3	14
1750	1536.7	1536.7	1536.4	1536.8	0.3	11
2000	1540.9	1540.9	1540.8	1541.1	0.0	4
2500	1549.7	1549.7	1549.7	1549.7	0.0	1
3000	1558.3	1558.3	1558.3	1558.3	0.0	1
4000	1576.1	1576.1	1576.1	1576.1	0.0	1

Table 3.1.2. Levantine Basin spring model profile envelope values, and variability. Sound speeds for model, mean, minimum, and maximum are given in meters per second.

Depth (m)	Model	Mean	Min.	Max.	Std. Dev.	# Obs.
0	1526.6	1526.3	1522.1	1537.3	3.0	36
10	1526.7	1525.2	1521.7	1529.9	2.1	36
20	1524.7	1523.8	1521.3	1526.2	0.9	36
30	1523.8	1522.6	1519.4	1525.0	1.6	36
50	1520.9	1520.6	1517.3	1523.1	1.5	36
75	1519.5	1519.5	1516.9	1522.2	1.5	36
100	1518.8	1519.1	1516.3	1521.6	1.5	35
125	1518.4	1518.9	1516.0	1521.6	1.4	35
150	1518.0	1518.6	1515.8	1521.9	1.3	35
200	1517.4	1518.1	1515.3	1521.3	1.3	34
250	1517.2	1517.7	1515.5	1520.8	1.3	34
300	1516.9	1517.3	1515.3	1520.2	1.5	34
400	1517.2	1517.2	1516.2	1519.2	0.3	31
500	1517.7	1517.7	1517.0	1518.8	1.1	31
600	1518.6	1518.6	1518.1	1519.5	0.6	31
700	1519.9	1519.9	1519.5	1520.4	0.7	31
800	1521.3	1521.2	1520.9	1521.5	0.3	30
900	1522.7	1522.7	1522.4	1523.0	0.7	29
1000	1524.2	1524.2	1523.9	1524.5	0.6	26
1100	1525.8	1525.8	1525.7	1526.1	0.8	24
1200	1527.5	1527.5	1527.3	1527.7	0.2	22
1300	1529.1	1529.1	1528.9	1529.3	0.4	19
1400	1530.7	1530.8	1530.6	1531.0	0.3	17
1500	1532.4	1532.4	1532.2	1532.7	0.6	15
1750	1536.6	1536.6	1536.5	1536.8	0.9	12
2000	1540.9	1540.9	1540.8	1541.1	0.5	8
2500	1549.7	1549.7	1549.7	1549.7	0.5	2
3000	1558.3	1558.3	1558.3	1558.3	0.0	1
4000	1576.1	1576.1	1576.1	1576.1	0.0	1

Table 3.1.3. Levantine Basin summer model profile, envelope values, and variability. Sound speeds for model, means, minimum, and maximum are given in meters per second.

Depth (m)	Model	Mean	Min.	Max.	Std Dev.	# Obs.
0	1540.4	1540.9	1528.1	1546.8	3.4	84
10	1540.5	1540.5	1528.2	1545.6	3.0	84
20	1540.7	1537.8	1525.7	1544.4	4.9	84
30	1534.3	1531.5	1521.6	1543.1	6.4	84
50	1523.2	1524.2	1519.1	1543.0	4.5	84
75	1519.6	1520.1	1515.9	1529.4	2.3	82
100	1518.4	1519.0	1514.8	1524.0	1.8	81
125	1517.9	1518.6	1514.9	1521.9	1.5	81
150	1517.3	1518.3	1514.9	1522.1	1.5	81
200	1516.6	1517.9	1515.0	1521.8	1.4	76
250	1516.4	1517.5	1515.2	1521.6	1.4	74
300	1516.1	1517.2	1514.9	1521.0	1.0	74
400	1516.4	1517.0	1515.7	1520.5	0.8	72
500	1517.1	1517.5	1516.6	1520.3	0.6	69
600	1518.2	1518.5	1517.9	1520.1	0.6	66
700	1519.5	1519.8	1519.3	1520.7	0.7	65
800	1520.9	1521.1	1520.7	1521.9	0.0	63
900	1522.5	1522.6	1522.2	1523.1	0.7	59
1000	1524.1	1524.2	1523.8	1524.6	0.0	55
1100	1525.7	1525.8	1525.4	1526.2	0.8	47
1200	1527.3	1527.5	1527.2	1527.9	0.7	42
1300	1529.0	1529.1	1528.8	1529.4	0.8	38
1400	1530.7	1530.7	1530.4	1531.0	0.5	33
1500	1532.3	1532.4	1532.2	1532.7	0.1	30
1750	1536.6	1536.7	1536.6	1536.9	0.4	25
2000	1540.9	1540.9	1540.8	1541.1	0.4	19
2500	1549.6	1549.6	1549.5	1549.7	0.0	3
3000	1558.3	1558.3	1558.3	1558.3	0.0	1
4000	1576.1	1576.1	1576.1	1576.1	0.0	1

Table 3.1.4. Levantine Basin autumn model profile, envelope values, and variability. Sound speeds for model, mean, minimum, and maximum are given in meters per second.

Depth (m)	Model	Mean	Min.	Max.	Std. Dev.	# Obs.
0	1533.4	1533.2	1523.5	1538.9	3.5	32
10	1533.7	1533.3	1523.5	1538.5	3.4	32
20	1533.7	1533.5	1523.8	1538.6	3.4	32
30	1534.0	1533.5	1523.9	1538.8	3.3	32
50	1532.3	1530.9	1521.7	1538.4	4.4	32
75	1524.8	1522.4	1517.5	1529.4	2.4	32
100	1521.3	1519.7	1516.3	1523.0	1.8	31
125	1520.1	1519.1	1516.3	1522.1	1.9	31
150	1519.0	1518.6	1516.2	1521.2	1.0	31
200	1517.9	1518.0	1516.0	1520.3	1.1	30
250	1517.6	1517.6	1515.9	1520.2	1.2	30
300	1517.3	1517.3	1516.0	1520.0	1.1	30
400	1516.9	1517.3	1516.2	1519.9	0.9	29
500	1517.5	1517.7	1516.9	1519.7	0.7	29
600	1518.5	1518.7	1518.3	1520.2	0.7	26
700	1519.8	1519.9	1519.5	1521.0	0.3	25
800	1521.2	1521.3	1521.0	1521.8	0.9	23
900	1522.7	1522.8	1522.5	1523.3	0.3	23
1000	1524.2	1524.3	1524.1	1524.7	0.6	23
1100	1525.8	1525.9	1525.6	1526.2	0.6	23
1200	1527.5	1527.5	1527.2	1527.7	0.7	21
1300	1529.1	1529.2	1528.9	1529.4	0.8	18
1400	1530.8	1530.8	1530.7	1531.0	0.4	17
1500	1532.4	1532.5	1532.3	1532.7	0.7	16
1750	1536.7	1536.7	1536.6	1536.9	0.4	15
2000	1540.9	1541.0	1540.9	1541.4	0.0	12
2500	1549.6	1549.6	1549.5	1549.6	0.5	4
3000	1558.3	1558.3	1558.3	1558.3	0.0	1
4000	1576.1	1576.1	1576.1	1576.1	0.0	1

3.2 Cretan Basin

A MOODS extraction was obtained for each month for an area covering 31.5–35°N, 023–027°E. Profiles were grouped into seasons based on obvious changes observed in sound speed gradients. Seasonal profile groups were edited to remove those with less than five data points, duplicates, and those that did not begin at the surface or extend beyond 50 m in depth. The edited seasonal profiles were interpolated to standard ocean depths and were statistically analyzed to obtain a mean value at each depth. The routine selects the real profile that is closest to the mean and produces a model profile, which is this same profile extended beyond its maximum depth with mean values. Model profiles were visually evaluated to determine if they were representative of their season. Minimum and maximum observed values and the standard deviation at each standard depth are also provided with each model profile.

In the winter (January–March), the Cretan Basin profiles exhibited a weak negative sound speed gradient from the surface to approximately 1000 m with some exceptions (Fig. 3.2.1). This sound speed minimum resulted from the vertical advection of the cooled, high-salinity surface waters during frontal passages with the formation of new Levantine intermediate water. The maximum standard deviation was 3.5 m/sec at a 250-m water depth (Table 3.2.1).

Spring (April and May) was deemed to begin when profiles exhibited a reasonably strong seasonal thermocline resulting from surface warming (Fig. 3.2.1). Only one profile for the months of April and May was available from MOODS (Table 3.2.2). This profile was compared to profiles from the adjacent areas in the Ionian Sea and the Levantine Basin and appears to be a reasonable spring profile.

The summer (June–October) profiles exhibited a strong seasonal thermocline (Fig. 3.2.2). The summer season duration increased toward the southeast section of the Mediterranean Sea. Maximum standard deviation was 6.7 m/sec at 30 m (Table 3.2.3).

The autumn (November and December) profiles were selected based on the formation of a significant surface mixed layer resulting from increasing periods of high winds (Fig. 3.2.2). The maximum standard deviation of 7.1 m/sec at 100 m (Table 3.2.4) was based on only seven profiles. Variability in the intensity and location of the semipermanent eddy in this area also affected the profile distribution in the MOODS data base.

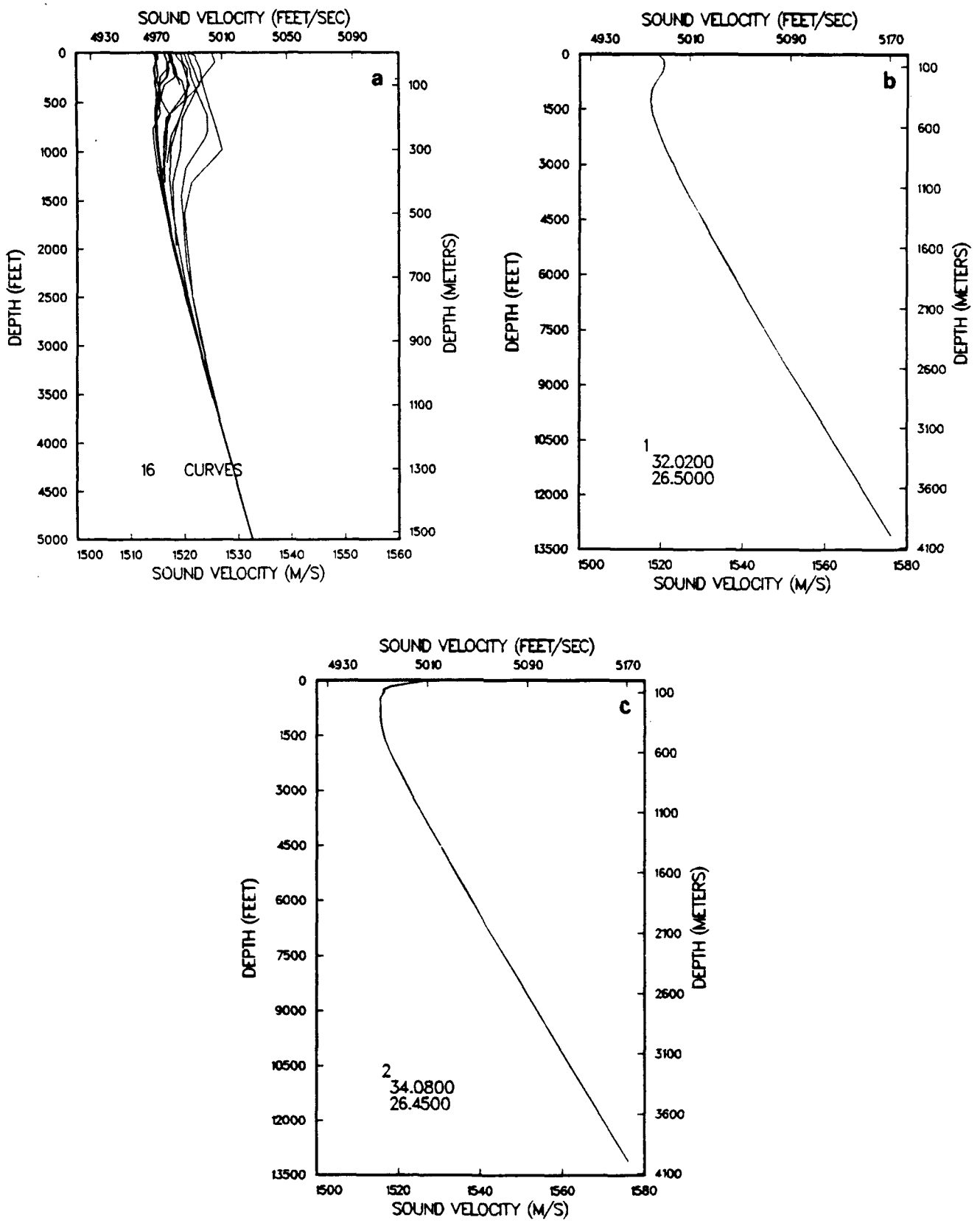

Figure 3.2.1. Cretan Basin: (a) winter profiles (January-March), (b) winter model profile,(c) spring profile and model (April-May)

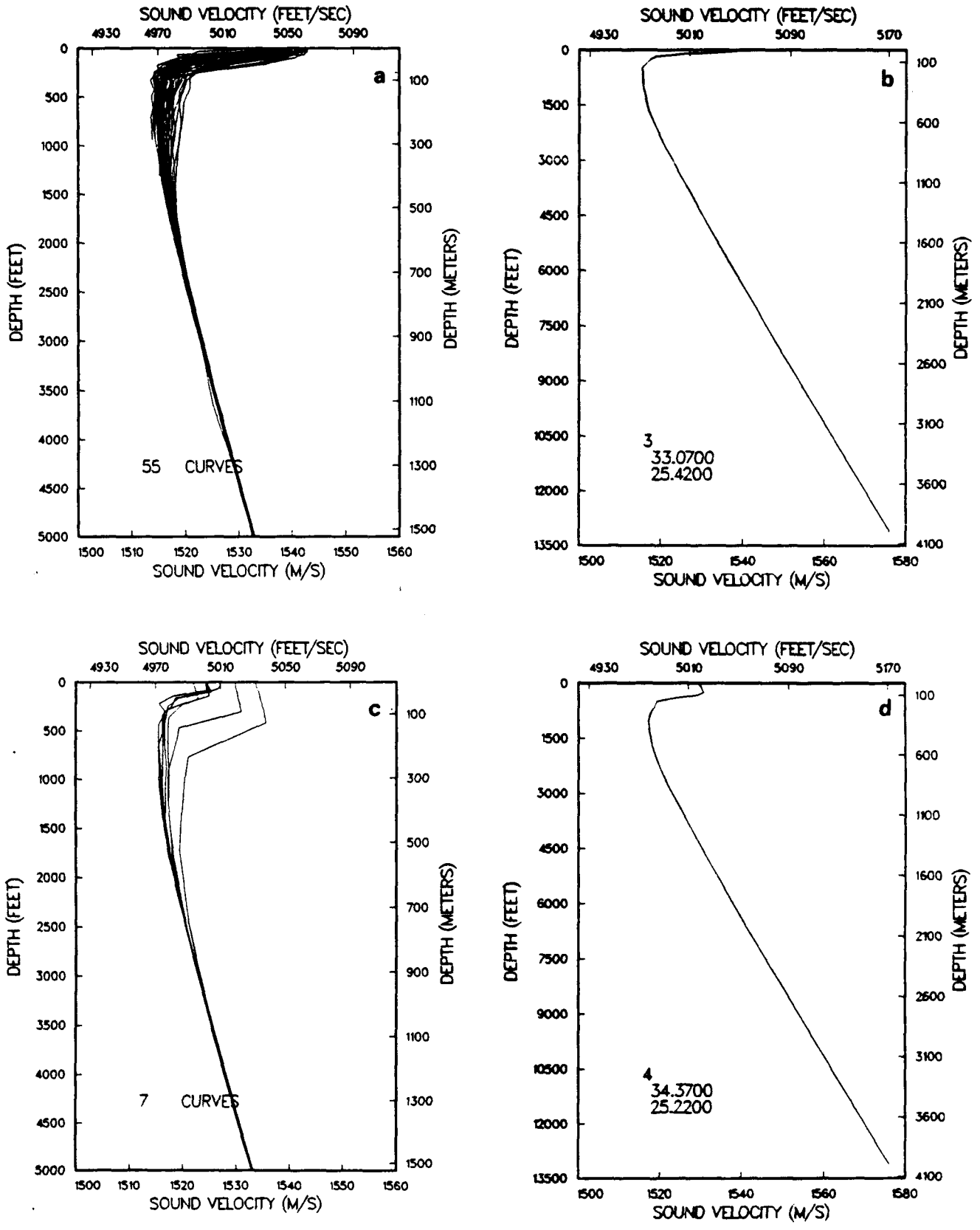

Figure 3.2.2. Cretan Basin: (a) summer profiles (June-October), (b) summer model profile, (c) autumn profiles (November-December), (d) autumn model profile

Table 3.2.1. Cretan Basin winter model profile, envelope values, and variability Sound speeds for model, mean, minimum, and maximum are given in meters per second.

Depth (m)	Model	Mean	Min.	Max.	Std. Dev.	# Obs.
0	1519.2	1518.0	1514.5	1525.3	2.8	15
10	1519.7	1518.3	1514.6	1525.4	2.9	15
20	1519.7	1518.5	1514.8	1525.7	2.9	15
30	1519.9	1518.6	1514.7	1525.8	3.0	15
50	1520.6	1518.8	1514.5	1524.8	3.1	15
75	1520.6	1518.8	1514.7	1523.6	2.9	15
100	1520.7	1518.6	1514.7	1523.6	3.3	14
125	1520.5	1518.5	1514.8	1524.0	3.2	14
150	1520.3	1518.3	1514.8	1524.4	3.2	14
200	1519.3	1517.8	1514.7	1525.4	3.4	14
250	1518.3	1517.5	1514.3	1526.3	3.5	14
300	1517.5	1517.3	1514.6	1527.0	3.4	14
400	1517.3	1516.9	1515.4	1521.3	1.8	13
500	1517.9	1517.5	1516.6	1519.9	1.0	12
600	1518.9	1518.5	1517.8	1520.5	1.0	11
700	1520.0	1519.8	1519.2	1521.1	0.9	9
800	1521.2	1521.2	1520.7	1522.0	0.2	9
900	1522.7	1522.7	1522.3	1523.3	0.5	7
1000	1524.2	1524.2	1523.9	1524.5	0.0	6
1100	1525.7	1525.7	1525.6	1525.9	0.0	4
1200	1527.3	1527.3	1527.2	1527.4	0.3	3
1300	1529.0	1529.0	1528.9	1529.0	0.3	3
1400	1530.6	1530.6	1530.5	1530.7	0.5	3
1500	1532.2	1532.2	1532.1	1532.3	0.3	3
1750	1536.4	1536.4	1536.4	1536.5	0.0	2
2000	1540.6	1540.6	1540.6	1540.6	0.0	2
2500	1549.1	1549.1	1549.1	1549.1	0.0	1
3000	1558.3	1558.3	1558.3	1558.3	0.0	1
4000	1576.1	1576.1	1576.1	1576.1	0.0	1

Table 3.2.2. Cretan Basin spring model profile (envelope values and variability are not available because only one profile was available for this area and season). Sound speeds for model, mean, minimum, and maximum are given in meters per second.

Depth (m)	Model	Mean	Min.	Max.	Std. Dev.	# Obs.
0	1526.3	1526.3	1526.3	1526.3	0	1
10	1525.3	1525.3	1525.3	1525.3	0	1
20	1524.2	1524.2	1524.2	1524.2	0	1
30	1522.0	1522.0	1522.0	1522.0	0	1
50	1518.0	1518.0	1518.0	1518.0	0	1
75	1516.3	1516.3	1516.3	1516.3	0	1
100	1516.3	1516.3	1516.3	1516.3	0	1
125	1515.9	1515.9	1515.9	1515.9	0	1
150	1515.4	1515.4	1515.4	1515.4	0	1
200	1515.5	1515.5	1515.5	1515.5	0	1
250	1515.4	1515.4	1515.4	1515.4	0	1
300	1515.4	1515.4	1515.4	1515.4	0	1
400	1515.8	1515.8	1515.8	1515.8	0	1
500	1516.7	1516.7	1516.7	1516.7	0	1
600	1517.9	1517.9	1517.9	1517.9	0	1
700	1519.4	1519.4	1519.4	1519.4	0	1
800	1520.9	1520.9	1520.9	1520.9	0	1
900	1522.4	1522.4	1522.4	1522.4	0	1
1000	1523.9	1523.9	1523.9	1523.9	0	1
1100	1525.6	1525.6	1525.6	1525.6	0	1
1200	1527.2	1527.2	1527.2	1527.2	0	1
1300	1528.9	1528.9	1528.9	1528.9	0	1
1400	1530.6	1530.6	1530.6	1530.6	0	1
1500	1532.3	1532.3	1532.3	1532.3	0	1
1750	1536.5	1536.5	1536.5	1536.5	0	1
2000	1540.8	1540.8	1540.8	1540.8	0	1
2500	1549.6	1549.6	1549.6	1549.6	0	1
3000	1558.3	1558.3	1558.3	1558.3	0	1
4000	1576.1	1576.1	1576.1	1576.1	0	1

Table 3.2.3. Cretan Basin summer model profile, envelope values, and variability. Sound speeds for model, mean, minimum, and maximum are given in meters per second.

Depth (m)	Model	Mean	Min.	Max.	Std. Dev.	# Obs.
0	1540.5	1538.9	1532.0	1545.3	3.1	55
10	1537.1	1537.6	1522.4	1542.9	4.1	55
20	1535.2	1533.2	1518.4	1542.2	6.1	55
30	1526.2	1528.1	1518.7	1540.6	6.7	55
50	1519.1	1520.9	1515.2	1534.9	4.3	55
75	1517.7	1517.7	1514.2	1522.6	2.2	55
100	1516.9	1516.7	1513.5	1520.9	1.4	55
125	1516.3	1516.4	1514.0	1520.8	1.9	55
150	1515.6	1516.2	1513.7	1520.2	1.3	55
200	1515.7	1516.0	1513.8	1519.6	1.6	55
250	1515.7	1515.9	1513.7	1519.2	0.5	52
300	1515.8	1515.9	1514.5	1518.8	1.2	51
400	1516.4	1516.3	1515.1	1518.2	0.9	51
500	1517.1	1517.1	1516.4	1518.2	0.9	46
600	1518.3	1518.3	1517.8	1519.1	0.1	45
700	1519.7	1519.6	1519.2	1520.1	0.8	45
800	1521.1	1521.1	1520.7	1521.5	0.8	45
900	1522.7	1522.6	1522.3	1523.0	0.8	45
1000	1524.2	1524.2	1523.7	1524.6	0.6	43
1100	1525.8	1525.8	1525.0	1526.0	0.7	39
1200	1527.5	1527.4	1526.8	1527.7	1.1	36
1300	1529.1	1529.1	1528.8	1529.3	0.7	30
1400	1530.7	1530.8	1530.4	1531.0	0.3	28
1500	1532.3	1532.4	1532.2	1532.6	0.7	23
1750	1536.5	1536.6	1536.4	1536.7	0.5	17
2000	1540.9	1540.9	1540.7	1541.1	0.7	9
2500	1549.4	1549.4	1549.4	1549.5	0.3	5
3000	1558.3	1558.3	1558.3	1558.3	0	1
4000	1576.1	1576.1	1576.1	1576.1	0	1

Table 3.2.4. Cretan Basin autumn model profile, envelope values, and variability. Sound speeds for model, mean, minimum, and maximum are given in meters per second.

Depth (m)	Model	Mean	Min.	Max.	Std. Dev.	# Obs.
0	1529.8	1526.5	1522.0	1533.6	3.7	7
10	1529.9	1526.6	1522.2	1533.8	3.6	7
20	1529.9	1526.7	1522.4	1533.9	3.7	7
30	1530.2	1526.5	1522.6	1534.2	3.9	7
50	1530.4	1523.8	1517.4	1534.5	5.9	7
75	1530.8	1522.2	1516.0	1534.9	6.9	7
100	1529.2	1521.3	1516.4	1535.3	7.1	7
125	1523.5	1520.2	1515.7	1535.5	6.7	7
150	1519.3	1519.1	1515.5	1532.3	5.6	7
200	1518.6	1517.9	1515.5	1525.7	3.3	7
250	1517.8	1517.2	1515.5	1521.0	1.7	7
300	1517.3	1517.1	1515.5	1520.5	1.5	7
400	1517.4	1517.2	1516.1	1519.9	1.3	7
500	1518.0	1517.7	1517.0	1519.5	0.9	7
600	1518.9	1518.7	1518.2	1520.0	0.9	7
700	1520.0	1519.9	1519.6	1520.8	0.5	7
800	1521.3	1521.3	1521.1	1521.8	0.6	6
900	1522.8	1522.9	1522.7	1523.1	0.3	6
1000	1524.4	1524.4	1524.2	1524.6	0.6	6
1100	1526.0	1526.0	1525.8	1526.2	0.0	6
1200	1527.6	1527.6	1527.5	1527.9	0.3	6
1300	1529.2	1529.2	1529.2	1529.5	0.4	6
1400	1530.8	1530.9	1530.8	1531.1	0.3	6
1500	1532.5	1532.5	1532.4	1532.7	0.4	6
1750	1536.7	1536.7	1536.6	1536.9	0.2	5
2000	1540.9	1540.9	1540.8	1541.0	0.4	5
2500	1549.6	1549.6	1549.6	1549.6	0.0	1
3000	1558.3	1558.3	1558.3	1558.3	0	1
4000	1576.1	1576.1	1576.1	1576.1	0	1

3.3 Ionian Sea

A MOODS extraction was obtained for each month for an area covering 32.5–37.5 °N, 015–022.5 °E. The extraction was divided into northern and southern halves with 35 °N selected as the dividing limit. Profiles were grouped into seasons based on obvious changes observed in sound speed gradients. Seasonal profile groups were edited to remove those with less than five data points, duplicates, and those that did not begin at the surface or extend beyond 50 min depth. Because there was no significant variation between the northern and southern profiles, they were combined into one area. The edited seasonal profiles were interpolated to standard ocean depths and were statistically analyzed to obtain a mean value at each depth. The routine selects the real profile that is closest to the mean and produces a model profile, which is this same profile extended beyond its maximum depth with mean values. Model profiles were visually evaluated to determine if they were representative of their season. Minimum and maximum observed values and the standard deviation at each standard depth are also provided with each model profile.

In the winter (December–April), Ionian Sea profiles exhibited a positive sound speed gradient from the surface to the bottom with some exceptions (Fig. 3.3.1). The maximum standard deviation was only 3.0 m/sec at a 30-m water depth (Table 1).

Spring (May and June) was deemed to begin when profiles exhibited a reasonably strong seasonal thermocline resulting from surface warming (Fig. 3.3.1). The maximum standard deviation was 4.2 m/sec at a 20-m water depth (Table 3.3.2).

The summer (July–September) profiles were similar to the spring profiles in exhibiting a strong seasonal thermocline. The difference was that surface sound speeds typically exceeded spring seasonal values by approximately 15 m/sec (Fig. 3.3.2). The maximum standard deviation was 7 m/sec at a 30-m depth (Table 3.3.3). This increased variation at this depth was due to the spatial variability in the influx of Atlantic water combined with the reduced vertical mixing over the Ionian during the summer months when wind speeds are low.

The autumn (October and November) profiles were selected based on the formation of a significant surface mixed layer that results from increasing periods of high winds, which is the beginning of the formation process for Levantine intermediate water (Fig. 3.3.2). The maximum standard deviation was 5.5 m/sec, the bottom of this mixed layer (Table 3.3.4). Profiles still exhibited a reduced seasonal thermocline.

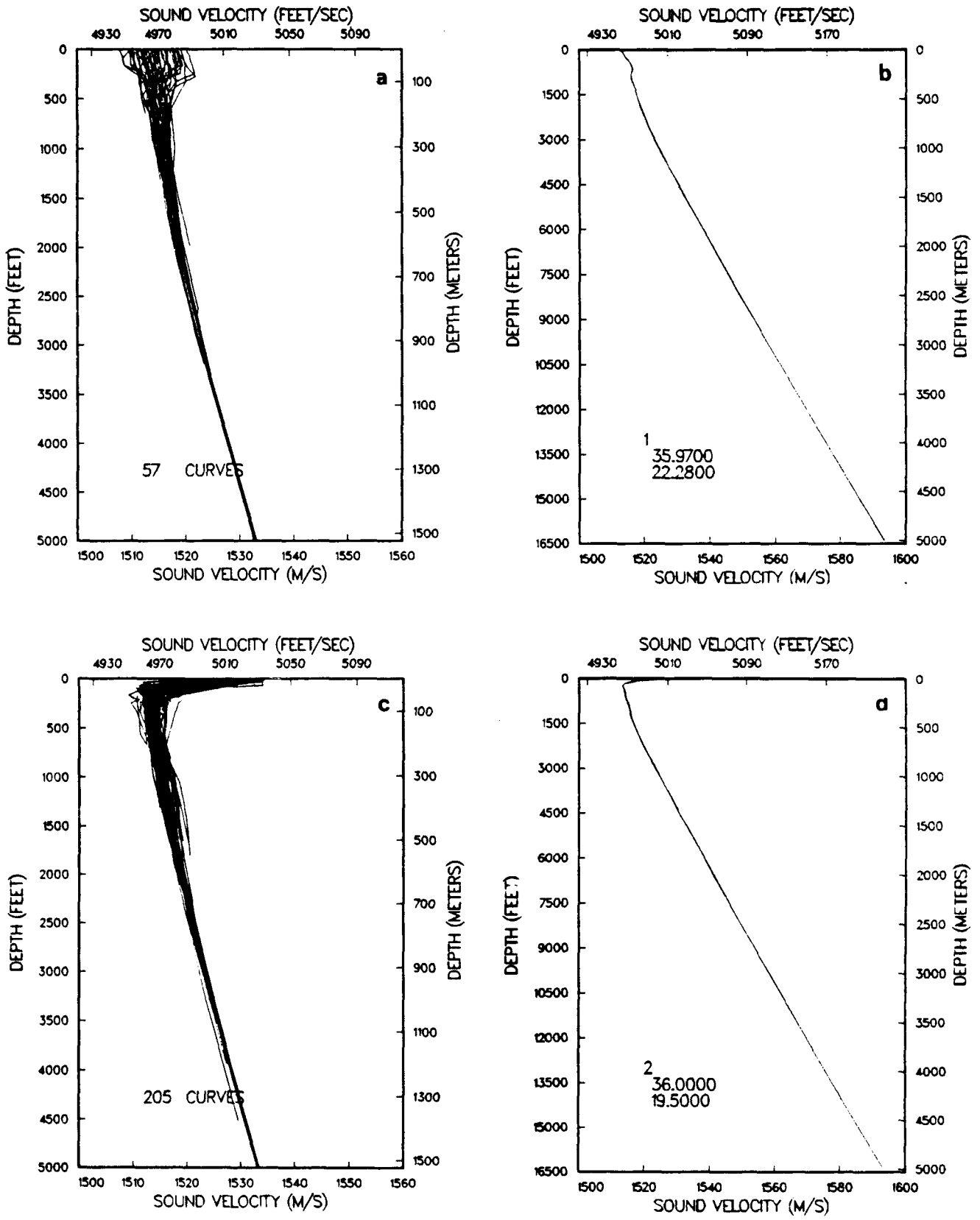

Figure 3.3.1. Ionian Sea: (a) winter profiles (December-April), (b) winter model profile,(c) spring profiles (May-June), (d) spring model profile

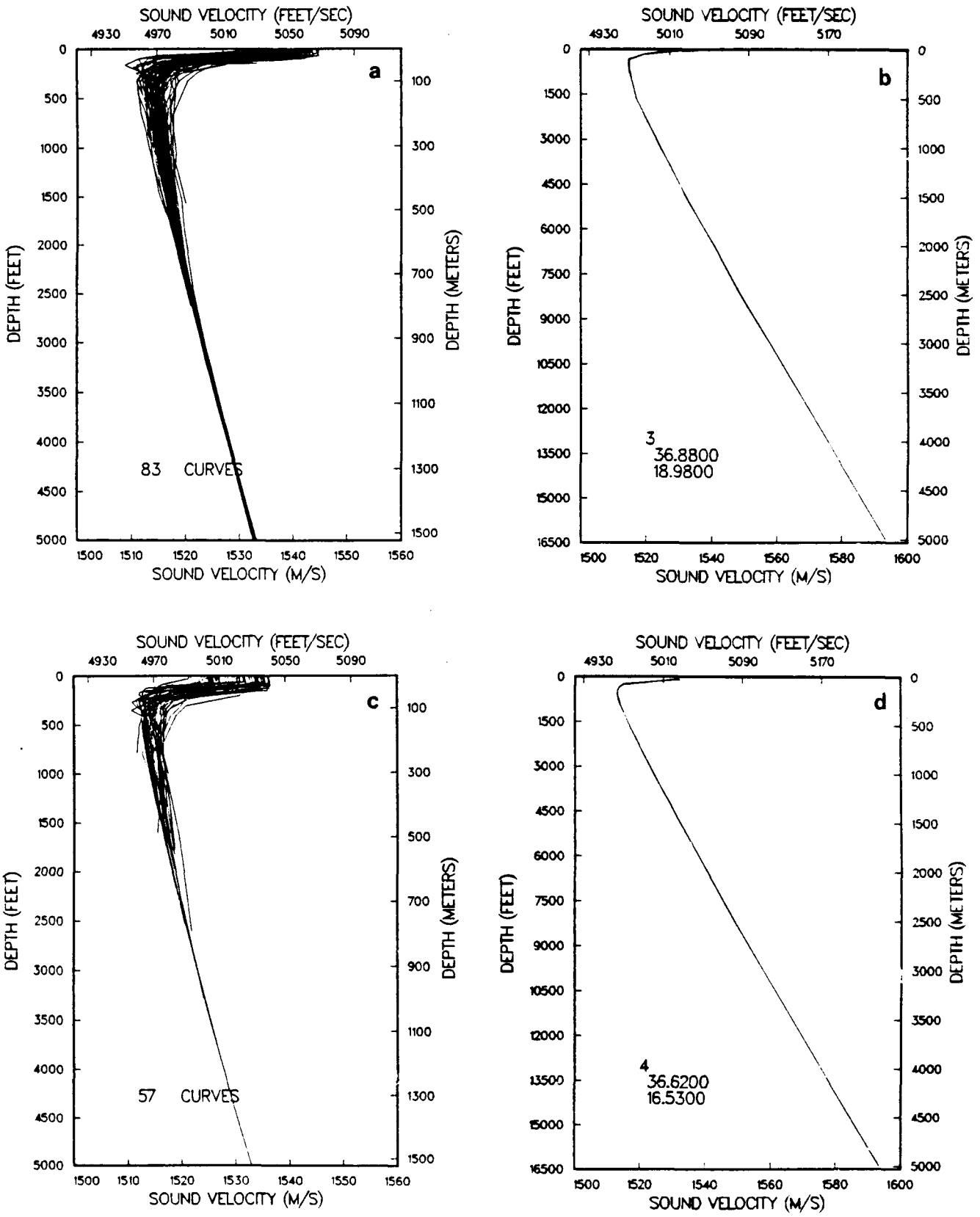

Figure 3.3.2. Ionian Sea: (a) summer profiles (July-September), b) summer model profile, (c) autumn profiles (October-November), (d) autumn model profile

Table 3.3.1. Ionian Sea winter model profile, envelope values, and variability. Sound speeds for model, mean, minimum, and maximum are given in meters per second.

Depth (m)	Model	Mean	Min.	Max.	Std. Dev.	# Obs.
0	1513.7	1513.9	1507.8	1520.2	2.8	57
10	1513.6	1514.0	1508.0	1520.4	2.8	57
20	1513.2	1514.1	1508.3	1520.8	3.0	57
30	1513.4	1514.1	1508.3	1520.9	3.0	57
50	1513.8	1514.4	1508.7	1521.3	3.0	57
75	1514.3	1514.6	1510.6	1521.7	2.6	57
100	1514.9	1514.5	1511.4	1520.1	1.9	54
125	1515.5	1514.6	1511.7	1519.2	1.4	53
150	1516.0	1514.7	1511.8	1518.4	1.4	53
200	1516.4	1515.2	1513.2	1517.4	1.4	51
250	1515.9	1515.5	1513.6	1517.7	0.6	48
300	1516.0	1515.9	1514.2	1518.0	0	47
400	1517.2	1516.7	1515.3	1518.0	0.9	42
500	1518.1	1517.7	1516.5	1519.3	0.4	37
600	1519.1	1518.8	1517.7	1520.8	0.4	23
700	1520.3	1520.0	1519.1	1521.0	0.5	22
800	1521.5	1521.3	1520.7	1522.3	0.2	22
900	1522.9	1522.8	1522.2	1523.2	0.6	17
1000	1524.4	1524.4	1524.0	1524.5	0.8	15
1100	1526.0	1525.9	1525.6	1526.2	0.7	15
1200	1527.6	1527.5	1527.3	1527.8	0.4	15
1300	1529.2	1529.2	1528.9	1529.5	0.7	15
1400	1530.9	1530.8	1530.5	1531.1	0.6	15
1500	1532.5	1532.5	1532.2	1532.7	0.5	15
1750	1536.6	1536.6	1536.4	1536.9	0.6	14
2000	1540.8	1540.7	1540.5	1540.8	0.8	12
2500	1549.2	1549.2	1549.1	1549.2	0.4	12
3000	1557.9	1557.8	1557.8	1557.9	0	10
4000	1575.7	1575.7	1575.7	1575.7	0	1
5000	1593.5	1593.5	1593.5	1593.5	0	1

Table 3.3.2. Ionian Sea spring model profile, envelope values, and variability. Sound speeds for model, mean, minimum, and maximum are given in meters per second.

Depth (m)	Model	Mean	Min.	Max.	Std. Dev.	# Obs.
0	1527.4	1525.5	1515.7	1534.9	3.3	153
10	1523.6	1524.2	1511.8	1534.0	3.8	153
20	1518.2	1519.6	1511.0	1534.1	4.2	153
30	1516.4	1516.5	1510.4	1525.4	3.1	153
50	1513.9	1514.0	1509.0	1520.2	2.1	153
75	1513.3	1513.4	1509.4	1518.2	0.5	152
100	1513.7	1513.4	1510.5	1517.8	0.6	147
125	1513.9	1513.7	1511.1	1517.4	1.4	145
150	1514.0	1514.0	1511.2	1517.0	0.7	145
200	1514.3	1514.5	1512.3	1516.1	0.7	142
250	1514.9	1514.9	1513.2	1516.7	1.4	138
300	1515.3	1515.5	1513.6	1518.0	0.2	134
400	1516.1	1516.4	1514.8	1519.4	1.1	124
500	1517.3	1517.4	1516.3	1520.2	0.2	68
600	1518.6	1518.6	1517.8	1519.9	0.6	37
700	1519.9	1520.0	1519.2	1521.0	0.8	37
800	1521.5	1521.5	1520.6	1522.2	0.9	37
900	1523.1	1523.0	1522.1	1523.6	1.1	34
1000	1524.7	1524.6	1523.5	1525.1	0.4	34
1100	1526.3	1526.2	1525.1	1526.6	0.4	30
1200	1527.9	1527.9	1526.7	1528.1	0.2	30
1300	1529.5	1529.5	1528.3	1529.8	0.7	28
1400	1531.2	1531.2	1530.9	1531.4	0.4	27
1500	1532.9	1532.9	1532.7	1533.1	0.7	27
1750	1537.0	1537.0	1536.9	1537.3	0.8	27
2000	1541.2	1541.2	1541.0	1541.4	0.4	25
2500	1549.7	1549.7	1549.5	1550.0	0.2	22
3000	1558.4	1558.4	1558.1	1558.7	0.8	15
4000	1575.7	1575.7	1575.7	1575.7	0	1
5000	1593.4	1593.4	1593.4	1593.4	0	1

Table 3.3.3. Ionian Sea Summer Model Profile, Envelope Values and Variability. Sound speeds for model, mean, minimum, and maximum are given in meters per second.

Depth (m)	Mode	Mean	Min.	Max.	Std. Dev.	# Obs.
0	1539.9	1539.5	1531.3	1544.8	2.5	82
10	1534.1	1538.3	1527.7	1544.9	3.9	82
20	1528.3	1533.9	1515.2	1544.9	6.9	82
30	1524.2	1526.8	1511.4	1542.1	7.0	82
50	1519.2	1518.2	1508.9	1527.5	3.6	82
75	1517.0	1515.4	1510.9	1522.2	2.1	82
100	1514.8	1514.7	1511.0	1520.5	2.0	78
125	1514.8	1514.6	1511.2	1519.9	1.7	78
150	1514.8	1514.6	1511.5	1519.2	1.5	78
200	1514.8	1515.0	1511.8	1517.9	1.3	76
250	1515.2	1515.3	1512.7	1517.9	1.0	75
300	1515.5	1515.7	1513.2	1518.2	1.1	73
400	1516.3	1516.6	1514.6	1518.9	0.6	70
500	1517.0	1517.5	1516.2	1519.5	0.3	59
600	1518.5	1518.7	1517.9	1520.2	0.5	38
700	1519.9	1520.0	1519.4	1521.1	0.4	36
800	1521.4	1521.4	1520.9	1522.1	0.4	36
900	1522.9	1522.9	1522.6	1523.4	0.2	34
1000	1524.3	1524.4	1524.1	1524.9	0.8	33
1100	1525.9	1526.0	1525.7	1526.4	0.7	26
1200	1527.5	1527.6	1527.4	1528.0	1.1	26
1300	1529.0	1529.2	1529.0	1529.6	0.4	26
1400	1530.6	1530.9	1530.6	1531.2	0.7	26
1500	1532.1	1532.5	1532.1	1532.9	0.8	24
1750	1536.4	1536.6	1535.5	1537.0	0.3	23
2000	1540.7	1540.9	1540.5	1541.2	0.7	18
2500	1549.0	1549.3	1549.0	1549.5	0.5	14
3000	1558.0	1558.0	1557.8	1558.1	0.3	6
4000	1575.7	1575.7	1575.7	1575.7	0	1
5000	1593.4	1593.4	1593.4	1593.4	0	1

Table 3.3.4. Ionian Sea Autumn Model Profile, Envelope Values and Variability. Sound speeds for model, mean, minimum, and maximum are given in meters per second.

Depth (m)	Model	Mean	Min.	Max.	Std. Dev.	# Obs.
0	1530.2	1529.7	1521.4	1536.2	4.4	55
10	1530.9	1529.8	1521.1	1536.3	4.2	55
20	1531.0	1529.9	1518.4	1536.4	4.3	55
30	1531.8	1528.7	1516.0	1536.5	5.1	55
50	1524.3	1521.6	1512.3	1533.0	5.5	55
75	1514.8	1516.0	1511.6	1526.7	2.7	54
100	1513.8	1514.8	1511.5	1520.4	2.0	48
125	1513.2	1514.5	1512.5	1519.0	1.6	48
150	1512.9	1514.6	1512.2	1518.3	1.2	44
200	1513.2	1514.7	1511.8	1516.9	1.0	43
250	1513.6	1515.0	1512.8	1516.7	1.2	37
300	1514.1	1515.5	1514.0	1517.5	0.9	35
400	1515.5	1516.4	1515.2	1518.4	1.0	31
500	1516.8	1517.4	1516.6	1519.6	0.5	25
600	1518.3	1518.6	1518.0	1520.3	0.8	6
700	1519.8	1520.0	1519.5	1521.1	0.2	5
800	1521.2	1521.3	1521.1	1521.4	0	3
900	1522.8	1522.7	1522.7	1522.8	0.4	3
1000	1524.3	1524.2	1524.1	1524.3	0	3
1100	1525.9	1525.9	1525.8	1525.9	0	2
1200	1527.5	1527.5	1527.5	1527.5	0	2
1300	1529.2	1529.1	1529.1	1529.2	0.5	2
1400	1530.8	1530.8	1530.8	1530.8	0.5	2
1500	1532.5	1532.5	1532.5	1532.5	0	1
1750	1536.6	1536.6	1536.6	1536.6	0	1
2000	1540.8	1540.8	1540.8	1540.8	0	1
2500	1549.2	1549.2	1549.2	1549.2	0	1
3000	1557.9	1557.9	1557.9	1557.9	0	1
4000	1575.7	1575.7	1575.7	1575.7	0	1
5000	1593.5	1593.5	1593.5	1593.5	0	1

3.4 Strait of Sicily

A MOODS extraction was obtained for each month for the area covering 36.5–3824°N, 010–013°E. Although studies in the strait have shown that Atlantic water enters the strait from the western Mediterranean along its southern portion, the area is extremely variable over time. The result is that this difference is not apparent from profiles in the MOODS data base. The variability from year to year results in an averaging process that makes the inflow along the southern part indistinguishable; therefore, the entire strait area is presented with only one typical profile per season. Profiles were grouped into seasons based on obvious changes observed in sound speed gradients. Seasonal profile groups were edited to remove those with less than five data points, duplicates, and those that did not begin at the surface or extend beyond 50 m in depth. The edited seasonal profiles were interpolated to standard ocean depths and were statistically analyzed to obtain a mean value at each depth. The routine selects the real profile that is closest to the mean and produces a model profile, which is this same profile extended beyond its maximum depth with mean values. Model profiles were visually evaluated to determine if they were representative of their season. Minimum and maximum observed values and the standard deviation at each standard depth are also provided with each model profile.

In the winter (December–April), the strait of Sicily profiles exhibited a positive sound speed gradient from the surface to the bottom with some exceptions (Fig. 3.4.1). The maximum standard deviation was 2.8 m/sec at a 20- to 50-m water depth (Table 3.4.1).

Spring (May and June) was deemed to begin when the profiles exhibited a reasonably strong seasonal thermocline resulting from surface warming (Fig. 3.4.1). The sound channel at 100 m results from Atlantic water overlying the Levantine intermediate waters. The maximum standard deviation was 3.5 m/sec at the surface (Table 3.4.2).

The summer (July–September) profiles were similar to the spring profiles in exhibiting a strong seasonal thermocline. The difference was that surface sound speeds typically exceeded spring seasonal values by approximately 15 m/sec (Fig. 3.4.2). The maximum standard deviation was 5.1 m/sec at 30 m (Table 3.4.3).

The autumn (October and November) profiles were selected based on the formation of a significant surface mixed layer resulting from increasing periods of high winds (Fig. 3.4.2). The maximum standard deviation was 5.9 m/sec at 50 m but remained close to this value from the surface down to the bottom of this mixed layer at 75 m (Table 3.4.4). Profiles still exhibited a reduced seasonal thermocline.

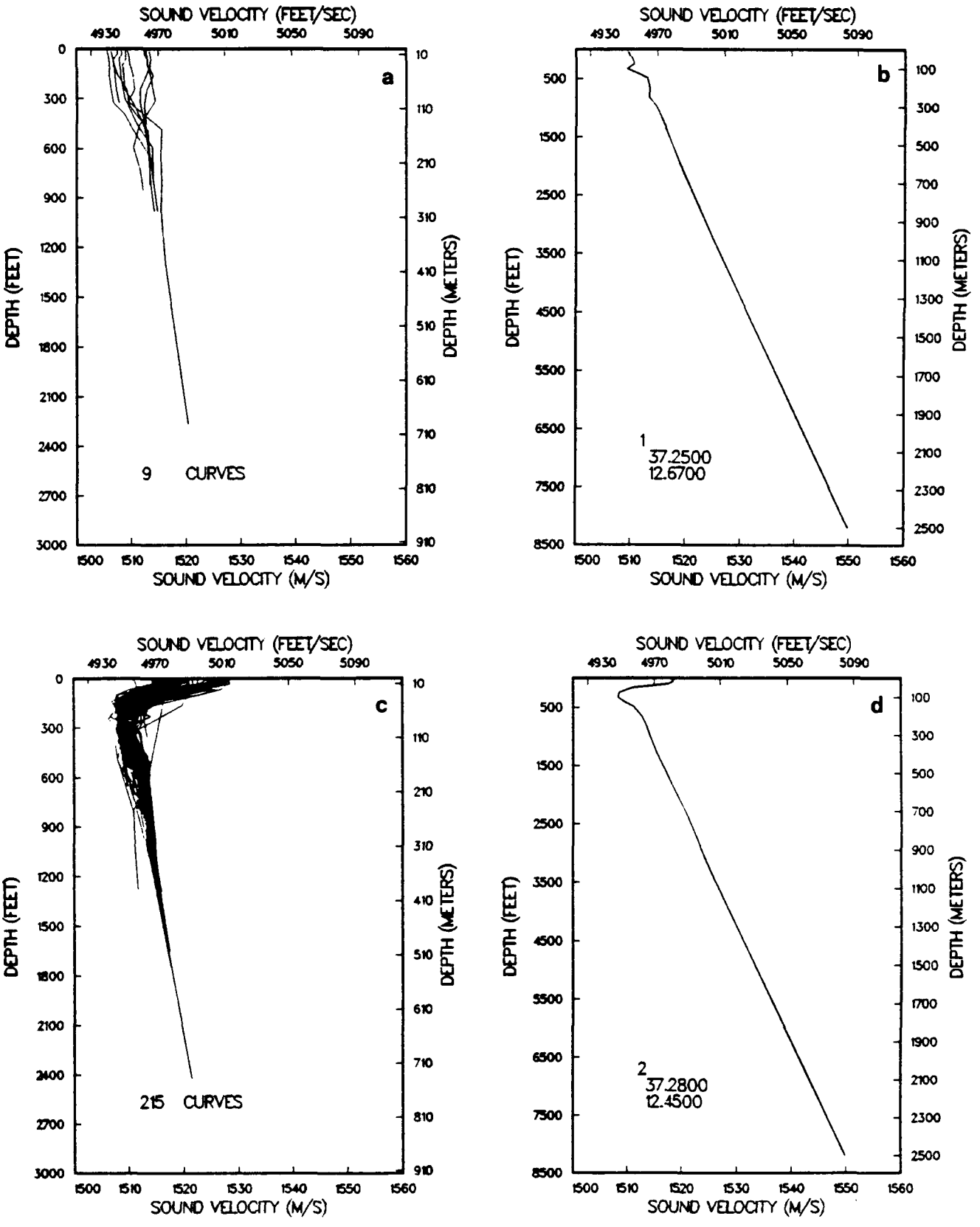

Figure 3.4.1. Strait of Sicily: (a) winter profiles (December-April), (b) winter model profile, (c) spring profiles (May-June), (d) spring model profile

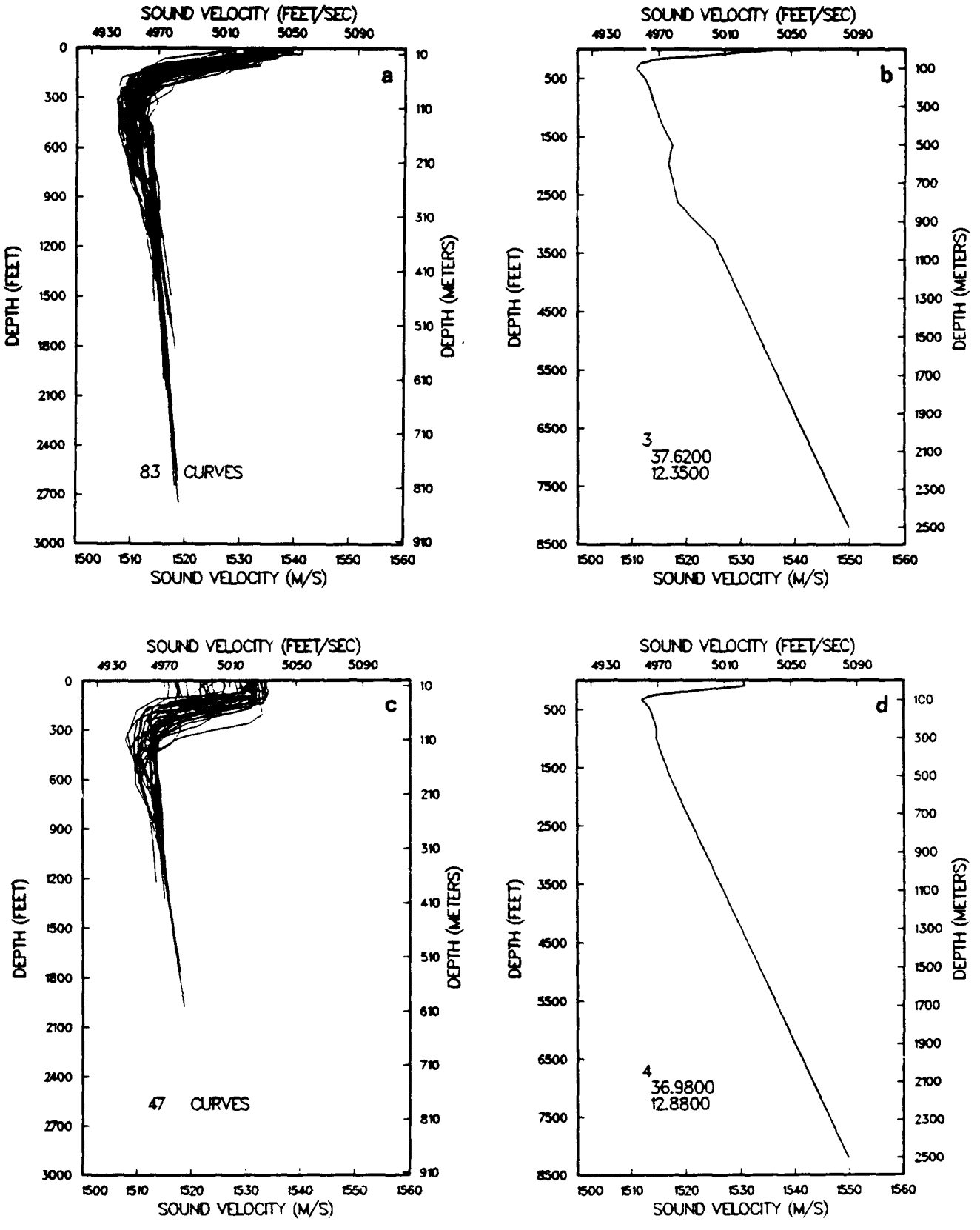

Figure 3.4.2. Straits of Sicily: (a) summer profiles (July-September), (b) summer model profile, (c) autumn profiles (October-November),(d)autumn model profile

Table 3.4.1. Strait of Sicily winter model profile, envelope values, and variability. Sound speeds for model, means, minimum, and maximum are given in meters per second.

Depth (m)	Model	Mean	Min.	Max.	Std. Dev.	# Obs.
0	1509.2	1509.3	1505.6	1513.2	2.7	9
10	1509.5	1509.5	1505.7	1513.5	2.7	9
20	1509.7	1509.5	1505.9	1513.6	2.8	9
30	1509.8	1509.5	1506.0	1513.4	2.8	9
50	1510.3	1509.7	1505.9	1513.9	2.8	9
75	1510.6	1509.9	1506.3	1513.9	2.4	9
100	1509.3	1510.1	1506.7	1514.0	2.1	9
125	1511.2	1511.5	1509.0	1512.7	1.1	8
150	1513.0	1512.5	1510.4	1515.5	1.4	8
200	1513.4	1513.4	1511.0	1515.4	1.2	7
250	1513.3	1513.7	1512.0	1515.5	1.1	5
300	1514.7	1514.7	1514.1	1515.4	0.4	3
400	1516.2	1516.2	1516.2	1516.2	0	1
500	1517.6	1517.6	1517.6	1517.6	0	1
600	1519.0	1519.0	1519.0	1519.0	0	1
1000	1525.1	1525.1	1525.1	1525.1	0	1
1500	1533.3	1533.3	1533.3	1533.3	0	1
2000	1541.6	1541.6	1541.6	1541.6	0	1
2500	1549.9	1549.9	1549.9	1549.9	0	1

Table 3.4.2. Strait of Sicily spring model profile, envelope values, and variability. Sound speeds for model, mean, minimum, and maximum are given in meters per second.

Depth (m)	Model	Mean	Min.	Max.	Std. Dev.	# Obs.
0	1519.4	1519.1	1510.9	1528.4	3.5	209
10	1518.3	1518.6	1511.3	1528.4	2.8	209
20	1518.3	1516.9	1510.5	1525.7	2.7	209
30	1517.5	1514.2	1507.9	1522.7	2.0	209
50	1510.8	1510.0	1507.0	1519.7	2.0	209
75	1508.5	1509.0	1506.4	1515.7	1.4	196
100	1508.3	1509.2	1507.8	1515.2	1.6	155
125	1509.2	1509.9	1507.6	1514.7	0.8	147
150	1511.2	1511.1	1507.9	1514.2	0.9	142
200	1512.6	1512.8	1509.5	1513.8	0.5	136
250	1513.5	1513.5	1510.9	1514.3	0.8	109
300	1514.1	1514.0	1511.0	1514.7	0.7	81
400	1515.5	1515.6	1515.1	1515.9	0.8	34
500	1517.2	1517.2	1517.0	1517.3	0	8
600	1518.9	1518.9	1518.9	1518.9	0	1
700	1520.7	1520.7	1520.7	1520.7	0	1
1000	1525.1	1525.1	1525.1	1525.1	0	1
1500	1533.3	1533.3	1533.3	1533.3	0	1
2000	1541.6	1541.6	1541.6	1541.6	0	1
2500	1549.9	1549.9	1549.9	1549.9	0	1

Table 3.4.3. Strait of Sicily summer model profile, envelope values, and variability. Sound speeds for model, mean, minimum, and maximum are given in meters per second.

Depth (m)	Model	Mean	Min.	Max.	Std.Dev.	# Obs.
0	1536.3	1533.5	1526.5	1541.5	3.2	80
10	1532.4	1532.7	1523.1	1541.2	3.0	80
20	1527.7	1529.6	1515.8	1535.4	3.3	80
30	1525.1	1523.3	1514.1	1533.5	5.1	80
50	1514.8	1514.9	1509.9	1524.6	3.2	80
75	1511.5	1511.4	1508.0	1517.4	1.8	76
100	1510.8	1510.4	1507.3	1514.8	1.8	76
125	1511.5	1510.5	1507.7	1513.3	1.2	69
150	1512.2	1510.9	1507.6	1513.8	1.4	67
200	1513.1	1511.8	1508.9	1514.0	1.4	58
250	1513.6	1512.9	1510.1	1514.8	0.4	46
300	1514.2	1513.8	1511.8	1515.1	0.9	41
400	1515.6	1515.3	1513.9	1516.6	0.5	34
500	1517.3	1516.8	1515.4	1517.4	0.6	23
600	1516.6	1516.6	1516.0	1517.1	0.4	7
700	1517.6	1517.6	1517.4	1517.9	0.5	4
800	1518.3	1518.3	1518.1	1518.5	0	2
1000	1525.1	1525.1	1525.1	1525.1	0	1
1500	1533.3	1533.3	1533.3	1533.3	0	1
2000	1541.6	1541.6	1541.6	1541.6	0	1
2500	1549.9	1549.9	1549.9	1549.9	0	1

Table 3.4.4. Strait of Sicily autumn model profile, envelope values, and variability. Sound speeds for model, mean, minimum, and maximum are given in meters per second.

Depth (m)	Model	Mean	Min.	Max.	Std. Dev.	# Obs.
0	1530.6	1527.3	1515.6	1533.6	5.5	44
10	1530.6	1527.3	1515.8	1533.7	5.5	44
20	1530.7	1527.4	1515.6	1534.1	5.4	44
30	1530.8	1526.6	1515.5	1533.7	5.5	44
50	1522.9	1520.5	1510.8	1532.8	5.9	44
75	1514.1	1514.9	1509.2	1531.1	3.9	41
100	1511.9	1512.8	1508.2	1520.1	2.5	35
125	1512.8	1511.9	1508.5	1514.8	1.6	33
150	1513.5	1511.8	1509.4	1513.6	1.6	33
200	1514.1	1512.8	1510.1	1514.2	1.1	29
250	1514.6	1513.5	1512.2	1514.6	0.9	16
300	1514.6	1514.1	1512.8	1514.6	0.6	9
400	1515.7	1515.5	1515.0	1515.8	0	6
500	1517.0	1517.1	1517.0	1517.3	0.5	4
600	1518.6	1518.6	1518.6	1518.6	0	1
1000	1525.1	1525.1	1525.1	1525.1	0	1
1500	1533.3	1533.3	1533.3	1533.3	0	1
2000	1541.6	1541.6	1541.6	1541.6	0	1
2500	1549.9	1549.9	1549.9	1549.9	0	1

3.5 Strait of Sardinia

A MOODS extraction was obtained for each month for an area covering 37–39.5°N, 008–010°E. Profiles were grouped into seasons based on obvious changes observed in sound speed gradients. Seasonal profile groups were edited to remove those with less than five data points, duplicates, and those that did not begin at the surface or extend beyond 50 m in depth. The edited seasonal profiles were interpolated to standard ocean depths and were statistically analyzed to obtain a mean value at each depth. The routine selects the real profile that is closest to the mean and produces a model profile, which is this same profile extended beyond its maximum depth with mean values and near-bottom historical sound speeds. Model profiles were visually evaluated to determine if they were representative of their season. Minimum and maximum observed values and the standard deviation at each standard depth are also provided with each model profile.

In the winter (December–April), the Strait of Sardinia profiles exhibited a positive sound speed gradient from the surface to the bottom with some exceptions (Fig. 3.5.1). The maximum standard deviation was only 1.6 m/sec at a 20-m water depth (Table 3.5.1).

Spring (May and June) was deemed to begin when profiles exhibited a reasonably strong seasonal thermocline resulting from surface warming (Fig. 3.5.1). The maximum standard deviation was 4.4 m/sec at the surface (Table 3.5.2).

The summer (July–September) profiles were similar to the spring profiles in exhibiting a strong seasonal thermocline. The difference was that surface sound speeds typically exceeded spring seasonal values by approximately 13 m/sec (Fig. 3.5.2). The maximum standard deviation was 5.3 m/sec at 30 m (Table 3.5.3).

The autumn (October and November) profiles were selected based on the formation of a significant surface mixed layer resulting from increasing periods of high winds (Fig. 3.5.2). The maximum standard deviation was 5.9 m/sec at 10 m but remained close to this value down to the bottom of this mixed layer at 30 to 50 m (Table 3.5.4). Profiles still exhibited a reduced seasonal thermocline.

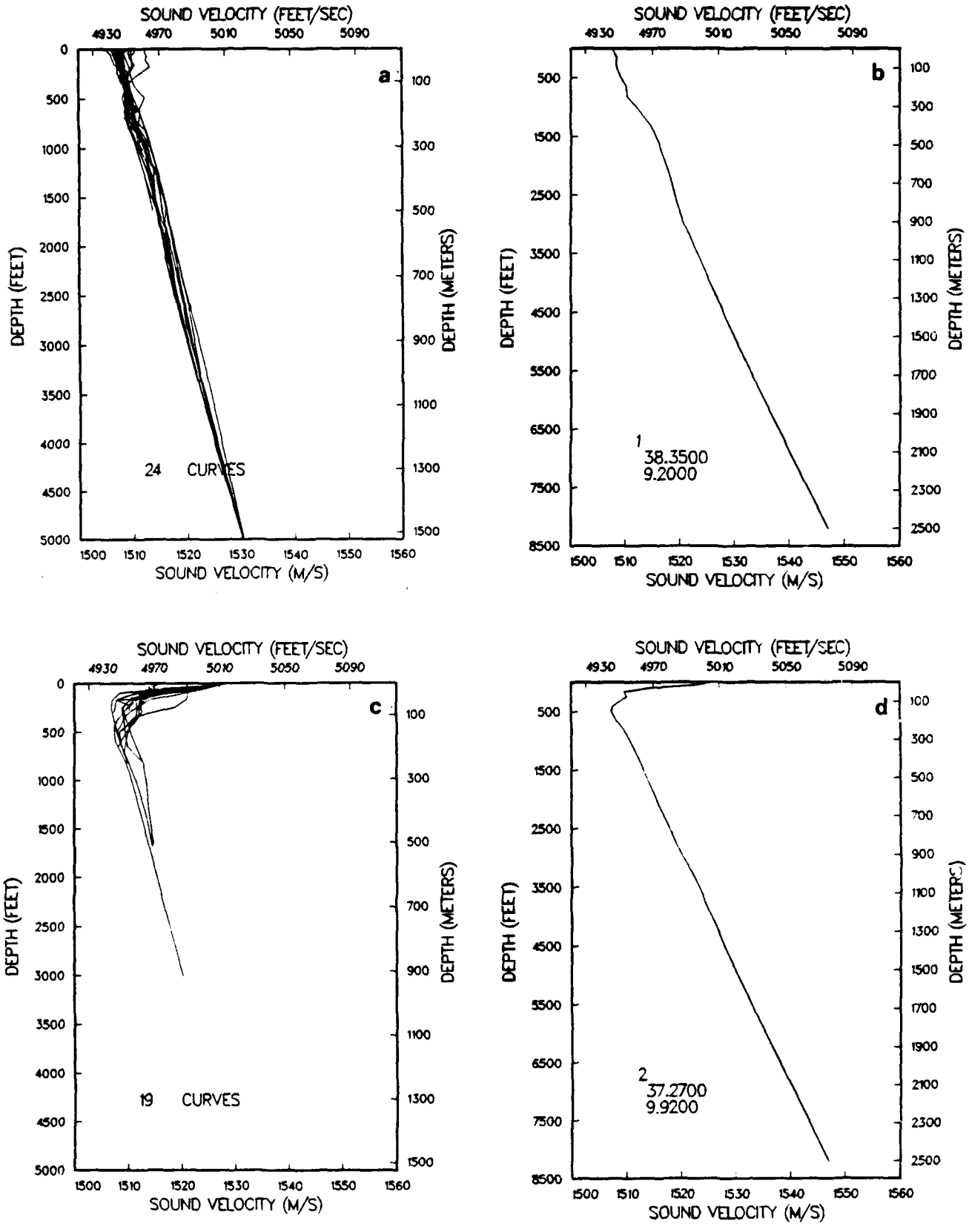

Figure 3.5.1. Strait of Sardinia:(a)winter profiles (December-April), (b) winter model profile,(c) spring profiles (May-June),(d) spring model profile

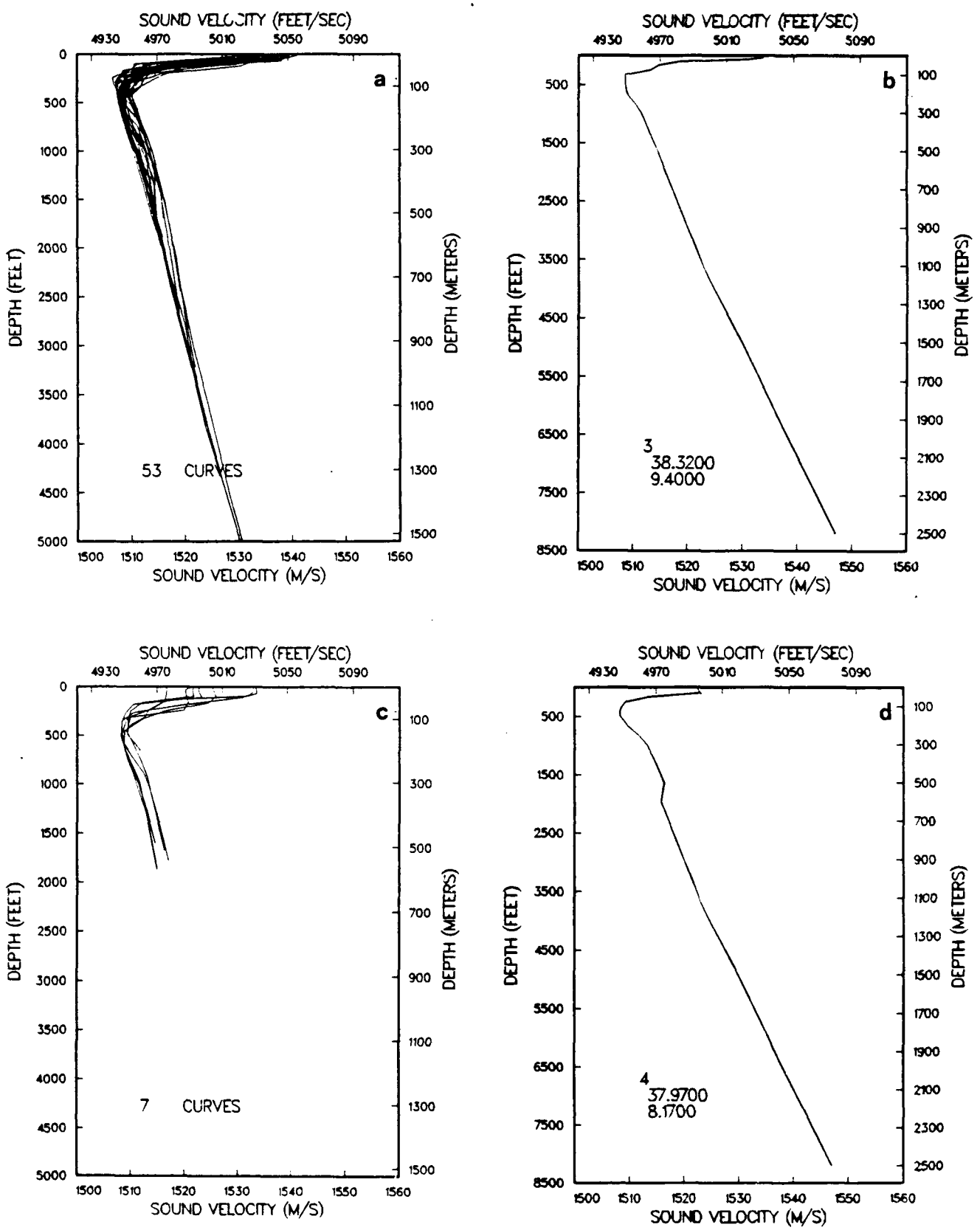

Figure 3.5.2. Strait of Sardinia:(a) summer profiles (July-September), (b) summer model profile, (c) autumn profiles (October-November),(d)autumn model profile

Table 3.5.1. Strait of Sardinia winter model profile, envelope values, and variability. Sound speed profiles for model, mean, minimum, and maximum are given in meters per second.

Depth (m)	Model	Mean	Min.	Max.	Std. Dev.	# Obs.
0	1507.6	1507.6	1505.3	1512.2	1.5	22
10	1507.8	1507.7	1505.5	1512.2	1.4	22
20	1508.0	1507.7	1506.0	1512.5	1.6	22
30	1508.1	1507.8	1506.2	1512.4	1.5	22
50	1508.4	1508.2	1506.7	1513.0	1.4	22
75	1508.3	1508.3	1507.0	1511.3	1.0	22
100	1508.4	1508.7	1507.7	1510.0	0.7	22
125	1508.7	1509.0	1508.4	1510.9	0.6	22
150	1509.1	1509.3	1508.1	1512.1	0.9	22
200	1510.2	1509.8	1508.5	1511.4	1.1	19
250	1510.3	1510.8	1509.4	1512.4	0.9	19
300	1511.9	1512.0	1510.5	1513.3	1.0	19
400	1514.6	1513.9	1512.2	1514.9	1.0	17
500	1516.1	1515.1	1513.6	1516.3	0.9	16
600	1517.3	1516.5	1515.5	1517.6	1.0	12
700	1518.4	1517.7	1516.7	1519.0	0.6	12
800	1519.3	1519.0	1518.1	1520.5	0.8	12
900	1520.5	1520.4	1519.7	1522.0	0.9	12
1000	1522.1	1521.9	1521.4	1523.5	0.5	11
1100	1523.7	1523.4	1523.0	1524.8	0.3	11
1200	1525.2	1525.0	1524.7	1526.2	0.5	11
1300	1526.8	1526.6	1526.4	1527.5	0.2	11
1400	1528.3	1528.2	1528.0	1528.8	0.5	11
1500	1529.9	1529.8	1529.7	1530.1	0	10
1750	1534.0	1534.1	1534.0	1534.1	0.4	10
2000	1538.3	1538.4	1538.3	1538.4	0.8	9
2500	1547.0	1547.0	1547.0	1547.0	0.7	8

Table 3.5.2. Strait of Sardinia spring model profile, envelope values, and variability. Sound speeds for model, mean, minimum, and maximum are given in meters per second.

Depth (m)	Model	Mean	Min.	Max.	Std. Dev.	# Obs.
0	1525.0	1524.2	1514.8	1528.2	4.4	17
10	1524.0	1522.6	1514.0	1526.1	4.0	17
20	1520.8	1519.2	1513.9	1523.4	3.7	17
30	1514.4	1514.9	1508.3	1521.2	3.1	17
50	1509.6	1511.7	1507.1	1520.9	3.0	17
75	1510.0	1510.7	1506.9	1518.7	2.7	17
100	1508.7	1510.1	1507.2	1512.2	1.5	12
125	1507.6	1509.4	1507.4	1511.0	1.3	9
150	1507.3	1508.8	1507.3	1510.3	1.0	8
200	1508.1	1509.2	1508.0	1511.5	1.2	7
250	1509.5	1510.6	1509.5	1512.8	1.3	4
300	1510.5	1511.7	1510.5	1513.3	1.2	3
400	1512.2	1513.0	1512.2	1513.8	0.8	3
500	1513.7	1514.3	1513.7	1514.7	0.6	3
600	1515.2	1515.2	1515.2	1515.2	0	1
700	1516.8	1516.8	1516.8	1516.8	0	1
800	1518.4	1518.4	1518.4	1518.4	0	1
900	1520.0	1520.0	1520.0	1520.0	0	1
1000	1522.1	1522.1	1522.1	1522.1	0	1
1100	1523.7	1523.7	1523.7	1523.7	0	1
1200	1525.2	1525.2	1525.2	1525.2	0	1
1300	1526.8	1526.8	1526.8	1526.8	0	1
1400	1528.3	1528.3	1528.3	1528.3	0	1
1500	1529.9	1529.9	1529.9	1529.9	0	1
1750	1534.0	1534.0	1534.0	1534.0	0	1
2000	1538.3	1538.3	1538.3	1538.3	0	1
2500	1547.0	1547.0	1547.0	1547.0	0	1

Table 3.5.3. Strait of Sardinia summer model profile, envelope values, and variability. Sound speeds for model, mean, minimum, and maximum are given in meters per second.

Depth (m)	Model	Mean	Min.	Max.	Std. Dev.	# Obs.
0	1533.7	1534.5	1527.4	1541.4	3.6	49
10	1533.7	1533.4	1526.3	1539.5	3.7	49
20	1531.0	1529.4	1518.3	1538.0	4.6	49
30	1518.7	1522.8	1510.6	1531.6	5.3	49
50	1514.6	1513.9	1508.4	1523.1	2.5	49
75	1513.2	1510.3	1506.5	1514.7	2.0	47
100	1508.5	1508.9	1506.8	1511.9	1.2	43
125	1508.5	1508.6	1507.3	1510.4	0.9	41
150	1508.5	1508.6	1507.5	1510.6	1.1	39
200	1508.8	1509.5	1508.3	1511.6	1.1	32
250	1510.3	1510.5	1509.2	1512.7	1.3	29
300	1511.5	1511.7	1510.2	1513.8	1.3	25
400	1513.0	1513.5	1512.1	1515.3	0.4	24
500	1514.5	1514.7	1513.6	1516.7	1.0	22
600	1515.8	1516.4	1515.4	1517.8	1.3	11
700	1517.2	1517.6	1516.8	1518.8	0.4	11
800	1518.6	1518.8	1518.2	1520.0	0.5	10
900	1520.0	1520.3	1519.8	1521.3	0.3	10
1000	1521.4	1521.8	1521.4	1522.8	0.5	8
1100	1522.8	1523.3	1522.8	1524.3	0.4	5
1200	1524.4	1524.8	1524.4	1525.8	0.5	5
1300	1526.2	1526.5	1526.2	1527.2	0.3	5
1400	1528.1	1528.2	1528.1	1528.6	0.3	5
1500	1529.9	1529.9	1529.8	1530.3	0.5	5
1750	1534.1	1534.2	1534.1	1534.4	0.5	5
2000	1538.3	1538.3	1538.3	1538.3	0	1
2500	1547.0	1547.0	1547.0	1547.0	0	1

Table 3.5.4. Strait of Sardinia autumn model profile, envelope values, and variability. Sound speeds for model, means, minimum, and maximum are given in meters per second.

Depth (m)	Model	Mean	Min.	Max.	Std. Dev.	# Obs.
0	1522.8	1524.8	1516.5	1533.2	5.7	7
10	1522.6	1524.7	1516.7	1533.5	5.9	7
20	1522.8	1524.7	1516.6	1533.5	5.8	7
30	1523.1	1524.2	1516.5	1531.3	4.9	7
50	1513.4	1517.8	1512.1	1524.5	4.4	7
75	1509.4	1513.3	1509.4	1519.0	3.2	7
100	1508.6	1510.1	1508.6	1512.3	1.4	7
125	1508.3	1509.1	1508.3	1510.0	0.8	7
150	1508.3	1508.7	1508.1	1509.6	0.7	7
200	1509.6	1509.8	1508.9	1511.8	1.2	7
250	1511.6	1510.7	1509.9	1512.4	0.9	6
300	1513.1	1512.0	1511.0	1513.4	1.0	6
400	1514.9	1513.7	1512.9	1514.9	0.7	5
500	1516.4	1515.2	1514.1	1516.4	0.9	4
600	1515.8	1515.8	1515.8	1515.8	0	1
700	1517.2	1517.2	1517.2	1517.2	0	1
800	1518.6	1518.6	1518.6	1518.6	0	1
900	1520.0	1520.0	1520.0	1520.0	0	1
1000	1521.4	1521.4	1521.4	1521.4	0	1
1100	1522.8	1522.8	1522.8	1522.8	0	1
1200	1524.4	1524.4	1524.4	1524.4	0	1
1300	1526.2	1526.2	1526.2	1526.2	0	1
1400	1528.1	1528.1	1528.1	1528.1	0	1
1500	1529.9	1529.9	1529.9	1529.9	0	1
1750	1534.1	1534.1	1534.1	1534.1	0	1
2000	1538.3	1538.3	1538.3	1538.3	0	1
2500	1547.0	1547.0	1547.0	1547.0	0	1

3.6 Alboran Sea

A MOODS extraction was obtained for each month for several areas in the Alboran Sea. Profiles were grouped into seasons based on obvious changes observed in sound speed gradients. The Alboran Sea was grouped into three seasons: winter, summer, and transitional, which includes those months between summer and winter when the seasonal thermocline is developing or weakening. Because the strong Alboran Sea front was present, the area was divided into two parts for both the summer and transitional seasons. The first area is primarily northern and includes 36.5–37°N, 004.6–003.8°W and 36.2–37°N, 003.8–003°W. The second area is primarily southern but also includes the entire area to the immediate east of the Strait of Gibraltar. This southern part includes 35–36.3°N, 004.8–003.8°W and 35–36°, 003.8–003°W. The northern section contains cooler Mediterranean water with a resulting shallow sound channel axis and a strong thermocline. Southern profiles tended to have a weaker seasonal thermocline during these summer and transitional seasons and displayed more variability due to the mixing of Atlantic and Mediterranean waters.

The Alboran Sea was not divided into these two parts for the winter because there were only five profiles in this version of the MOODS data base, and differences across the frontal region could not be perceived. The water column appeared to be well mixed during the winter; therefore, frontal variations would be minimized. Acoustic implications of the Alboran Sea front may also be minimal due to the small spatial dimensions of this area.

Seasonal profile groups were edited to remove those with less than five data points, duplicates, and those that did not begin at the surface or extend beyond 50 m in depth. The edited seasonal profiles were interpolated to standard ocean depths and were statistically analyzed to obtain a mean value at each depth. The routine selects the real profile that is closest to the mean and produces a model profile, which is this same profile extended beyond its maximum depth with mean values and with historical deep water sound speeds. Model profiles were visually evaluated to determine if they were representative of their season. Minimum and maximum observed values and the standard deviation at each standard depth are also provided with each model profile.

In the winter (January–March), the Alboran Sea profiles exhibited a positive sound speed gradient from the surface to the bottom with some exceptions (Fig. 3.6.1). The maximum standard deviation was only 1.6 m/sec at the surface (Table 3.6.1).

The summer (July–October) profiles exhibited a strong seasonal thermocline. The northern Alboran profiles displayed a shallow sound channel axis at 100 m, but the southern Alboran profiles had a deeper sound channel axis at 200 m that resulted from the influx and mixing of Atlantic water (Fig. 3.6.2). The maximum standard

deviation was 6.0 m/sec at 20 m for the northern section (Table 2) and 5.7 m/sec at the surface for the southern section (Table 3.6.3).

The transition (April–June, November–December) profiles were selected based on the reduced seasonal sound speed negative gradients (Fig. 3.6.3). Like the summer season, the northern section profiles are cooler than those of the southern section. The maximum standard deviation was 6.3 m/sec at the surface for the northern section (Table 3.6.4) and 3.5 m/sec at 50 m for the southern section but remained close to this value down to 150 m (Table 3.6.5).

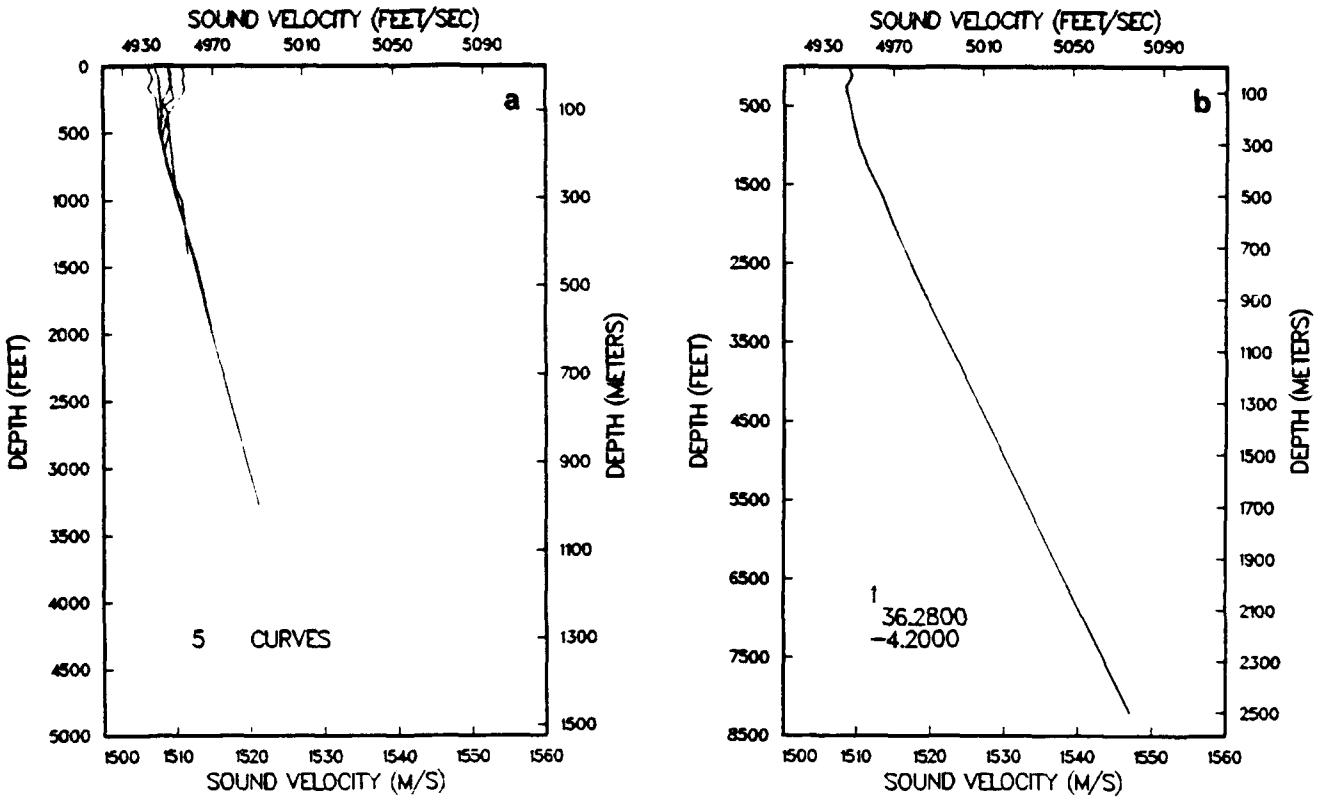

Figure 3.6.1. Alboran sea: (a) winter profiles (January-March), (b) winter model profile

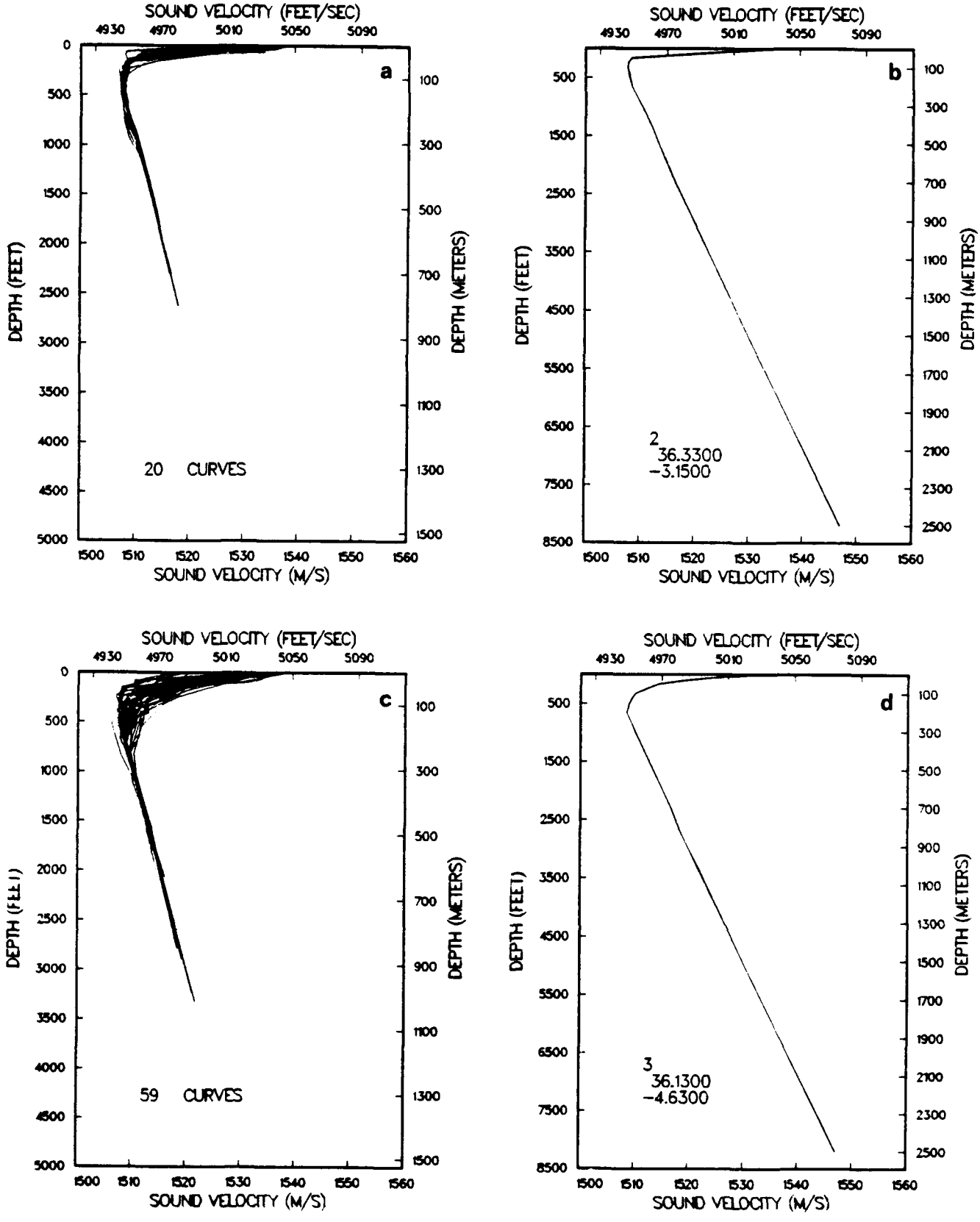

Figure 3.6.2. Alboran sea summer (July-October): (a) northern section profiles, (b) northern section model profile, (c) southern section profiles, (d) southern section model profile.

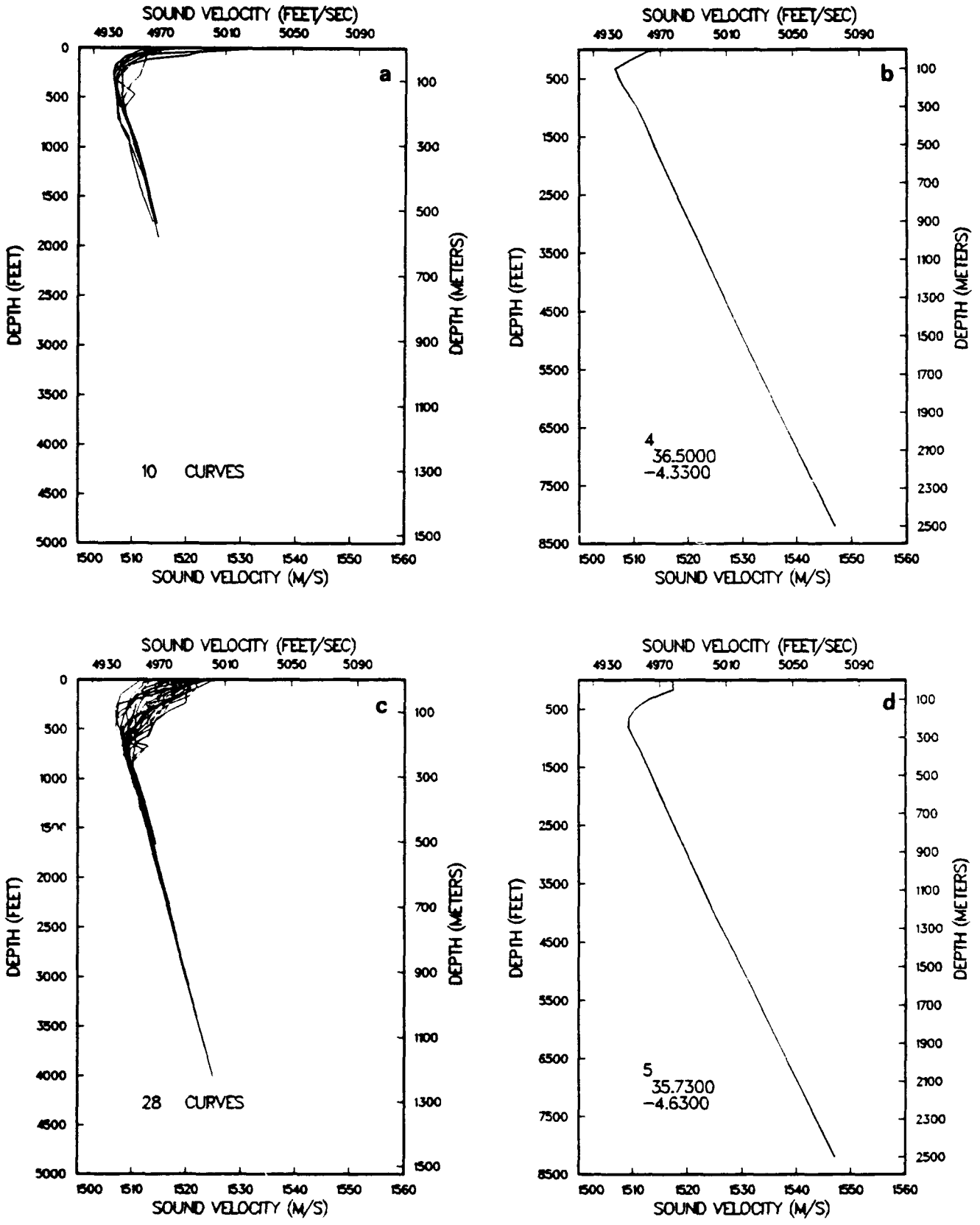

Figure 3.6.3. Alboran sea transition season (April-June, November-December) (a) northern section profiles, (b) northern section model profile, (c) southern section profiles,(d) southern section model profile

Table 3.6.1. Alboran Sea winter model profile, envelope values, and variability. Sound speeds for model, mean, minimum, and maximum are given in meters per second.

Depth (m)	Model	Mean	Min.	Max.	Std. Dev.	# Obs.
0	1509.0	1508.4	1506.2	1510.8	1.6	5
10	1508.9	1508.5	1506.3	1510.9	1.4	5
20	1509.0	1508.7	1506.6	1511.0	1.4	
30	1509.2	1508.7	1506.8	1510.9	1.4	5
50	1509.1	1508.7	1506.3	1511.1	1.7	5
75	1508.4	1508.8	1507.3	1510.5	1.1	5
100	1508.6	1508.2	1507.4	1509.4	0.7	5
125	1508.9	1508.2	1507.5	1508.9	0.5	5
150	1509.0	1508.3	1507.6	1509.0	0.5	5
200	1509.3	1508.5	1508.3	1509.3	0	5
250	1509.7	1509.3	1509.1	1509.7	0.5	4
300	1510.1	1510.2	1509.9	1510.6	0	4
400	1511.6	1511.6	1511.4	1511.8	0.3	3
500	1513.3	1513.3	1513.1	1513.4	0	2
600	1514.7	1514.7	1514.7	1514.7	0	1
700	1516.3	1516.3	1516.3	1516.3	0	1
800	1517.8	1517.8	1517.8	1517.8	0	1
900	1519.5	1519.5	1519.5	1519.5	0	1
1500	1529.8	1529.8	1529.8	1529.8	0	1
2000	1538.4	1538.4	1538.4	1538.4	0	1
2500	1547.0	1547.0	1547.0	1547.0	0	1

Table 3.6.2. Northern section of Alboran Sea summer model profile, envelope values, and variability. Sound speeds for model, mean, minimum, and maximum are given in meters per second.

Depth (m)	Model	Mean	Min.	Max.	Std. Dev.	# Obs.
0	1534.3	1533.3	1525.1	1538.0	3.7	20
10	1529.1	1527.4	1512.9	1535.7	5.9	20
20	1524.0	1520.4	1508.2	1533.6	6.0	20
30	1518.8	1514.5	1508.2	1522.2	3.8	20
50	1508.4	1509.1	1508.0	1513.6	1.5	20
75	1507.8	1507.9	1507.0	1509.8	0.3	20
100	1507.7	1507.6	1507.1	1508.4	0.7	19
125	1507.9	1507.6	1507.0	1508.3	0.5	18
150	1508.1	1507.7	1507.1	1508.2	0.5	17
200	1508.5	1508.3	1507.7	1508.6	0	14
250	1509.3	1509.2	1508.2	1509.8	0.7	14
300	1510.2	1510.2	1509.3	1510.7	0.9	14
400	1512.0	1512.1	1511.8	1512.3	0.4	12
500	1513.4	1513.6	1513.3	1513.9	0.4	10
600	1514.9	1515.0	1514.9	1515.1	0.7	7
700	1516.4	1516.6	1516.4	1516.7	0	4
800	1518.1	1518.1	1518.0	1518.1	0.5	2
1500	1529.8	1529.8	1529.8	1529.8	0	1
2000	1538.4	1538.4	1538.4	1538.4	0	1
2500	1547.0	1547.0	1547.0	1547.0	0	1

Table 3.6.3. Southern section of Alboran Sea summer model profile, envelope values, and variability. Sound speed profiles for model, mean, minimum, and maximum are given in meters per second.

Depth (m)	Model	Mean	Min.	Max.	Std. Dev.	# Obs.
0	1532.1	1530.4	1517.0	1539.9	5.7	58
10	1527.6	1526.3	1514.4	1535.2	4.9	58
20	1523.0	1522.0	1511.9	1533.6	5.0	58
30	1519.4	1519.0	1510.3	1531.0	4.7	58
50	1514.3	1514.6	1507.9	1523.3	3.2	58
75	1512.1	1511.8	1507.0	1518.4	2.7	58
100	1510.0	1510.4	1507.4	1515.3	1.9	58
125	1509.5	1509.5	1507.0	1514.1	1.6	57
150	1509.0	1509.0	1506.5	1512.6	1.5	56
200	1508.5	1508.7	1506.9	1511.2	1.1	54
250	1509.3	1509.3	1507.9	1510.3	0.5	51
300	1510.0	1510.1	1509.3	1510.6	0.3	49
400	1511.7	1511.7	1511.2	1512.2	0.9	43
500	1513.3	1513.4	1512.7	1513.8	0.3	38
600	1515.0	1514.9	1514.4	1515.4	0.8	31
700	1516.6	1516.5	1516.2	1516.8	0.8	21
800	1518.0	1518.0	1517.6	1518.2	0.4	11
900	1519.7	1519.7	1519.6	1519.8	0.5	4
1000	1521.4	1521.4	1521.4	1521.4	0	1
1500	1529.8	1529.8	1529.8	1529.8	0	1
2000	1538.4	1538.4	1538.4	1538.4	0	1
2500	1547.0	1547.0	1547.0	1547.0	0	1

Table 3.6.4. Northern section Alboran Sea transition model profile, envelope values, and variability. Sound speeds for model, mean, minimum, and maximum are given in meters per second.

Depth (m)	Model	Mean	Min.	Max.	Std. Dev.	# Obs.
0	1514.9	1516.8	1512.0	1532.8	6.3	10
10	1512.5	1514.7	1510.9	1523.2	4.2	10
20	1511.9	1512.4	1509.5	1520.4	2.9	10
30	1511.2	1510.5	1508.3	1515.2	1.9	10
50	1509.7	1508.7	1506.7	1512.0	1.5	10
75	1508.2	1507.6	1506.2	1511.4	1.5	10
100	1506.6	1507.1	1506.2	1510.2	1.0	10
125	1507.0	1507.4	1506.6	1509.2	0.9	10
150	1507.3	1507.7	1506.9	1509.9	0.7	10
200	1508.2	1508.1	1507.1	1508.7	0.6	10
250	1509.4	1509.2	1508.0	1509.7	0.2	10
300	1510.6	1510.2	1509.4	1510.8	0.4	9
400	1512.2	1512.0	1510.9	1512.4	0.3	7
500	1513.6	1513.5	1512.9	1513.8	0.4	5
1500	1529.8	1529.8	1529.8	1529.8	0	1
2000	1538.4	1538.4	1538.4	1538.4	0	1
2500	1547.0	1547.0	1547.0	1547.0	0	1

Table 3.6.5. Southern section Alboran Sea transition season model profile, envelope values, and variability. Sound speeds for model, mean, minimum, and maximum are given in meters per second.

Depth (m)	Model	Mean	Min.	Max.	Std. Dev.	# Obs.
0	1517.4	1518.6	1511.7	1524.8	3.1	28
10	1517.2	1517.8	1510.8	1523.7	3.0	28
20	1517.4	1517.3	1509.9	1522.5	3.0	28
30	1517.3	1516.6	1509.1	1521.6	3.3	28
50	1517.4	1514.8	1507.8	1520.5	3.5	28
75	1515.1	1513.0	1507.3	1519.4	3.1	28
100	1513.0	1511.8	1507.0	1516.4	2.4	28
125	1511.6	1510.8	1507.1	1514.4	2.3	28
150	1510.6	1510.1	1507.2	1513.6	1.9	28
200	1509.3	1509.0	1507.9	1511.8	1.1	28
250	1509.2	1509.4	1508.8	1510.4	0.7	26
300	1510.0	1510.2	1509.8	1510.9	8	26
400	1511.8	1511.9	1511.4	1512.7	0.4	24
500	1513.4	1513.5	1513.2	1514.3	0.8	19
600	1514.9	1515.0	1514.7	1515.3	0.8	15
700	1516.5	1516.6	1516.4	1516.9	0.6	14
800	1518.1	1518.1	1518.0	1518.2	0	10
900	1519.7	1519.7	1519.5	1519.8	0.7	7
1000	1521.3	1521.3	1521.2	1521.3	0.5	5
1100	1522.9	1522.9	1522.9	1522.9	0	2
1200	1524.5	1524.5	1524.5	1524.5	0	1
1500	1529.8	1529.8	1529.8	1529.8	0	1
2000	1538.4	1538.4	1538.4	1538.4	0	1
2500	1547.0	1547.0	1547.0	1547.0	0	1

3.7 Strait of Gibraltar

A MOODS extraction was obtained for each month for an area covering 35.5–6.5°, 005–06°. Only a limited number of profiles were available for September through April from the MOODS data base. Tidal currents and internal waves working in combination result in an increase in mixing of the surface layer. Levantine intermediate water can be found at the surface at certain times in the tidal cycle due to the slope of the isopycnal surfaces. Such variability in the Strait of Gibraltar is well documented in the literature. With the constraints of limited data availability and the extreme variability due to the dynamics of this region, profiles were grouped into two seasons based on observed presence of a seasonal thermocline and changes in sound speed gradients.

The first season is winter, when the water column is essentially well mixed. The second is summer, when a seasonal thermocline causes a negative sound speed gradient down to approximately 100 m. Profiles were edited to remove those with less than five data points, duplicates, and those that did not begin at the surface or extend beyond 50 m in depth. Edited seasonal profiles were interpolated to standard ocean depths and were statistically analyzed to obtain a mean value at each depth. The routine selects the real profile that is closest to the mean and produces a model profile, which is this same profile extended beyond its maximum depth with mean values. The summer model profile was then used to extend the winter model profile to an 800-m depth. Model profiles were visually evaluated to determine if they were representative of their season. Minimum and maximum observed values and the standard deviation at each standard depth are also provided with each model profile. Neither the MOODS nor model profiles appear to be smooth because original data are decimated to fairly large increments at greater depths; standard depths, which are used in analysis routines, are also at large increments at greater depths.

In the winter (October–April), the Strait of Gibraltar profiles exhibited an isovelocity or weak sound speed gradient from the surface to the bottom (Fig. 3.7.1). Maximum standard deviation was 2.2 m/sec at the surface (Table 3.7.1). The model was extended with values from the summer model below this depth.

Summer (May–September) profiles exhibit a strong seasonal thermocline which results from surface warming (Fig. 3.7.1). Maximum standard deviation was 3.5 m/sec at 30 m (Table 3.7.2).

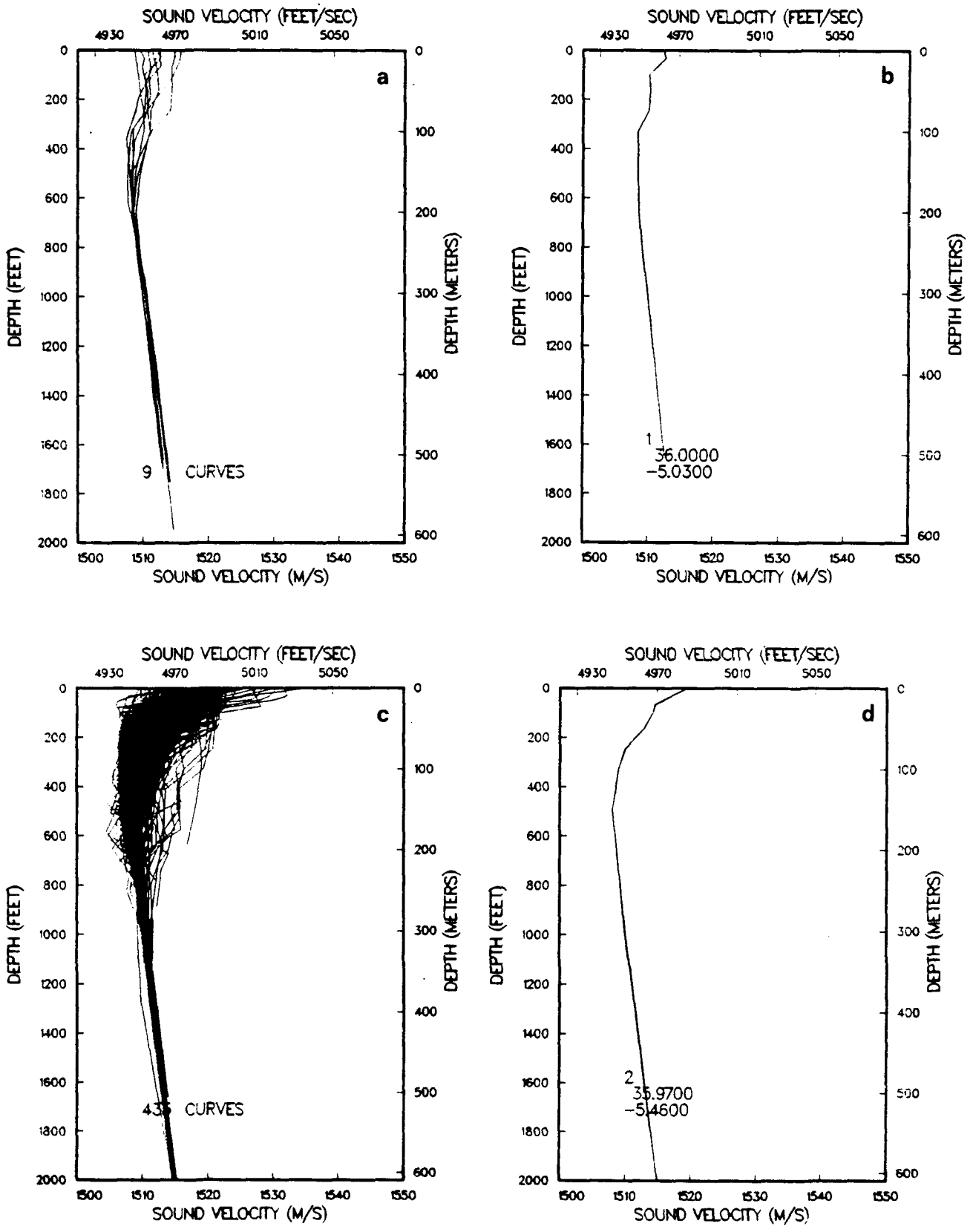

Figure 3.7.1. Strait of Gibraltar (a) Winter Profiles (b) Winter Model Profile (c) Summer Profiles (d) Summer Model Profile

Table 3.7.1. Strait of Gibraltar winter model profile, envelope values, and variability. Sound speeds for model, mean, minimum, and maximum are given in meters per second.

Depth (m)	Model Profile	Mean	Min.	Max.	Std. Dev.	# Obs.
0	1512.5	1512.1	1508.7	1515.8	2.2	9
10	1512.7	1512.1	1508.9	1515.6	1.9	9
20	1511.4	1511.9	1509.1	1515.1	1.9	9
30	1510.2	1511.5	1509.2	1514.6	1.9	9
50	1510.4	1511.2	1509.6	1514.5	1.4	9
75	1510.1	1510.5	1508.8	1514.2	1.6	9
100	1508.5	1509.5	1507.8	1511.3	1.4	9
125	1508.5	1508.9	1507.6	1510.3	1.1	9
150	1508.5	1508.5	1507.6	1509.6	0.6	9
200	1508.6	1508.5	1508.0	1509.0	0.4	9
250	1509.2	1509.3	1509.1	1509.6	0.3	9
300	1510.0	1510.1	1509.9	1510.6	0.4	9
400	1511.3	1511.7	1511.1	1512.1	0.3	9
500	1512.6	1513.1	1512.6	1513.6	0.5	8
600	1514.8	1514.8	1514.4	1515.1	0	1
700	1516.4	1516.4	1516.1	1516.7	0	1
800	1518.0	1518.0	1517.8	1518.2	0	1

Table 3.7.2.Strait of Gibraltar summer model profile, envelope values and variability. Sound speeds for model, mean, minimum, and maximum are given in meters per second.

Depth (m)	Model Profile	Mean	Min.	Max.	Std. Dev.	# Obs.
0	1519.5	1519.7	1509.6	1535.0	3.2	424
10	1516.9	1517.8	1507.8	1532.2	2.9	424
20	1514.5	1515.9	1506.1	1527.9	3.3	424
30	1514.2	1514.2	1506.4	1522.6	3.5	424
50	1512.9	1511.6	1506.3	1521.3	3.1	424
75	1509.9	1509.9	1506.1	1520.1	2.2	424
100	1508.9	1509.0	1505.7	1519.3	1.8	418
125	1508.5	1508.5	1505.9	1518.5	2.2	405
150	1508.0	1508.3	1505.1	1518.0	0.7	396
200	1508.6	1508.6	1505.4	1513.9	0.4	353
250	1509.3	1509.3	1507.6	1512.5	0.2	257
300	1509.9	1510.1	1509.3	1511.5	1.4	229
400	1511.6	1511.6	1510.1	1512.3	0.5	157
500	1513.2	1513.2	1512.2	1513.7	0.8	120
600	1514.8	1514.8	1514.4	1515.1	1.1	90
700	1516.4	1516.4	1516.1	1516.7	0.4	72
800	1518.0	1518.0	1517.8	1518.2	0.3	7

4.0 Currents in the Mediterranean Areas

4.1 Levantine Basin and the Cretan Sea

Very few current measurements were made in this area of the eastern Mediterranean Sea; hence, we must rely on geostrophic estimates (the current field derived from temperature and salinity data) and oceanographic model results to determine current velocity variations. Maximum current velocities at the surface are associated with the larger gyres and the mid-Mediterranean jet. Robinson et al. (1991) documented measured current speeds of 20–30 cm/sec. Hecht et al. (1988) calculated geostrophic velocities of 30–40 cm/sec (at a depth of 80 m) associated with these features. Hecht et al. indicated that the speeds decrease to 20 cm/sec at 230 m and to 5 cm/sec at 490 m. Independent researchers found similar speeds in the Mersa-Matruh eddy at the surface. Ovchinnikov (1965) documented measured currents in the upper layer (0–250 m) of the Cretan Sea as being a steady 50 cm/sec, with dynamic computations indicating an eastward direction. He also described measured current speeds at 1500 m to the south of Crete at less than 3 cm/sec. Surface currents measured by Accerboni and Grancini (1972) showed an intense flow that averaged 40 cm/sec from the Aegean Sea toward the Levantine Basin through the three straits: Kasos, Karpathos and Rhodes.

Numerical model simulations were used to determine the deep currents in the various study areas of the Mediterranean. The Naval Oceanographic and Atmospheric Research Laboratory's (NOARL) Layered Circulation Model (Dr. G. Heburn, NOARL, personal communication) was used to attain first-order current speed estimates. This model can predict, among other things, both circulation and integrated current speeds in the following three layers: 0–200 m, 200–600 m, and from 600 m to the seafloor (or 3700 m). The model, which has a resolution of 1/16°, uses the wind climatology of the European Center for Medium Range Weather Forecasting from 1981 to 1989 and the Synthetic Bathymetric Profiling System (SYNBAPS) data base. Mass transport exchanges in the Strait of Gibraltar are taken into account, and the Levantine intermediate water formation in the eastern Mediterranean is parameterized by assuming uniform mixing. The model is "spun up" from an ocean in the dormant state and, to date, has been climatologically forced for the equivalent of 34 years. Since the minimum depth at which predictions are made cannot be shoaler than 200 m, modeled current speed estimates in the shallow-water areas of the straits are not possible. It should be noted that the results of this model are preliminary, since the algorithms are still being tested and a complete set of forcing factors has not been incorporated.

Figures 4.1.1 and 4.1.2 show the modeled currents in the Levantine and Cretan Basins integrated over the depth of the third layer. These results indicate that maximum currents in both basins do not exceed 1.5 cm/sec. These maximum speeds are contained within a gyre in the Levantine Basin, but they are associated with

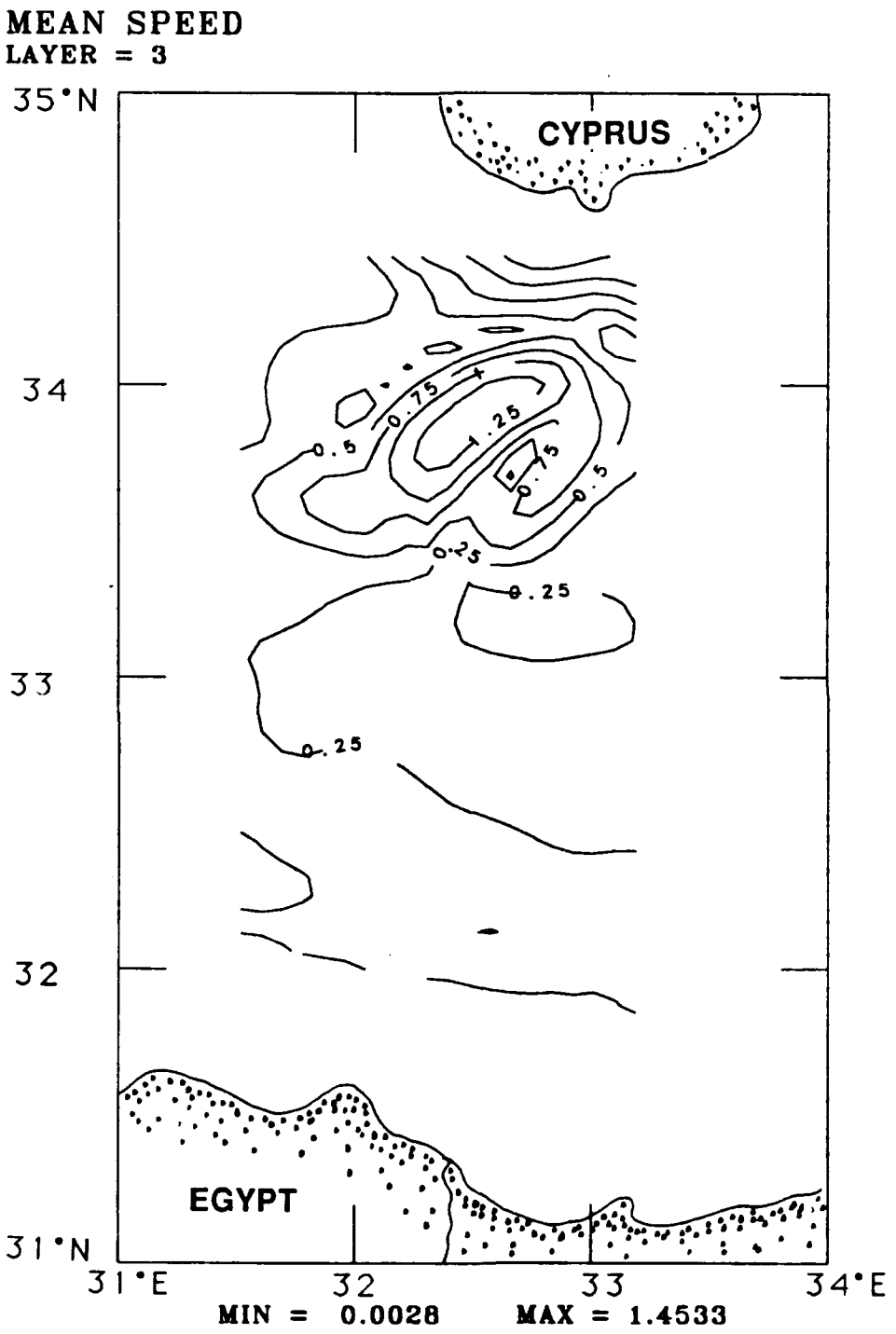

Figure 4.1.1. Modeled Deep Layer Circulation in the Levantine Basin.

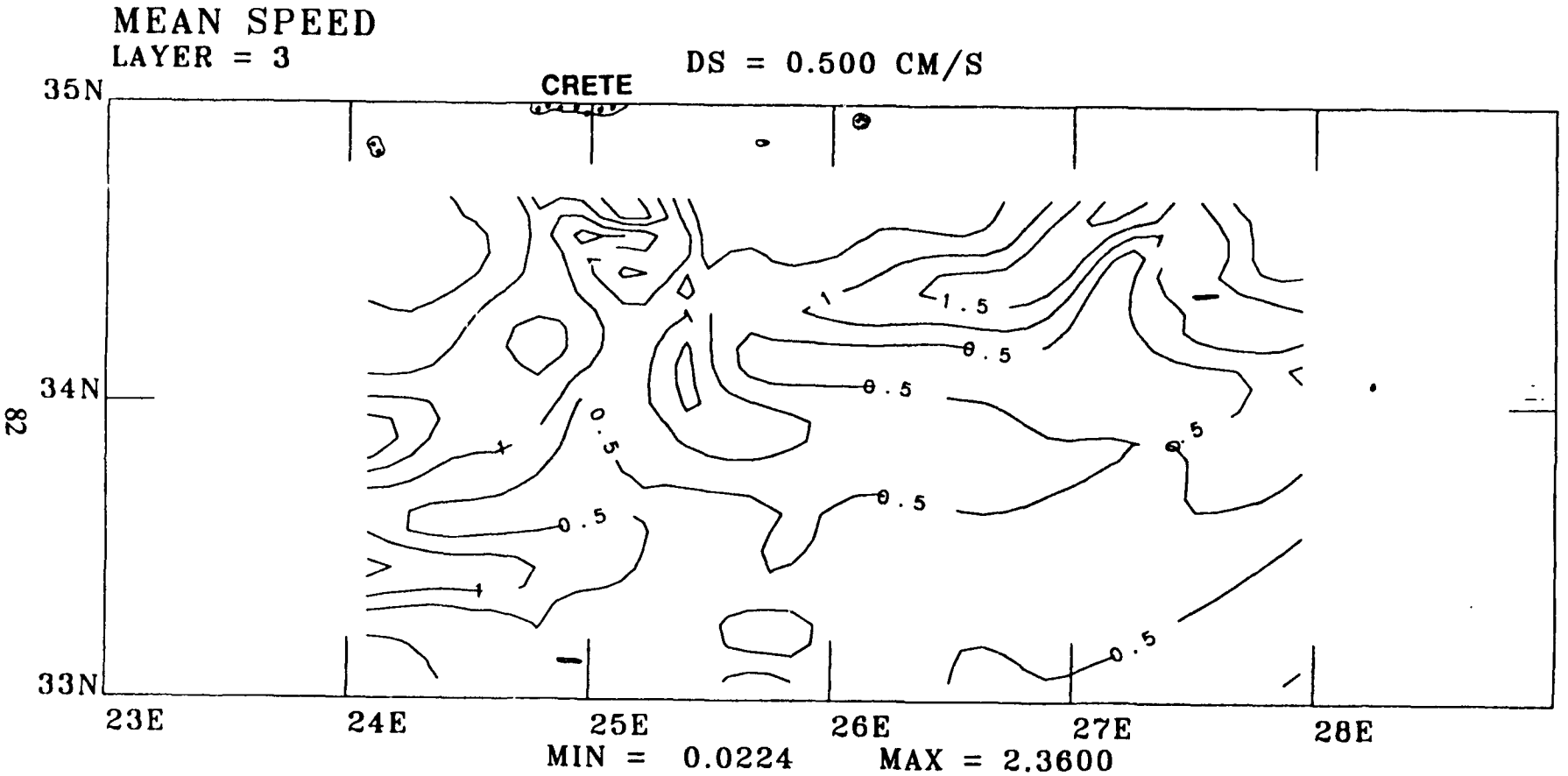

Figure 4.1.2. Modeled Deep Layer Circulation in the Cretan Basin.

circulation around both sides of Crete in the Cretan Basin. Figures 4.1.3 and 4.1.4 illustrate a time series of the currents in the abyssal waters of the Levantine and Cretan Basins at the locations specified over a 9-year period. A biannual periodicity of current speed maxima is evident in both basin time series illustrations. At this time, the only forcing factor that determines the abyssal circulation is the winds. Atmospheric biannual periodicities have been documented; however, an attempt to correlate these occurrences has not been undertaken.

4.2 Ionian Basin

Current velocities in the Ionian Basin are available from only a scattering of uncoordinated measurements. Like the Levantine and Cretan Basins, there is evidence that surface current speeds are geographically variable. For instance, the results of two current meter moorings during the IOMED 71 exercise (Miller, 1972) indicated velocities of 5-10 cm/sec at 36°N,17°E at 330 m, but currents of 25–45 cm/sec were observed at 121 m near 38.5°N,18°E. Geostrophic currents at 1000 m in the central Ionian Basin between 32° and 37°N showed current speeds between 0.6 and 3.0 cm/sec and highly variable directions. Documented bottom current velocities between 40 and 50 cm/sec at the sill between the Adriatic and Ionian Seas are related to the transport of heavy bottom water into the eastern Mediterranean basins.

The results of layer three (integrated current speeds between 600 m and the seafloor) of the NOARL Layered Circulation Model for the Ionian Basin (Figure 4.2.1) showed currents as high as 4 cm/sec at the base of the continental slope adjacent to the Strait of Sicily. Elsewhere in the basin, bottom currents are benign. Figure 4.2.2 contains a modeled time series of the deep (third) layer at 36°N, 18°E in the Ionian Basin. Like the deep modeled analyses in the previous two study areas, a biannual periodicity is evident.

4.3 Strait of Sicily

Geostrophic current estimates provided the first information concerning current speed and direction in this area. However, numerous current measurements have been made in the Strait of Sicily. The majority of these measurements were made using current meters; however, a body of data documents parachute drogue results and geomagnetic electrokinetograph tows. Table 4.3.1 summarizes various measurements known to the author, and Figure 4.3.1 shows their approximate locations in the strait.

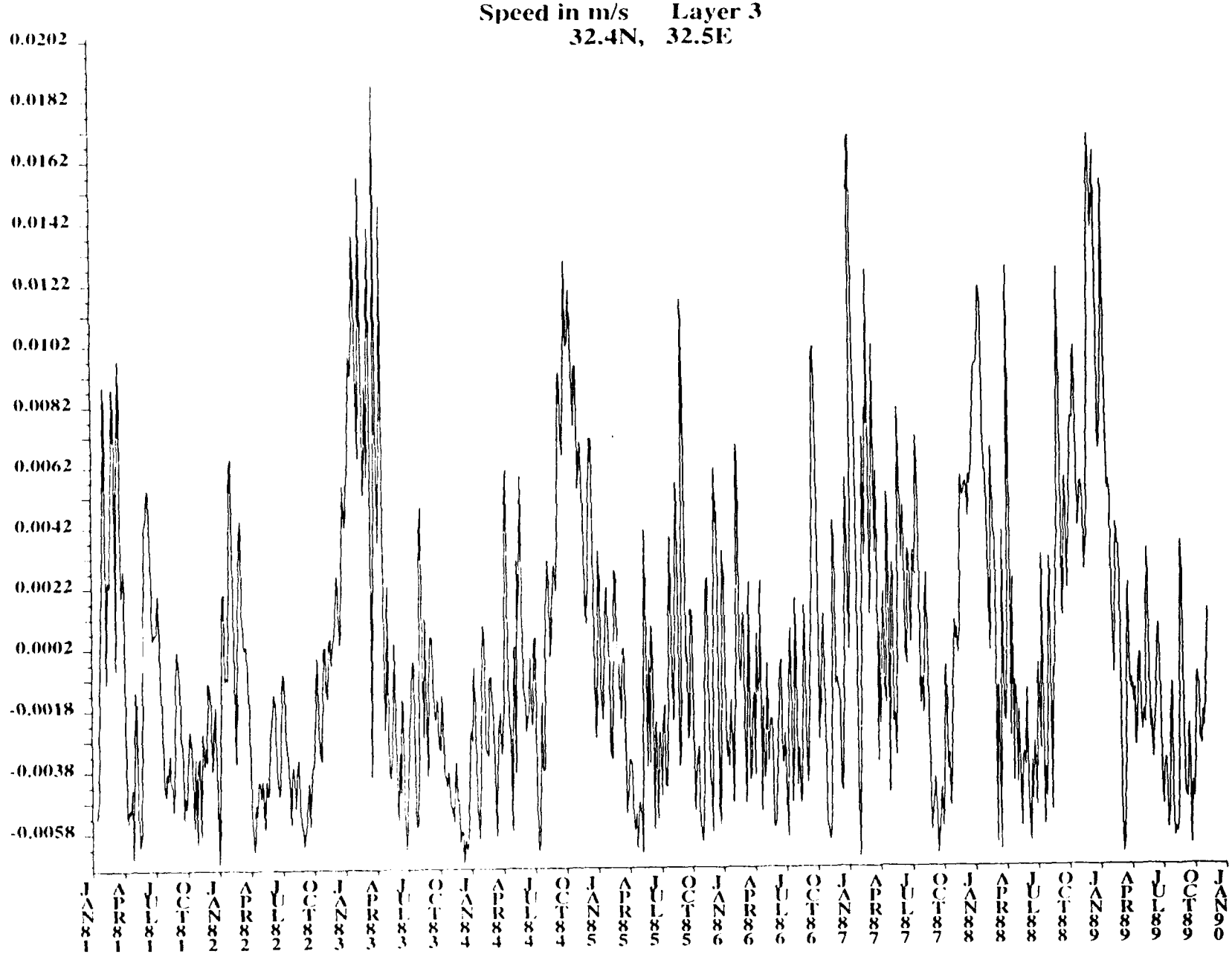

Figure 4.1.3. Modeled Temporal Variability of Deep Currents at 32.4°N, 32.5°E in the Levantine Basin.

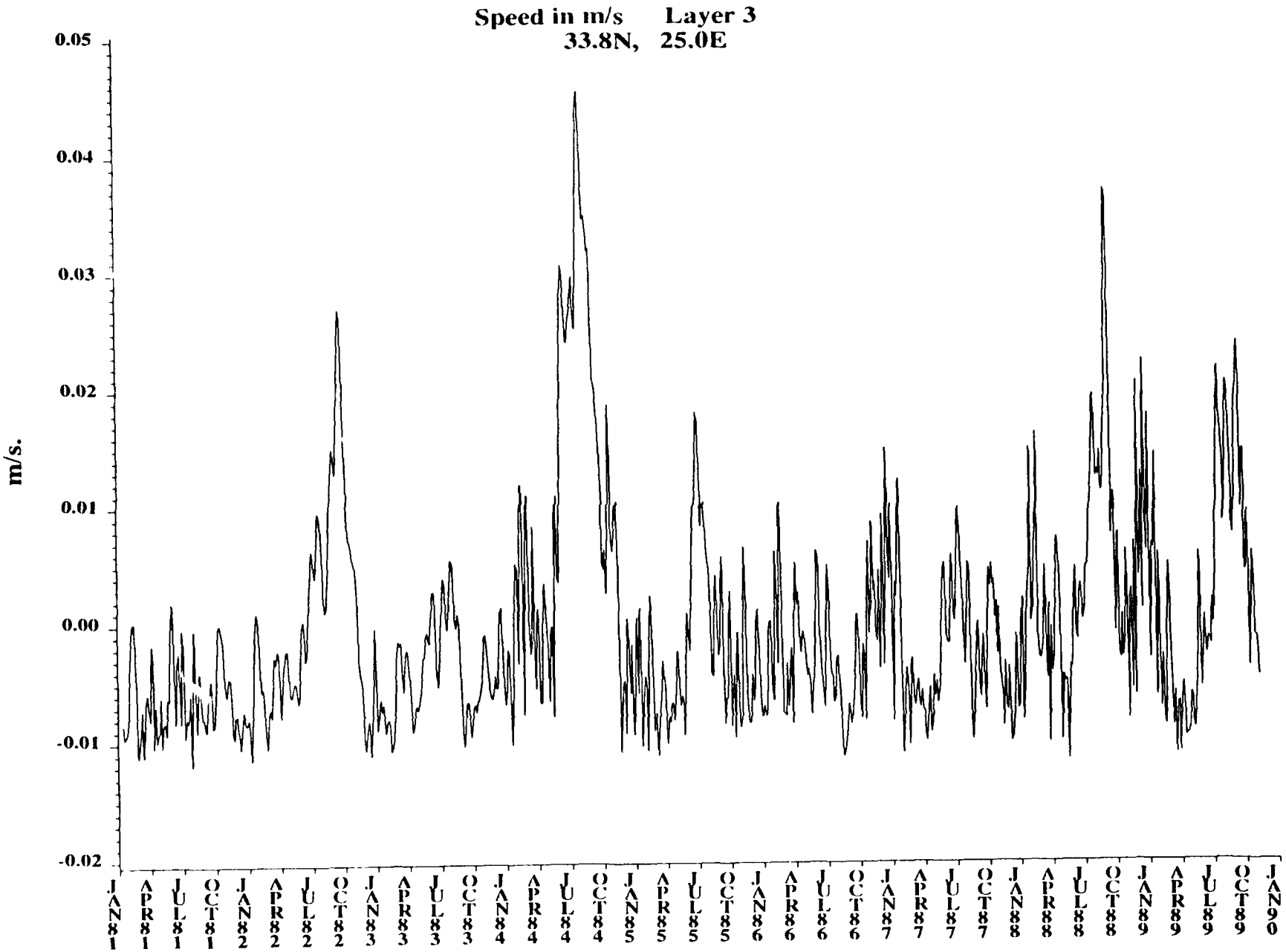

Figure 4.1.4. Modeled Temporal Variability of Deep Currents at 33.8°N, 25°E in the Cretan Basin.

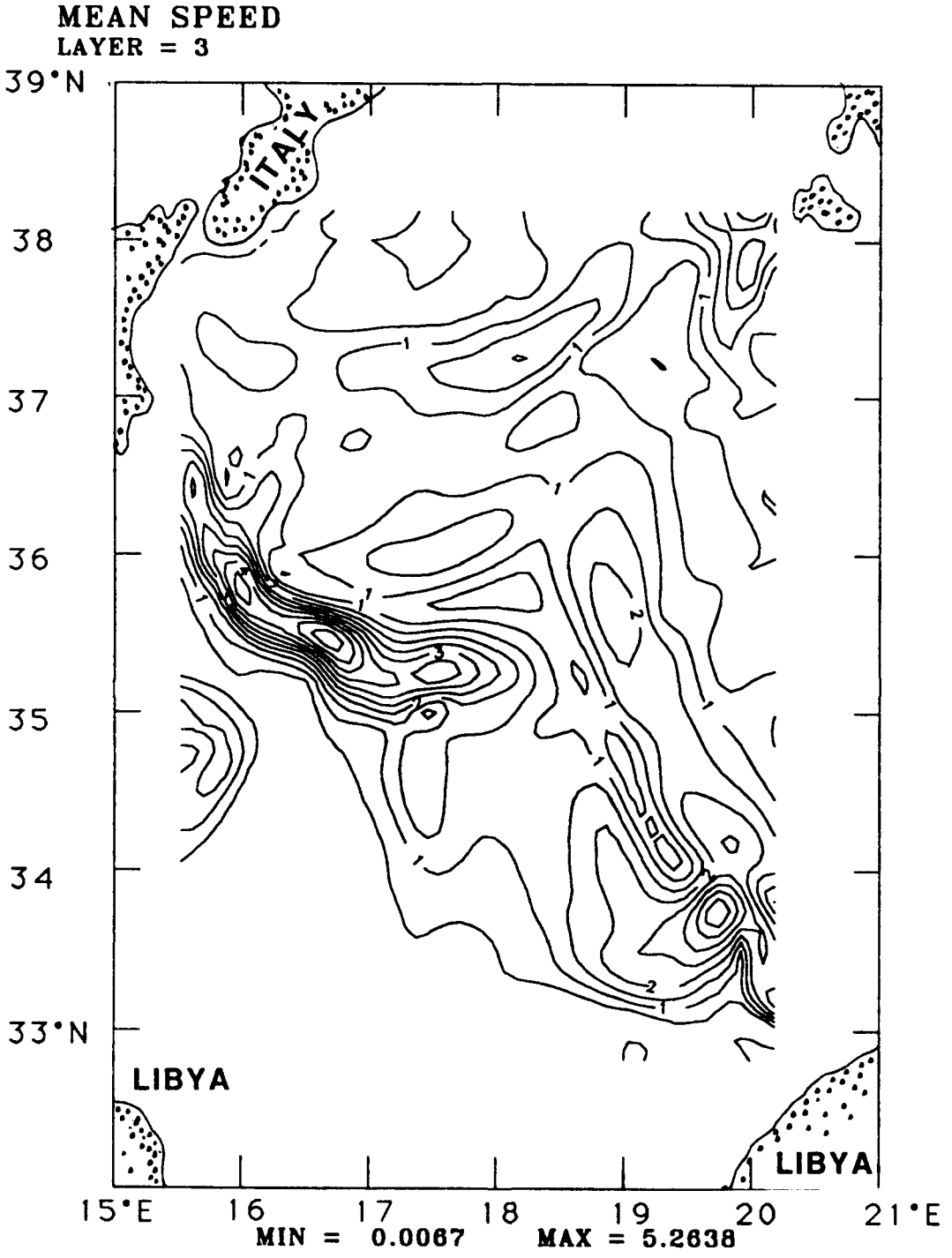

Figure 4.2.1. Modeled Deep Layer Circulation in the Ionian Basin.

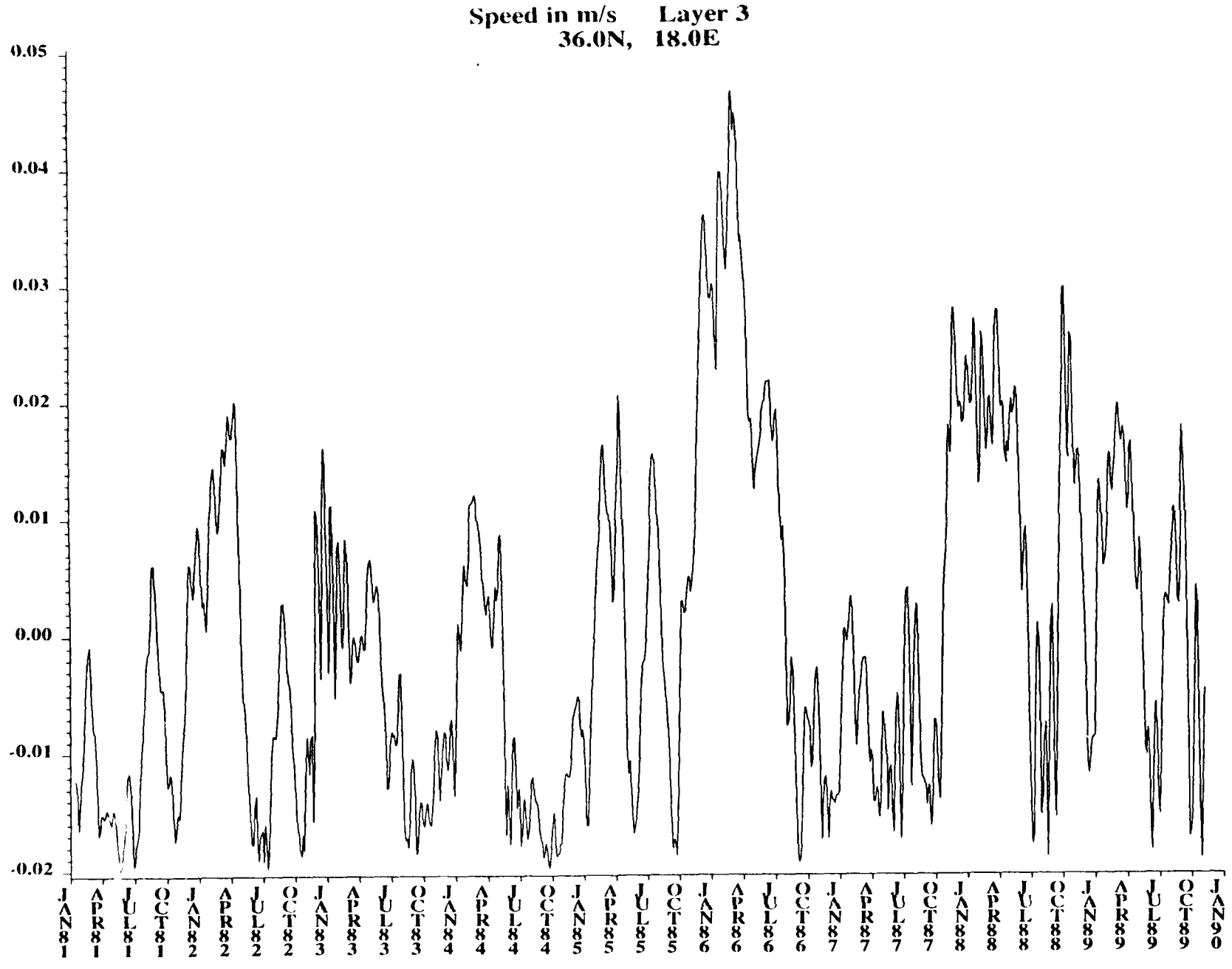

Figure 4.2.2. Modeled Temporal Variability of Deep Currents at 36°N, 18°E in the Ionian Basin.

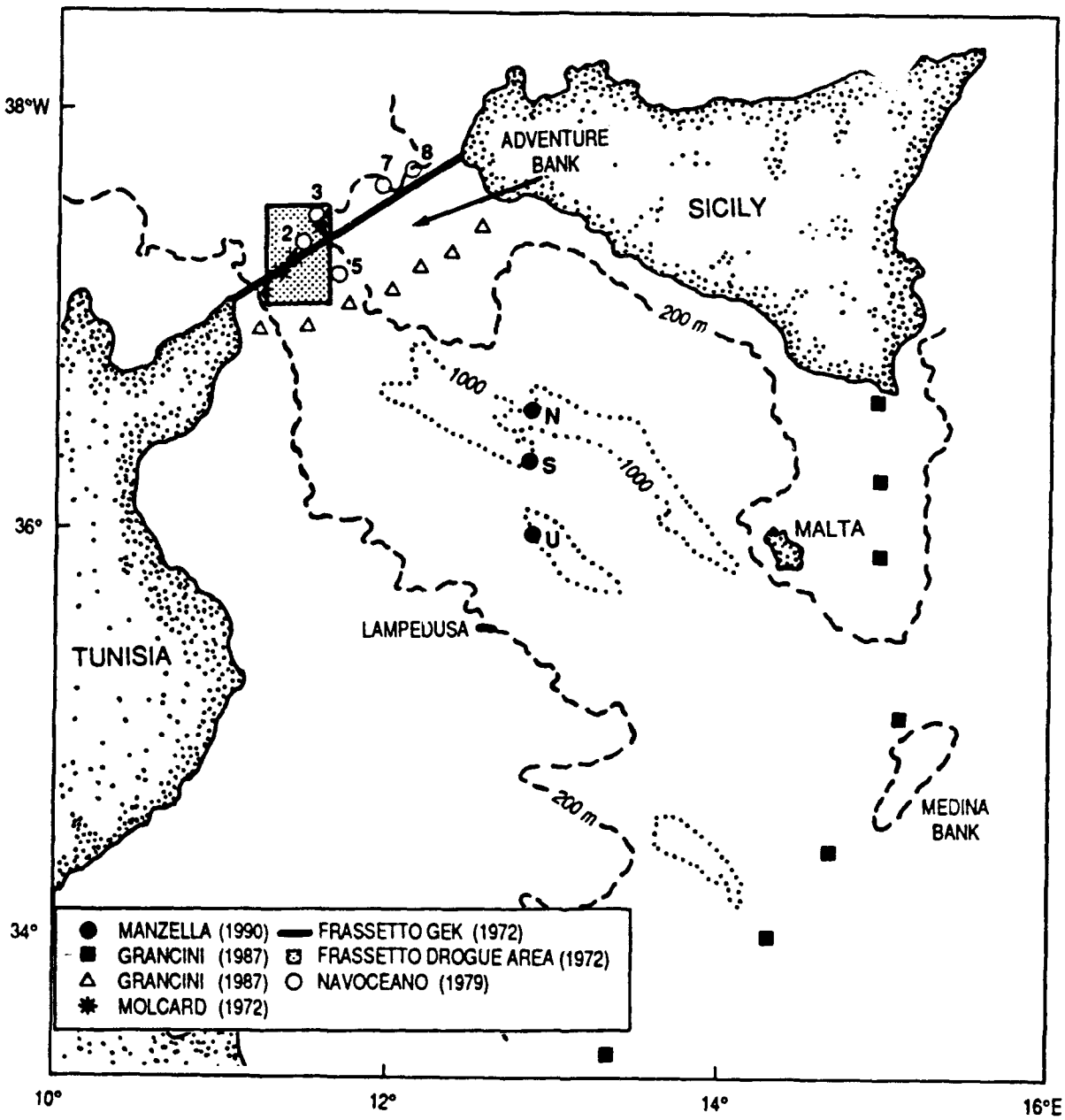

Figure 4.3.1. Location of Current Measurements in the Strait of Sicily.

Table 4.3.1. Summary of current measurements in the Strait of Sicily.

Reference	Location	Instrument	Depth (m)	Duration
Frassetto (1972)	N. Strait	GEK[1]	Surface	September–October 1963
Frassetto (1972)	N. Strait	Parachute drogue	20	October 1963
Frassetto (1972)	N. Strait	Parachute drogue	50–60	April 1963, September 1962
Frassetto (1972)	N. Strait	Parachute drogue	200	October 1962, 1963
Frassetto (1972)	N. Strait	Parachute drogue	300	April, October 1963
Molcard (1972)	N. Strait	Meters	50	May 1970 (4 days)
Molcard (1972)	N. Strait	Meters	50	May 1970 (13 days)
Molcard (1972)	N. Strait	Meters	50	May 1970 (13 days)
Molcard (1972)	N. Strait	Meters	50	May 1970 (13 days)
Molcard (1972)	N. Strait	Meters	150	May 1970 (4 days)
Molcard (1972)	N. Strait	Meters	150	May 1970 (13 days)
Molcard (1972)	N. Strait	Meters	150	May 1970 (13 days)
Molcard (1972)	N. Strait	Meters	300	May 1970 (4 days)
Molcard (1972)	N. Strait	Meters	300	May 1970 (13 days)
Molcard (1972)	N. Strait	Meters	300	May 1970 (13 days)
NAVOCEANO (1979)	N. Strait	Meters	58, 305, 428	December 1976–March 1977
NAVOCEANO (1979)	N. Strait	Meters	64	December 1976
NAVOCEANO (1979)	N. Strait	Meters	311, 468, 896	December 1976–March 1977
NAVOCEANO (1979)	N. Strait	Meters	69, 316, 450	December 1976–March 1977
NAVOCEANO (1979)	N. Strait	Meters	57, 140	December 1976–March 1977
NAVOCEANO (1979)	N. Strait	Meters	63, 146	December 1976–March 1977
Grancini and Michelato (1987)	N. Strait	Meters	11 stations[2]	March 1976–March 1977
Grancini and Michelato (1987)	S. Strait	Meters	8 stations[2]	July 1981–July 1982
Manzella et al. (1990)	C. Strait	Meters	80–107[3]	November 1985–June 1986
Manzella et al. (1990)	C. Strait	Meters	107–145[3]	November 1985–June 1986
Manzella et al. (1990)	C. Strait	Meters	80–130[3]	November 1985–June 1986

[1]Geomagnetic Electrokinetograph tow.
[2]The current meter depths of these stations are unspecified in the available literature; however, the results indicate that they extend throughout the water column.
[3]These current meters were redeployed at slightly different depths during March 1987.

Both the Atlantic and the Levantine waters attain their highest velocities and net transport through the strait in the winter (January-March). During the winter the Atlantic water adheres to the African coast, and during the summer (July-September) this water mass spreads across the channel from the Tunisian to the Sicilian coast. Manzella et al. (1990) estimated that, when comparing the summer to the winter, the mean eastward flow increased threefold (from 5 to 15 cm/sec). His analysis of several geographically and temporally diverse current data sets also revealed that the Atlantic water flow does not constitute a broad homogeneous current, but one characterized by high spatial and temporal variability. This property of the currents appears to be relatively consistent throughout the majority of the measurements throughout the strait.

The analysis of Grancini and Michelato (1987) indicated that the tidal component of the current is a prime contributor to the flow over the Sicilian shelf and the currents here are primarily wind driven, especially during the winter months, but that inertial currents dominate the flow characteristics on the Libyan shelf. Quantitatively, the tidal component on the Sicilian shelf appears to have an amplitude of about 10 cm/sec, and the amplitude of the inertial currents along the Libyan coast attain a maximum value of approximately 25 cm/sec, which may persist for several days.

The remainder of the Strait of Sicily current assessment will quantify the expected current speeds from a composite of all known measurements in following three generic areas: the southern strait along the approximate longitude of Malta, the central strait near Lampedusa, and the northern strait between Tunisia and Sicily.

The best set of current measurements in the southern strait was collected by Osservatorio Geofisico Sperimentale (OGS) from July 1981 to July 1982 and documented by Grancini and Michelato (1987) and Manzella et al. (1990). Unfortunately, little quantitative information concerning extreme and average currents measured at various depths was provided. However, an analysis of current time series along the moorings in the southern strait indicated that the Sicilian continental shelf is dominated by a steady southeasterly wind-induced current (25 cm/sec) which increases to 30 cm/sec in the winter. Near Malta the mean direction is southward at 10 cm/sec. In the vicinity of and to the south of Medina Bank, low-frequency, clockwise-rotating currents were present, an event that suggests the existence of eddies.

Manzella et al. (1988a&b; 1990) were instrumental in quantifying the currents in the central Strait of Sicily. During the Janus Experiment, the Stazione Oceanografica deployed three current meter moorings in the central strait to the north of Lampedusa. These moorings were recovered and replanted once over their 8-month duration (November 1985 to June 1986). Figure 4.3.2 (after Manzella et al., 1990) shows the current time series measured by the near-surface meters over the duration of the deployment. The numbers above the records indicate the current meter depths and the dashed lines indicate when the meters were recovered and redeployed. Maximum

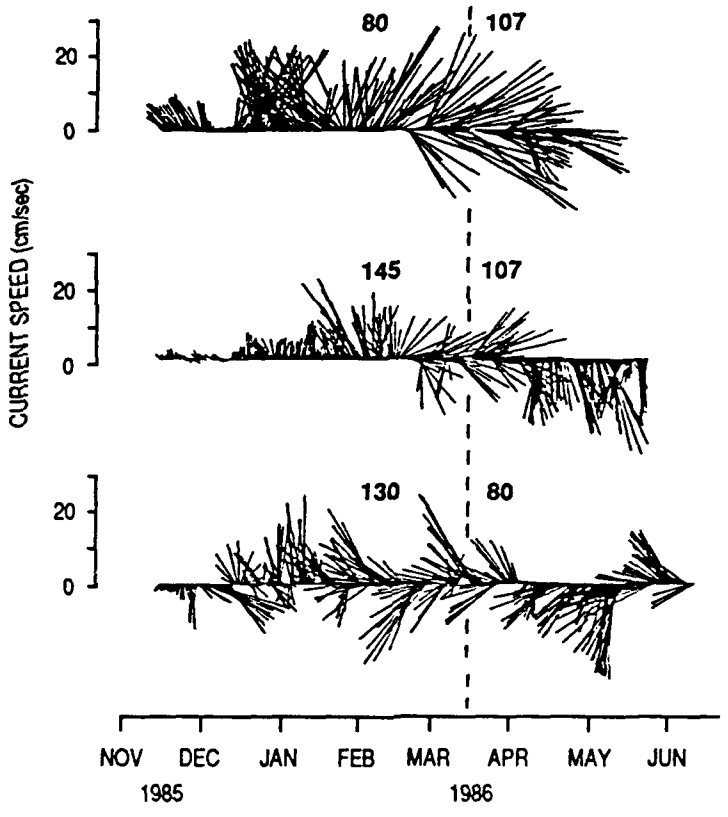

Figure 4.3.2. Current Meter Results in the Central Strait of Sicily from the Janus Experiment (Manzella, 1990).

current speeds observed over the duration of this time series were on the order of 30–35 cm/sec.

Two dynamic zones were apparent in the measurements. The northern and central moorings reflected a rectilinear flow with a single large-scale reversal in March; the southern mooring demonstrated evidence of numerous gyres. Attempts to correlate these data with numerous physical phenomena indicate that a variety of motions were probably superimposed on the mean Atlantic water flow during the measurement period. Figure 4.3.3 (after Manzella et al., 1988) contains the geostrophic velocities, which have been adjusted by the actual current meter data, along the moored current meter section to the north of Lampedusa during March and June 1986. Dashed lines indicate a generally northward flow (indicative of the Levantine intermediate water), and solid lines (characteristic of the Atlantic Water) indicate a generally southward flow. Bottom current velocities in the central strait are highly geographically dependent; the higher values are in the deeper portions of the strait. Since Levantine water seeks the deepest areas to pass into the western basins, this generalization is probably true for the entire Strait of Sicily region. In addition, the decreased current speed and, hence, net transport in the deep Levantine intermediate water from March to June is obvious. During June, a recirculation pattern of the Levantine water can be found in the current reversal near the seafloor. Table 4.3.2 statistically tabulates the currents observed at the three moorings during selected periods. The differences in current speed and transport observed in this data set are comparable to those documented by other researchers.

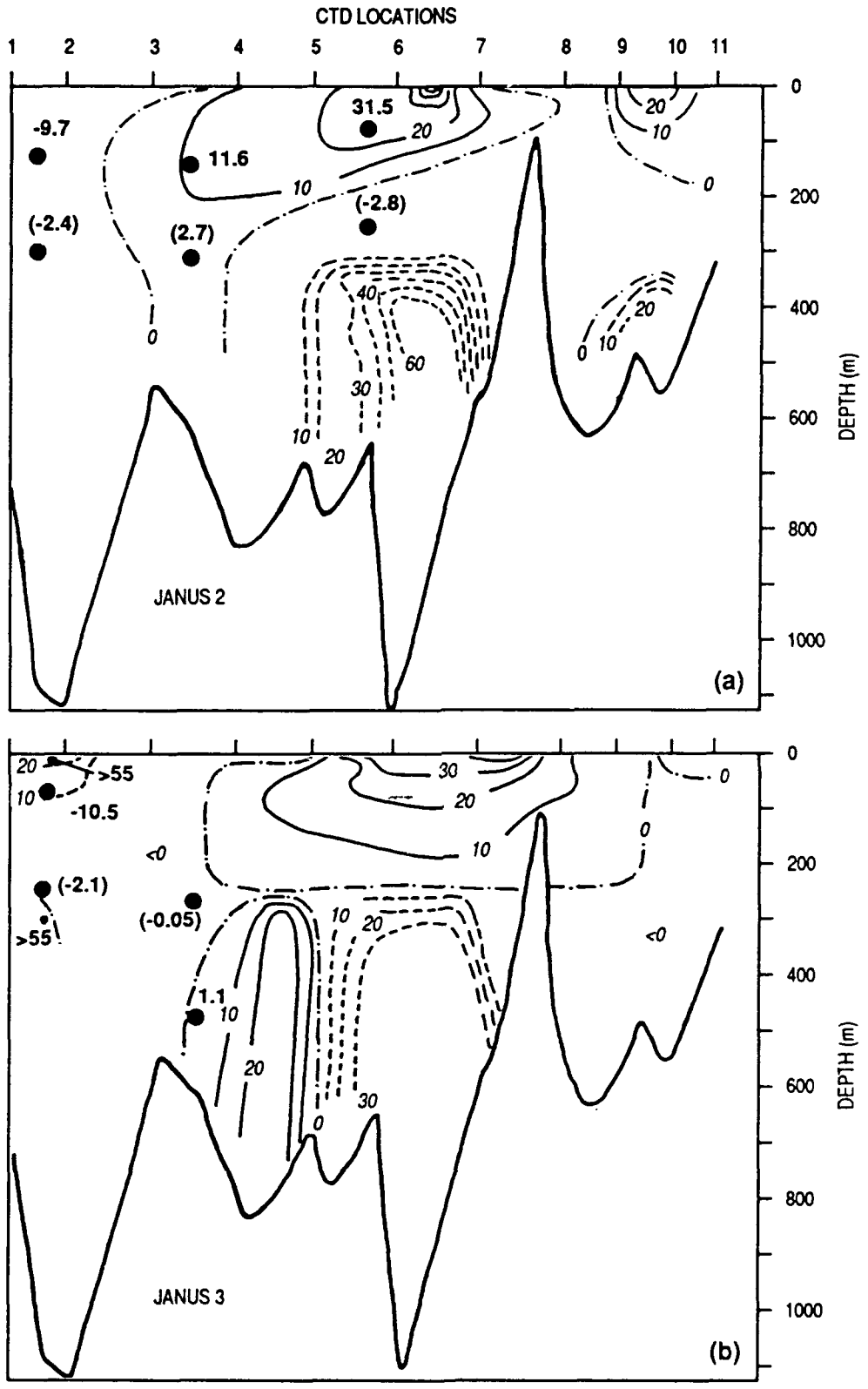

Figure 4.3.3. Measurement Adjusted Geostrophic Current Velocities in the Central Strait of Sicily During March (a) and June (b) 1965 (Manzella, 1988).

Table 4.3.2. Statistics of the Current Meter Moorings in the Central Strait (after Manzella et al., 1988a&b).

Mooring	Depth (m)	East-West (cm/sec)	Std. Dev.
15–30 Nov			
N	255	-3.91	2.67
N	355	-3.97	3.36
S	320	-2.19	2.37
S	520	0.42	1.15
U	305	1.64	2.29
U	405	1.29	1.37
15–30 March			
N	325	-9.38	3.15
N	450	-10.32	4.48
S	282	1.89	3.18
S	485	0.36	1.17
U	255	-3.81	5.03
25 May–5 June			
N	325	-3.20	1.95
N	450	-4.50	3.10
S	282	0.55	2.90
S	482	1.20	1.60
U	255	-2.05	3.60

By far, the largest quantity of current measurements was made in the northern strait between Sicily and Tunisia. An excellent set of current measurements in the northern strait was collected by OGS from March 1976 through March 1977 and documented by Grancini and Michelato (1987) and Manzella et al. (1990). Figure 4.3.4, based on these data, provides a cross section of the mean winter currents across the Strait of Sicily to the Tunisian coast. Positive values delineate a southerly flow that consists primarily of Atlantic water into the Ionian Sea, whereas negative values show the northerly subsurface flow of Levantine intermediate water into the western Mediterranean. The summer depiction along this section is qualitatively the same, but maximum values of both water masses are strongly reduced.

Molcard (1972) reported the results of a series of four vertical current moorings, which were made across the Tunisian half of the northern strait during May 1970. Although these measurements were over a short duration (three current meter strings were implanted for 13 days and one for 4 days), some meters were located in the Levantine intermediate water layer. A synopsis of these current measurements are tabulated in Table 4.3.3. Minus values of speed indicate a southeasterly flow; positive values denote a northwesterly flow. Moorings 2 and 3 were located over the preferential flow path of the Levantine intermediate water at the deepest part of the sills of the northern Strait of Sicily (see Fig. 4.3.1 for locations). Although the deepest current meters are not close to the seafloor, these data probably provide a liberal estimate of the average current speeds to be expected on the seafloor.

Frassetto's (1972) measurements include surface geomagnetic electrokinetograph (GEK) results across the northern strait and current drogue measurements in the vicinity of the deepest portions of the sills. The GEK results, measured at six time intervals during September–October 1963, show a south-southeast surface transport down the northern strait at speeds ranging from 4.1 to 151 cm/sec. The area where current drogue measurements were conducted is shown in Figure 4.3.1, and statistics of the observed currents at depths of from 20 to 300 m are tabulated in Table 4.3.4.

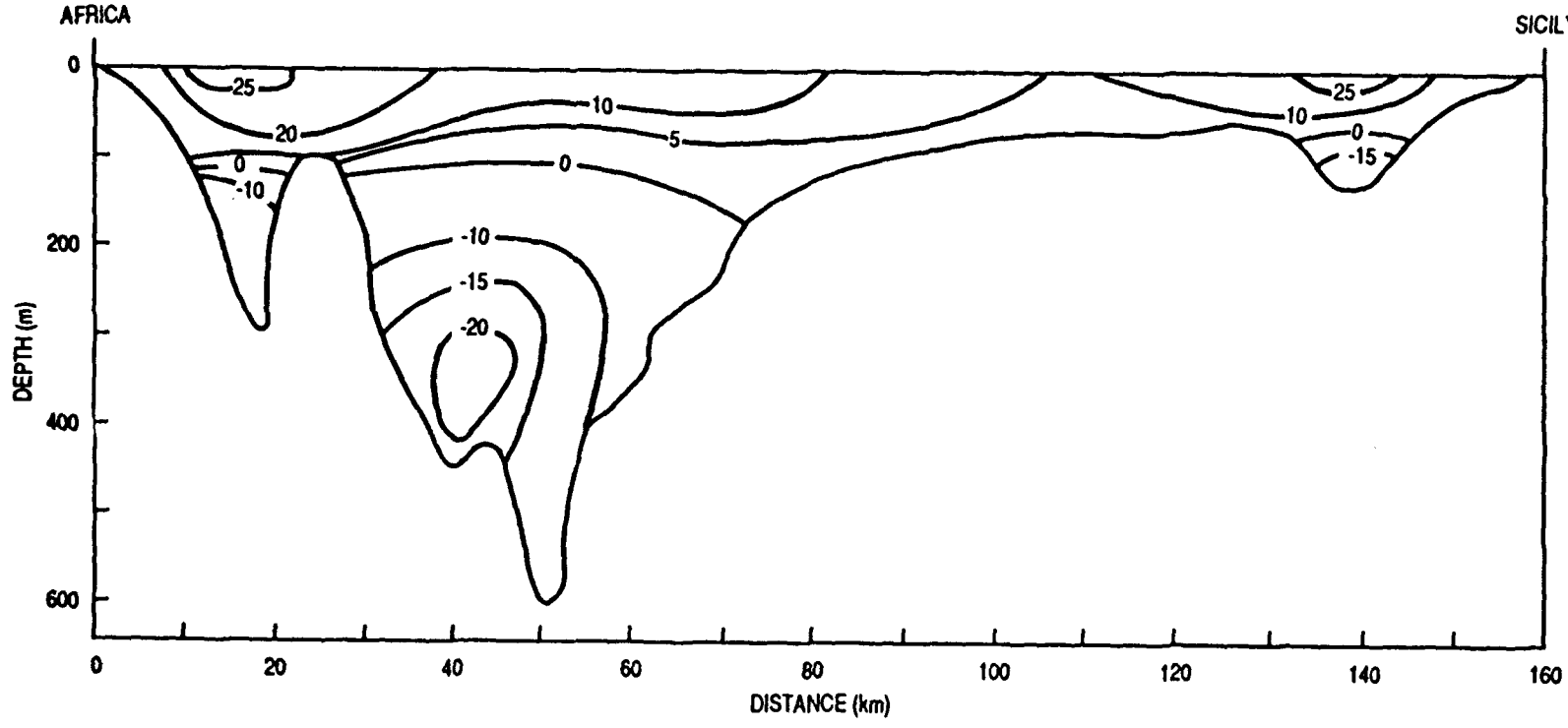

Figure 4.3.4. Measured Currents Across the Northern Strait of Sicily (Grancini, 1987).

Table 4.3.3. Current Statistics from Molcard (1972) Measurements in the Northern Strait.

Mooring Number	Position	Seafloor Depth (m)	Depth (m)	Average Speed (cm/sec)
4	37°11'N,11°10'E	190	50	-29.4
3	37°23'N,11°34'E	440	300	32.5
3	37°23'N,11°34'E	440	150	14.3
3	37°23'N,11°34'E	440	50	-2.0
2	37°19'N,11°24'E	550	300	1.7
2	37°19'N,11°24'E	550	150	-0.8
2	37°19'N,11°24'E	550	50	0
1	37°16'N,11°18'E	385	300	2.5
1	37°16'N,11°18'E	385	150	-0.7
1	37°16'N,11°18'E	385	50	-4.7

Table 4.3.4. Drogue Measurement Statistics of Frassetto (1972) in the Northern Strait.

Date	Depth (m)	Minimum Speed (cm/sec)	Maximum Speed (cm/sec)
April, September, October	20	0.2	0.9
April, September, October	50-60	0.15	1.6
October	200	0.01	0.55
April, October	300	0.05	0.43

In December 1976, the U.S. Naval Oceanographic Office (NAVOCEANO) deployed five current meter moorings in the northern strait (Fig. 4.3.1 gives the locations), some very near the seafloor. Table 4.3.5 presents statistical tabulations of these measurements, which were gathered over a 3-month period from mid-December 1976 until mid-March 1977. Moorings 2, 3, 5, 7, and 8 were in 444 m, 912 m, 465 m, 156 m, and 162 m of water, respectively (the latter two were atop Adventure Bank adjacent to the Sicilian side of the strait).

Figure 4.3.5 shows the modeled results of temporal variability in three layers at 37.2°N, 11.7°E in the northern strait over a 9-year period. Although the boundaries between these layers are determined by an undulating isopycnal, the upper layer is typical of Atlantic Water circulation and the lower two layers are influenced by the Levantine flow, since the bottom layer is very thin. This position nearly coincides with that of NAVOCEANO current mooring no. 5 on which meters were located at 69 m, 316 m, and 450 m deep. A cursory comparison of the modeled and measured data sets indicates that both similarities and differences exist. For example, the bimodal properties of both speed and direction in the shallow current meter measurements are reflected in the modeled results. However, the modeled deep currents are considerably lower than those recorded on the deep current meter.

A summary of the numerous current measurements in the northern Strait of Sicily provides coherent trends over long periods; however, large temporal and geographic variabilities exist over shorter periods. Specifically, long-period current characteristics that depict the core positions and magnitude of the Atlantic and Levantine waters during the winter are probably accurately represented in Figure 4.3.4. The magnitudes for both water masses are greatly diminished in the summer. Time series current measurements at all depths shown in the above tables demonstrate considerable variability over short periods. Generally, however, the highest current speeds observed are in the near-surface Atlantic water layer (as great as 2.95 kt), with speeds in all layers containing high standard deviations as a function of both time and space. Current speeds at intermediate and deep levels in the northern strait can attain a velocity as great as 40 cm/sec.

The tidal components of the currents in the Strait of Sicily vary greatly in magnitude. The data of Grancini and Michelato (1987) in the southern portion of the strait indicate that the diurnal and semidiurnal tidal components are greatest on the Sicilian shelf (10 cm/sec) and decrease markedly toward the Libyan shelf. The long time series measurements made by NAVOCEANO (1979) at the near-surface layers in the northern strait indicate that tidal currents are highly variable and range from near-zero values to as great as 30 cm/sec.

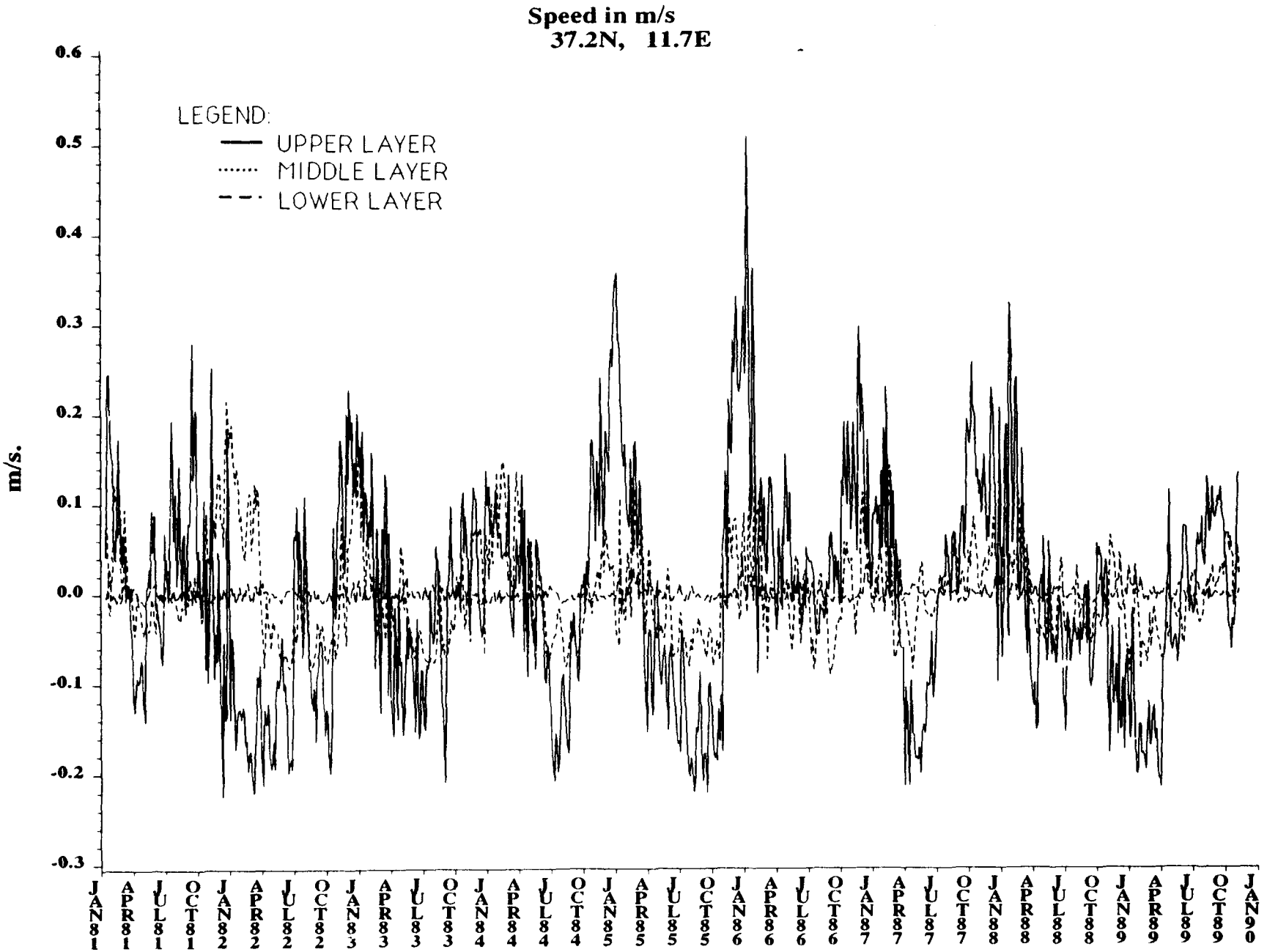

Figure 4.3.5. Modeled Temporal Variability of Currents in Three Layers at 37.2°N, 11.7°E in the Strait of Sicily.

Table 4.3.5. Statistics of the NAVOCEANO deployed current meters in the Northern Strait.

Mooring Number	Depth (m)	Max. Speed (cm/sec)	50% Speed (cm/sec)	Modal Speed (percentile)	Modal Speed (cm/sec)	Modal Direction (°T)
2	58	39	10	15	5	Variable
2	428	25	5	Bimodal	Bimodal	≈360
				29	1	
				27	6	
3	311	27	9	15	7	≈165
3	468	27	9	18	8	≈180
3	896	29	9	15	7	200
5	69	39	9	Bimodal	Bimodal	Bimodal
				18	3	≈100
				12	31	335
5	316	23	9	18	7	345
5	450	21	8	20	7	015
7	57	39	14	5–10	0–20	150–359
7	140	39	14	10	9	150–240
8	63	39	14	10	10	110
8	146	37	9	14	5	Bimodal
						50
						270

4.4 Strait of Sardinia

Features associated with significant currents in the Strait of Sardinia are the eastward-flowing Algerian current, which near the coast of Africa, and the semi-permanent eddies, the primary of which has been observed in the central strait. Unfortunately, no current measurements could be located in this region; therefore, geostrophic approximations must be used to quantify current speeds and directions. Garzoli and Maillard (1979) documented geostrophic calculations from several historical hydrographic sections in the area of the strait. A vertical section of geostrophically derived current speeds (based on an 800-m level of assumed no motion) across the strait at approximately 8°30'E is shown in Figure 4.4.1.

The surface velocities that range from 20 to 30 cm/sec and the slopes of the current speed that decay below these values agree well with the data set of Perkins and Pistek (1990). However, the 100-cm/sec surface velocity associated with an eastward-flowing

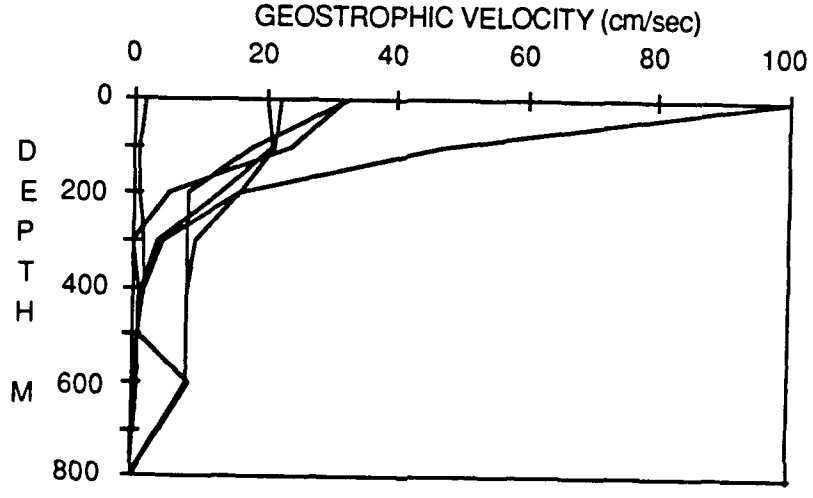

Figure 4.4.1. Geostrophic currents across the Strait of Sardinia after Garzoli and Maillard, 1979.

current in the northern portion of the strait in Garzoli's data is unique. The reason for this large difference in surface speeds may be due to the existence of the gyre in the strait when the high speeds were derived and its absence when speeds were lower. Note that since all estimates in the strait of Sardinia were geostrophically derived and referenced to a level of no motion in the abyssal waters, the near-bottom currents may be stronger than estimated. A modeled time series of currents in the deep layer (layer 3) at 38.3°N, 9°E from 1981 to 1990 is shown in Figure 4.4.2. Average currents are extremely low and generally agree with the geostrophic calculations of Garzoli and Maillard (1979).

4.5 Western Alboran Basin

A large quantity of current measurements from numerous sources and with numerous devices at a variety of depths are available in the western portion of the Alboran basin. Unfortunately, much of this data is embedded in foreign journals and are difficult to obtain. Although all sources of known measurements are not available, a relatively coherent description of the current regime in this area is possible. Figure 4.5.1 presents a composite of the geographical distribution of current measurements available in the literature. The measurement devices used include current meters; neutrally buoyant, free-floating current measuring systems; sonobuoys from which drift rates were calculated; and geostrophic calculations. Oceanographic measurements that enabled the geostrophic estimates and the sonobuoy locations are too numerous to be displayed in this figure. The locations of the drifting floats represent positions of initial deployment. The large quantity of data, the variety of depths to which sensors were deployed, and the observed temporal variability in the measurements make an attempt to quantify the currents in portions this area difficult. The available data base of currents in this region can afford higher resolution analyses of specified areas. The remainder of this documentation will focus first on the circulation and current magnitudes for the surface layer, followed by that layer occupied by the Levantine intermediate water and, finally, the abyssal circulation of the deep-water mass.

At the surface, the east-northeast-flowing Atlantic jet enters the Alboran Basin through the Strait of Gibraltar and flows parallel to the coast of Spain. Between the Atlantic jet and the coast of Spain (landward of the 200-m depth contour) currents are light and directions are variable. At approximately 4°30'W the surface currents begin to deflect to the southeast and the south to form a clockwise gyre, which occupies the entire western basin. Figure 4.5.2 (after Burkov, 1979) provides an excellent depiction of the vertical extent of the Atlantic jet adjacent to the Strait of Gibraltar. Positions of these current meter moorings are provided in Figure 4.5.1. The 96-cm/sec current speed in the center of the Atlantic jet (Burkov, 1979) is higher than that documented by La Violette (1986) of 1.2 m/sec using short term sonobuoy drift rates. Kinder (1984) showed that nonlinear internal waves, which emanate from the strait, propagate eastward about 50 km into the basin with a phase velocity of 1.5 to 2.0 m/sec, which

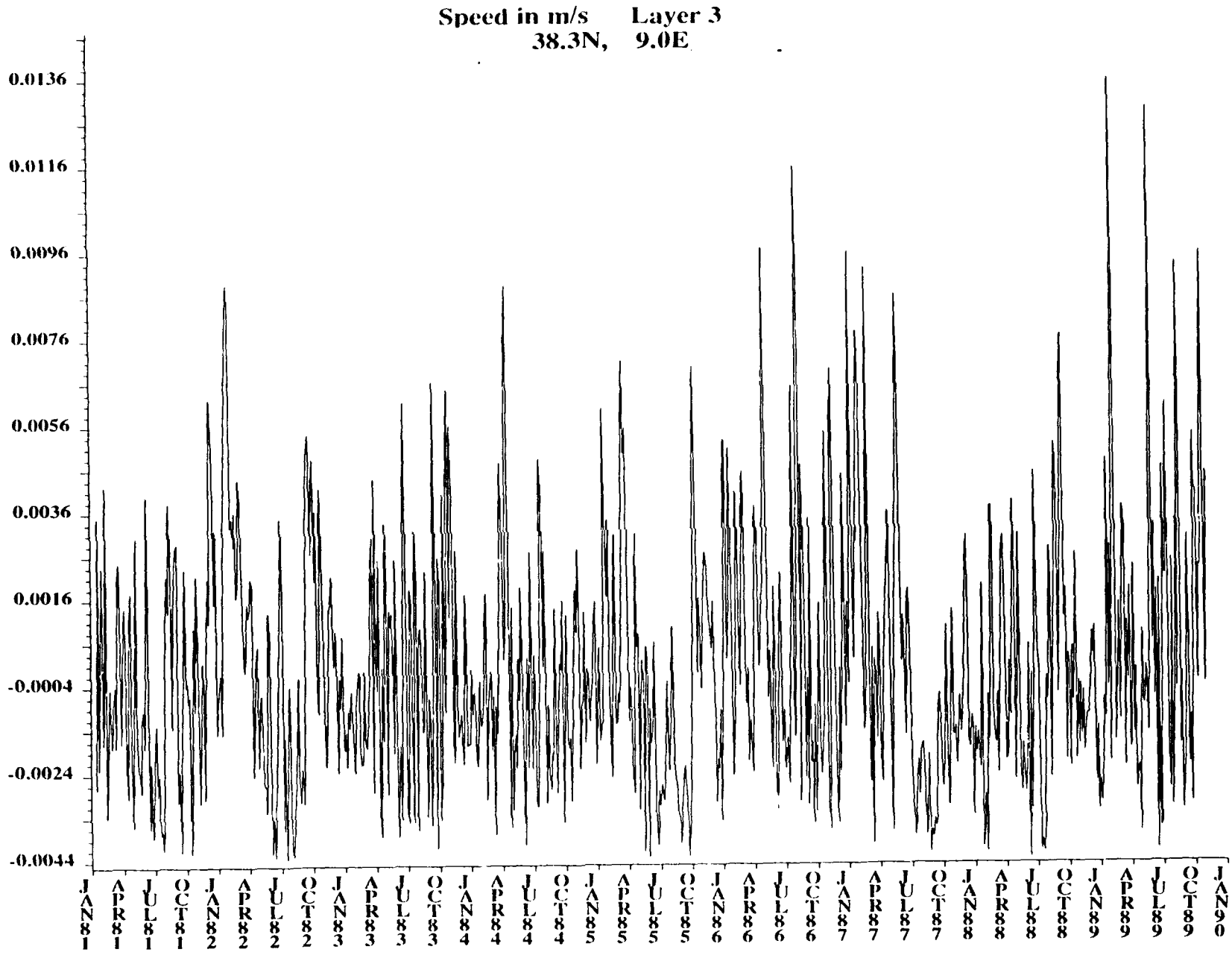

Figure 4.4.2. Modeled Temporal Variability of Deep Currents at 38.3°N, 9°E in the Strait of Sardinia.

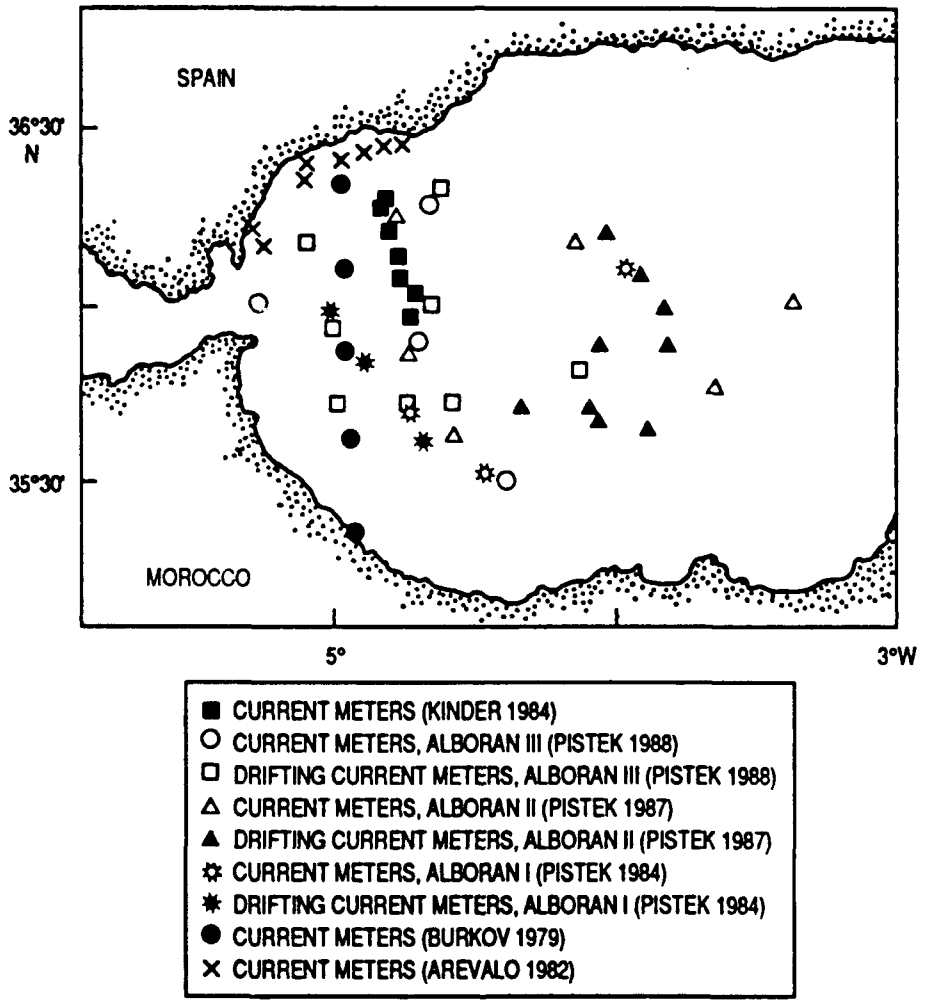

Figure 4.5.1. Location of Current Measurements in the Western Alboran Basin.

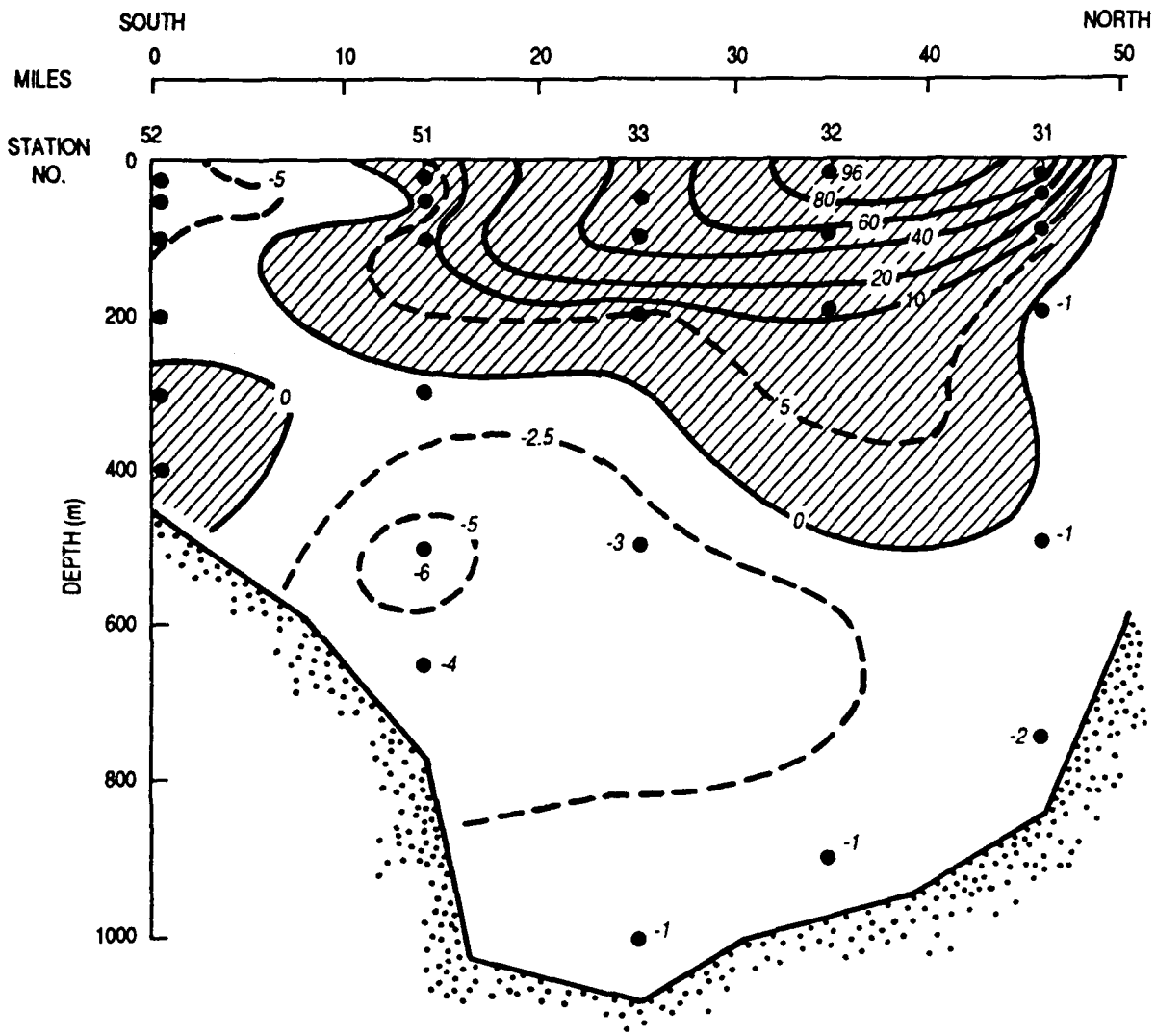

Figure 4.5.2. Measured Currents Across the Entrance to the Western Alboran Sea (Burkov, 1979).

resulted in a displacement peak velocity of approximately 40 cm/sec. In the western and southern branches of the Alboran gyre, velocities appear to be about half those in the north. Based on short-period sonobuoy drift studies, speeds in the central Alboran gyre ranged from 90 cm/sec on the edge to approximately 20 cm/sec near the center. Currents in the area between the coast of Spain and the seaward Atlantic jet in waters shoaler than 200 m were variable in direction and ranged from 5 to 20 cm/sec, depending on the time and depth of observation (Arevalo and Garcia, 1982).

Flow at intermediate depths (300 to 600 m) within the Levantine intermediate water mass is generally toward the strait; however, periods of stagnation are common and evidence of a counterclockwise flow has been observed (Kinder, 1984). Findings from the NATO-sponsored series of ALBORAN I, II, and III exercises (Pistek, 1984, 1987, and 1988) markedly contributed to the determination of the circulation at intermediate and abyssal depths in the western Alboran basin. Data from this exercise series included the deployment of 13 double current meter moorings, 21 neutrally buoyant current meter floats, and geostrophic currents from numerous oceanographic stations from 1980, 1982, and 1983 (Fig. 4.5.1). Current velocities in the intermediate water layer from the various current meter moorings appeared to range from averages of under 1 to 5 cm/sec. A maximum value of 13 cm/sec was observed in the 1980 and 1983 data set about 35–55 nm southeast of the strait.

A well-defined abyssal (from 600 m to the seafloor) boundary current along the Moroccan continental slope extends from Alboran Island at 3°W to the strait entrance. Speeds within this current are the highest observed in the abyssal circulation of the western Alboran basin. Just to the north of this flow is evidence of an eastward-flowing abyssal current. North of this current in the center of the basin is a weak counterclockwise flow that exhibits substantial periods of stagnation. Deep currents in the northern portion of the western Alboran Basin are erratic and slow (2 cm/sec), and net flow is to the west. Data from multiple moorings and floats along the Moroccan continental slope current, which extends from 400 to 800 m deep, indicate that current speeds between 5 and 9 cm/sec are common with a maximum speed in excess of 20 cm/sec observed during the ALBORAN III measurements. Currents in the central basin below 1000 m average 2.5 to 3.7 cm/sec; maximum observed value was 7 cm/sec. Currents at 403 m between the intermediate and deep-water masses in the northern Alboran basin are approximately 2 cm/sec. A current meter moored at the easternmost reaches of the strait at 712 m (near the seafloor) recorded average speeds of 12 cm/sec and maximum values of 22 cm/sec over a 31-day lifespan in the ALBORAN III exercise. The modeled time series of currents in the abyssal waters of the Alboran basin at 36°N, 5°W over a 9-year period are shown in Figure 4.5.3. This basin exhibits the strongest annual periodicity and the highest abyssal currents of all basins addressed in this document. Abyssal currents measured by Pistek during the ALBORAN series of exercises in the vicinity of the Moroccan continental slope current provide a good correlation with the modeled results.

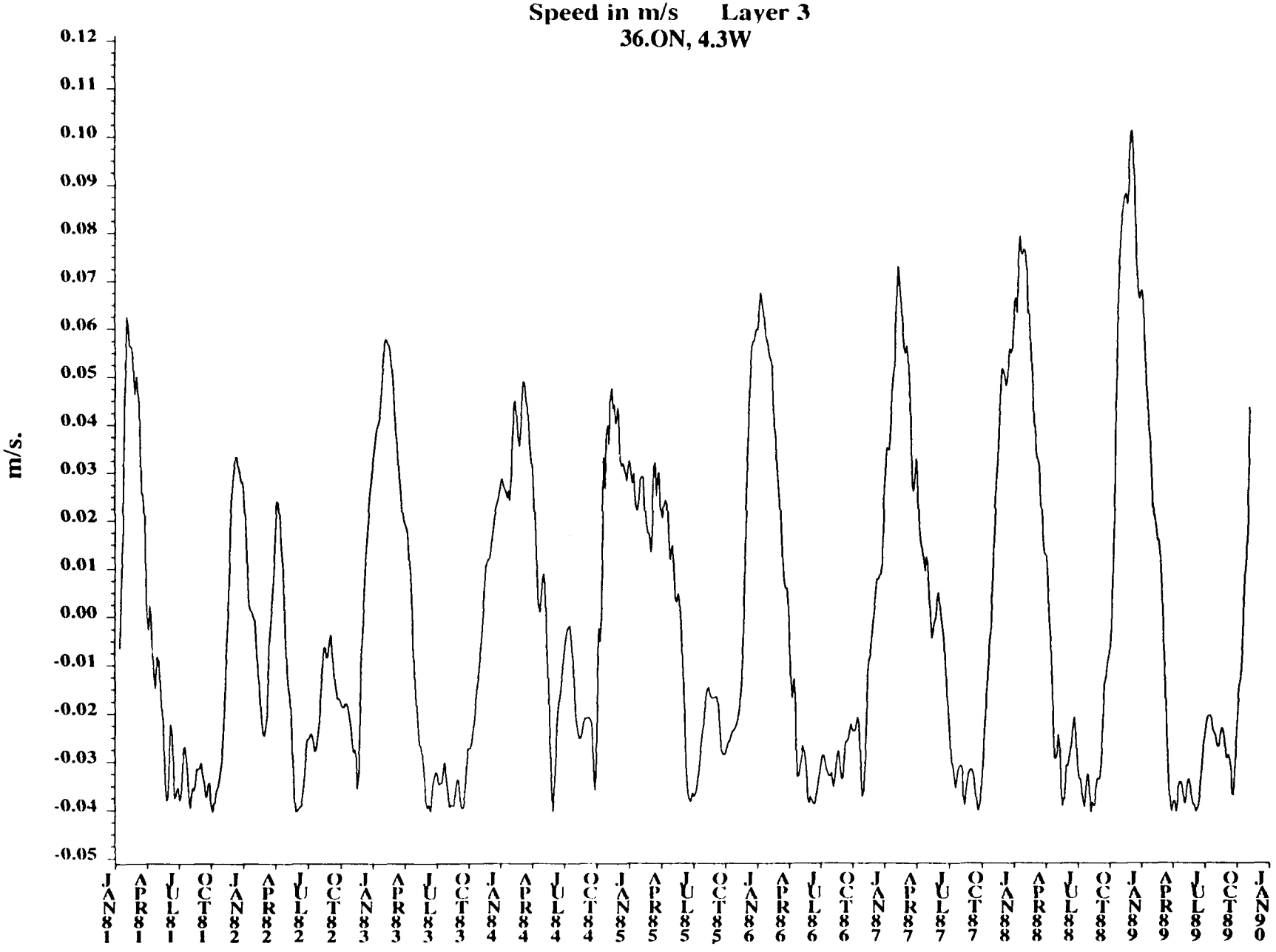

Figure 4.5.3. Modeled Temporal Variability of Deep Currents at 36°N, 4.3°W in the Alboran Basin.

4.6 Strait of Gibraltar

Literature concerning the oceanography and currents is abundant for this region. Although the first-order mechanisms and the quantification of the current regime is, for the most part, documented in the literature, the complexity of the dynamics in the area leaves many questions unanswered. Water exchange through the Strait of Gibraltar takes place over a wide range of time scales. It is estimated that 74% of the current variabilities result from the semidiurnal tides (Candela et al., 1990). At periods ranging from days to months, the isostatic responses of sea level to the atmospheric pressure field and wind stress are the primary forcing factors. Long-term (seasonal to interannual) variability is caused by the integrated effects of the mass and salt balances in the sea (Candela, 1991). Since the short-term variability is probably responsible for the highest currents at all depths in the strait, this description of current variability will be, for the most part, confined to the tidal time scales.

However, a brief explanation of the long-term variability that is present in the strait is appropriate before the effects of tidal time scales on current speed are quantified. Over a frequency range of multiple tidal cycles, the mean mass transport in the near-surface layer of the strait is to the east where Atlantic water enters the Mediterranean Sea. Mass transport in the bottom layers of the strait is to the west where Levantine intermediate water (and to a lesser extent, Mediterranean deep water) enters the Atlantic Ocean. Between these water masses is a strong shear interface layer, which is deeper at the western entrance of the strait and is shoalest at the main sill. Using multiple sources of historical current measurements, Lacombe and Richez (1982) provided an excellent portrayal of the average currents that can be expected on either side of the interface (Fig 4.6.1). From this figure, currents above the interface obviously are strongest in the vicinity of the sill and the currents below the interface are strongest to the west of the sill.

Lacombe and Richez (1982) used synoptically collected current measurements and hydrographic casts placed throughout the strait during the spring tides to produce a coherent description of the current processes and velocity structure throughout the water column for a frequency commensurate with the semidiurnal tide. The locations of the synoptic current moorings relevant to this discussion, overlaid on the generalized bathymetry, are shown in Figure 4.6.2. Although the primary current-generating forcing factor in the strait over short time scales is the semidiurnal tides, the topography of the channel exerts a considerable influence in the vertical current structure. Generically, the topography in the western approach to the strait (Figure 4.6.3) is composed of a wide shallow area with a narrow channel (at current mooring A4) oriented in an east-northeast direction. The shallowest point in the strait is the 300-m Camarinal Sill at mooring Ss. To the east of the sill at current mooring positions B'2 and C_2, the channel deepens to allow a larger area for mass transport through the strait.

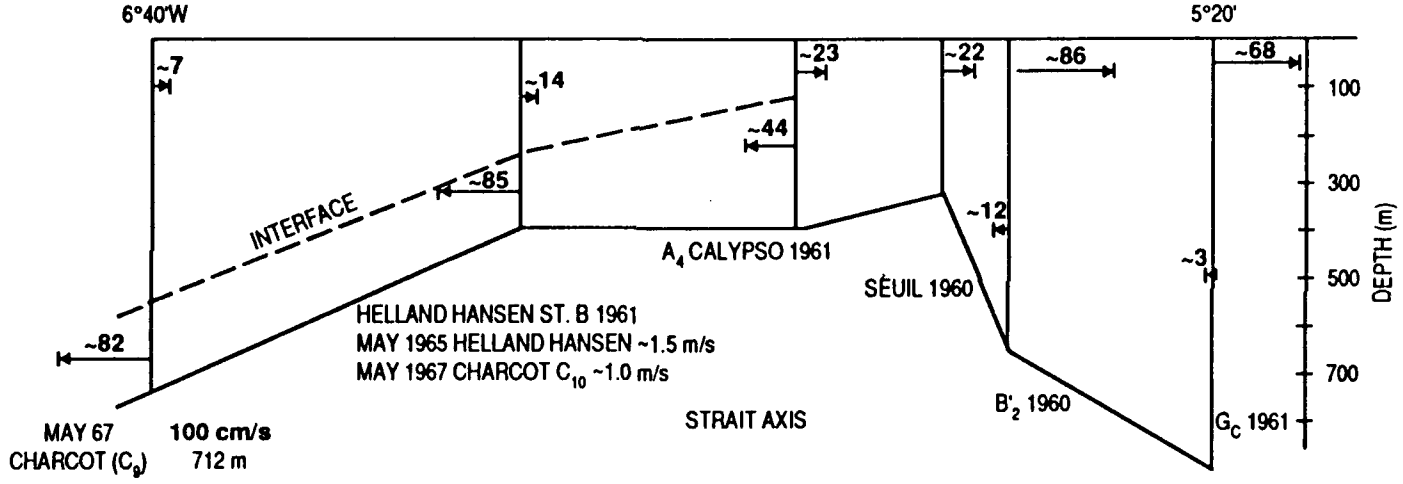

Figure 4.6.1. Average Currents in the Strait of Gibraltar (Lacombe, 1982).

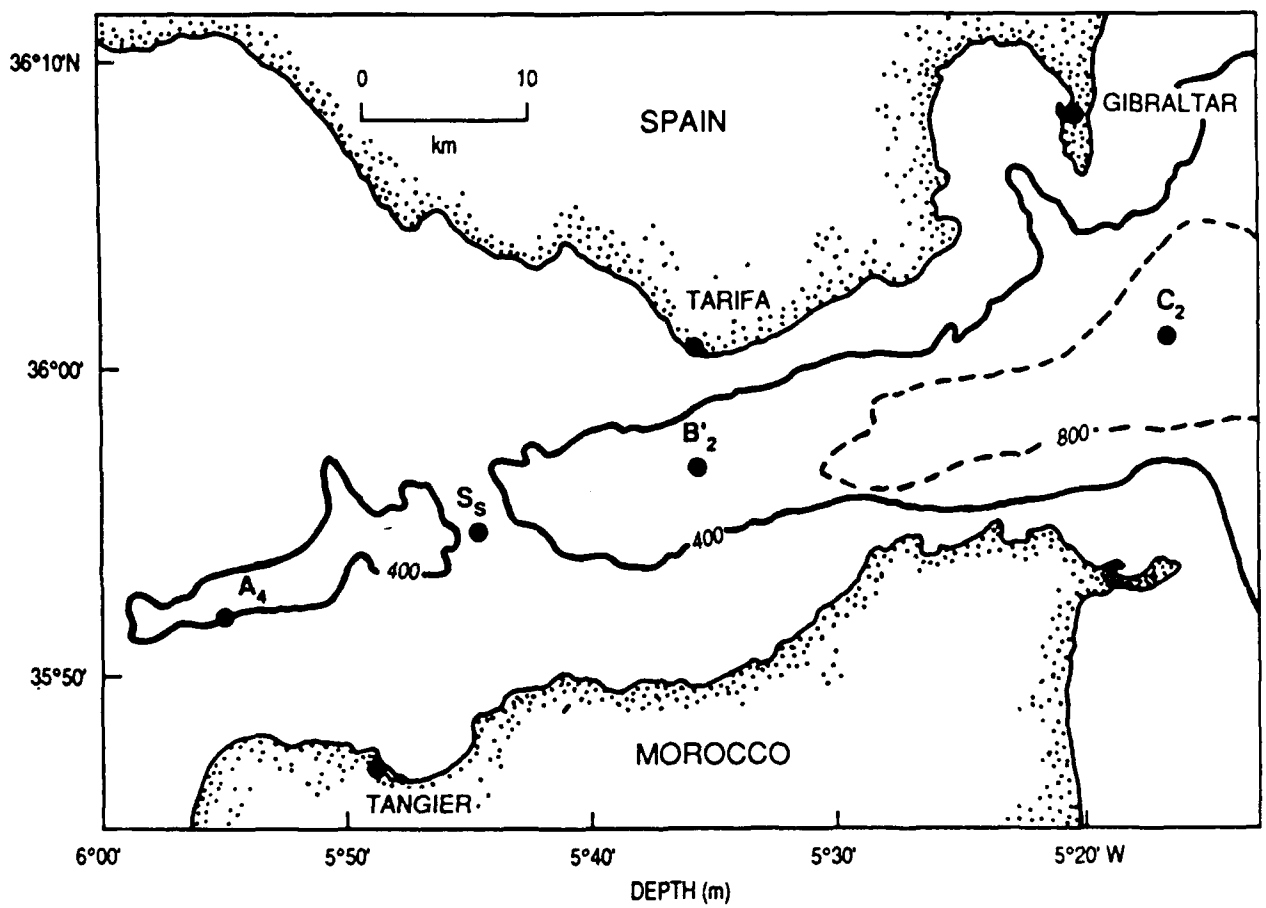

Figure 4.6.2. Location of Current Measurements in the Strait of Gibraltar.

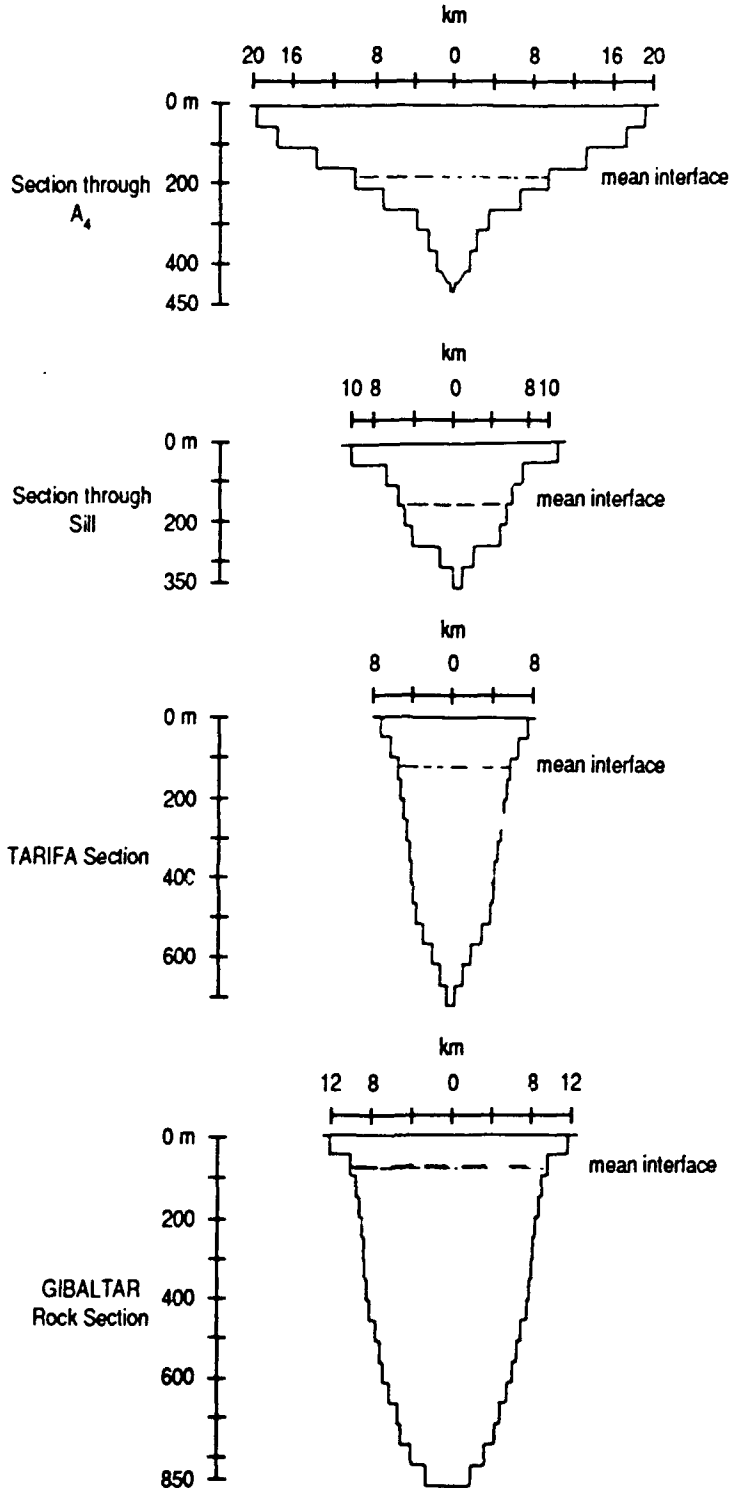

Figure 4.6.3. Topographical Cross Sections in the Strait of Gibraltar (Lacombe, 1982).

At the western entrance to the strait, the wide, shallow approaches result in a deep interface between the Atlantic and the Mediterranean waters, so the velocity of the deeper waters is very high. The mean velocity to the west of mooring A4 (at 6°15'W) above the interface is about 20 cm/sec, and the velocity below the interface between 250 m and the bottom is 140 cm/sec. At 6°20'W below a depth of 250 m, the velocity may exceed 150 cm/sec. A record speed of 245 cm/sec was observed in this area in one historical data set. Near-bottom velocities even farther to the west (at 6°44'W) are on the order of 80 to 100 cm/sec.

The temporal and vertical current variability measured simultaneously during a tidal cycle at all moorings (shown in Figure 4.6.2) are shown in Figure 4.6.4. Times on the vertical axis are either before (--) or after (+) high water (HW). The remainder of this documentation (largely extracted from Lacombe and Richez, 1982) explains the mechanisms responsible for the variability observed in this illustration, as well as a quantification of the currents at each mooring.

At mooring A4, the tidal component, which is superimposed on the mean regime, causes the deeper water to continuously flow to the west throughout the tidal cycle, while the waters above the interface tidally reverse. This event occurs because the amplitude of the tidal current is greater than the mean current in the surface layer but weaker than the mean current below the interface. Maximum near-bottom velocities at this mooring were 100 cm/sec.

Currents over the sill section at mooring Ss are much different than those to the west at A4. Currents in the upper 100 m here are about 180 cm/sec to the east and about 100 cm/sec to the west, much higher than those at A4. Unlike those at A4, currents below the interface at mooring Ss undergo a tidal reversal. Maximum current speeds below the interface are similar in both locations; however, as a consequence of the deep tidal reversing characteristics at Ss, the extreme velocity variation is greater.

At the Tarifa section (mooring B'2) near-surface currents are very high, but there is practically no important component to the west over the entire tidal cycle in the upper 50 m. In fact, during a period of approximately 4 hours, the surface current flows out over the sill while it flows in through the Tarifa section. Deep currents undergo a tidal reversal at the Tarifa section, but the deeper topography in the channel east of the sill causes the deep currents at mooring B'2 to be much more benign during both tidal cycles.

Currents in the upper 50 m at C_2, the easternmost mooring, assume a constant easterly direction with no tidal reversal, while a reversal takes place in the deeper layers. Since this area of the strait is the deepest, the Mediterranean water is much less restricted in its flow, deep current velocities here are the most benign of any area in the strait.

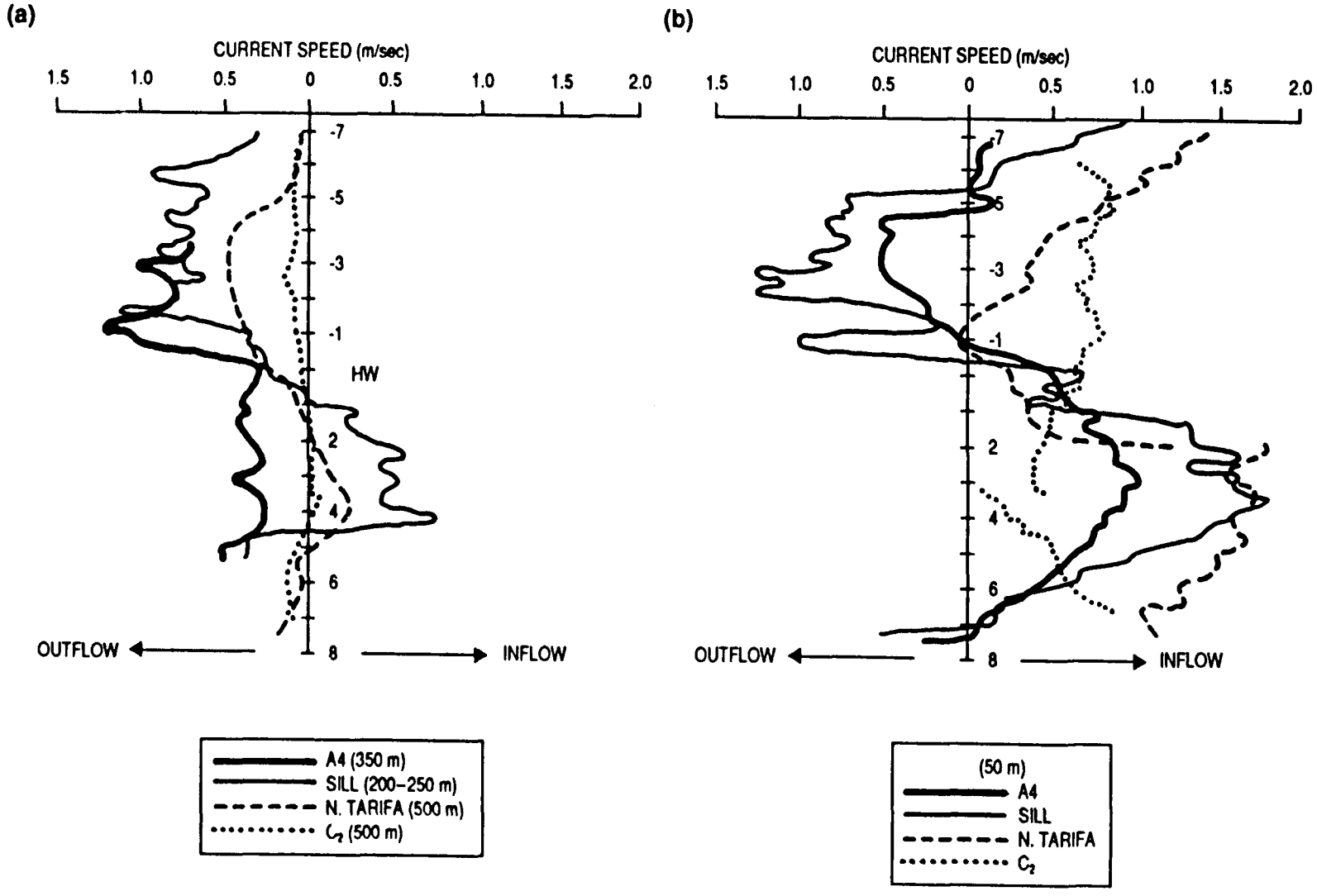

Figure 4.6.4. Deep (a) and Shallow (b) Currents Measured Simultaneously Over a tidal Cycle (modified after Lacombe, 1982).

The preceding discussion indicates that high current shear in the water column is present everywhere in the Strait of Gibraltar. Considerable difficulty can be expected in deploying any hardware in this environment. However, both surface and especially deep currents are lowest in the eastern approaches to the strait (in the vicinity of or to the east of mooring C_2).

5.0 References

Accerboni, E. and G. Grancini (1972). Mesures hydrologiques en Mediterranee Orientale (Septembre 1968). *Boll. Geofis, Teor. Appl.* 14(53-54): 3-16.

Ahmed, A. H. El-Gindy and S. H. Sharaf El-Din (1986). Water masses and circulation patterns in the deep layer of the eastern Mediterranean. *Oceanol. Acta* 9(3): 239-248.

Arevalo, L. and T. Garcia (1982). Corrientes de la Costa de Malaga, metodos y resultados. *Inf. Tecn. del I.E.O.*, Madrid (Spain), in press.

Bucca, P. J. and T. H. Kinder (1984). An example of meteorological effects on the Alboran Gyre. *J. Geophys. Res.* 89(C1): 751-757.

Burollet, P. M., J. M. Mugniot, and P. Sweer (1978). The geology of the pelagian block: margins and basins off southern Tunisia and Tripolitania. In *The Ocean Basins and Margins, 4A, The Western Mediterranean,* A. E. M. Narin, W. K. Kanes, and F. G. Stehli (eds.), New York: Plenum Press, v. 4b, p. 353.

Candela, J. (1991). The Gibraltar Strait and its role in the dynamics of the Mediterranean Sea. *Dyn. of Atmos. and Oc.* 15: 267-299.

Candela, J., C. D. Winant, and A. Ruiz (1990). Tides in the Strait of Gibraltar. *J. Geophys. Res.* 95: 7313-7335.

Carter, T. G., J. P. Flanagan, C. R. Jones, F. L. Marchant, R. R. Murchison, J. H. Rebman, and J. C. Sylvester (1972). New bathymetric chart and physiology of the Mediterranean Sea. In *The Mediterranean Sea: A Natural Sedimentation Laboratory*, D. J. Stanley (ed.), Stroudsburg (Pennsylvania): Dowden, Hutchinson and Ross, pp. 7-23.

Finetti, I. and C. Morelli (1972). Wide scale digital seismic exploration of the Mediterranean Sea. *Bollettino Di Geofisica Teorica Applicata* 14: 291-342.

Finetti, I. and C. Morelli (1973). Geophysical exploration of the Mediterranean. *Bollettino Di Geofisica Teorica Applicata* 15: 263-341.

Frassetto, R. (1972). A study of the turbulent flow and character of the water masses over the Sicilian Ridge in both summer and winter. SACLANT ASW Research Centre *Conference Proceedings No. 7*, La Spezia, Italy, September.

Garzoli, S. and C. Maillard (1979). Winter circulation in the Sicily and Sardinia Straits region. *Deep Sea Res.* 26A: 933-954.

Grancini, G. F. and A. Michelato (1987). Current structure and variability in the Strait of Sicily and adjacent area. *Ann. Geophys.* 5B(1): 75-88.

Hecht, Artur, N. Pinardi, and A. R. Robinson (1988). Currents, water masses eddies and jets in the Mediterranean Levantine Basin. *J. Phys. Oceanog.* 18: 1320-1353.

Hersey, J. B. (1965). Sedimentary basins of the Mediterranean Sea. In *Submarine Geology and Geophysics,* W. F. Whittard and R. Bradshaw (eds.), London: Butterworths, 75-91.

Keller G. H. and D. N. Lambert (1972). Geotechnical properties of submarine sediments, Mediterranean Sea. In *A Natural Sedimentation Laboratory*, Stroudsburg (Pennsylvania): Dowden, Hutchinson and Ross, 765 pp.

Kelling, G. and D. J. Stanley (1972). Sedimentation in the vicinity of the Strait of Gibraltar. In *A Natural Sedimentation Laboratory*, Stroudsburg (Pennsylvania), Dowden, Hutchinson and Ross, 765 pp.

Kinder, T. H. (1984). Net mass transport by internal waves near the Strait of Gibraltar. *Geophys. Res. Lett.* 11(10): 987-990.

La Violette, P. E. (1986). Short-term measurements of surface currents associated with the Alboran Sea Gyre during ¿Donde Va? *J. Phys. Oceanog.* 16: 262-279.

Lacombe, H. and C. Richez (1982) The regime of the Strait of Gibraltar. In *Hydrodynamics of Semi-enclosed Seas: Proc. of the 13th International Liege Colloquium on Ocean Hydrodynamics*, Jacques C.J. Nihoul (eds.), Elsevier Oceanography Series, 34.

Levine, E. R., and W. B. White (1972). Thermal frontal zones in the eastern Mediterranean Sea. *J. Geophys. Res.* 77(6): 1081-1086.

Lort, J. M. (1977). Geophysics of the Mediterranean Sea Basins. In *The Ocean Basins and Margins, 4A, The Eastern Mediterranean*, A. E. M. Narin, W. K. Kanes, and F. G. Stehli (eds.), New York: Plenum Press, pp. 151-213.

Malanotte-Rizzoli, P. and Artur Hecht (1988). Large-scale properties of the estern Mediterrnaean: a review. *Oceanol. Acta* 11(4): 323-355.

Malanotte-Rizzoli, P. and A. Bergamasco (1991). The wind and thermally driven circulation of the eastern Mediterranean Sea, Part II: The baroclinic case. *Dyn. Atmos. and Oc.* 15: 355-419.

Maldonado, Andres and D. J. Stanley (1976). Late Quaternary sedimentation and stratigraphy in the Strait of Sicily. *Smithsonian Institution Press* 16: 73 pp.

Manzella, G. M. R, G. P. Gasparini, and M. Astraldi (1988). Water exchange between eastern and western Mediterranean through the Strait of Sicily. *Deep Sea Res.* 35: 1021–1035.

Manzella, G. M. R., T. S. Hopkins, P. J. Minnett, and E. Nacini (1990). Atlantic water in the Strait of Sicily. *J. Geophys. Res.* 95(C2): 1569–1575.

Miller, A. R. (1972). The distributions of temperature, salinity, and sound velocity in the western Ionian Sea during spring, 1968. Woods Hole Oceanographic Institution Technical Report No. 72-5, January (unpublished).

Molcard, R. (1972). The Strait of Sicily in relation to the general circulation of the Mediterranean. SACLANTCENTRE Conference Proceedings No. 7, SACLANT ASW Research Centre, La Spezia, Italy, September.

Ovchinnikov, I. M. (1965). Formation of Mediterranean deep water masses. *Oceanology* 5(4): 40–46.

Ozoy, E. et al. (1991). A review of the Levantine Basin circulation and its variability during 1985-1988. *Dyn. Atmos. and Oc.* 15: 421-456.

Perkins, H. and P. Pistek (1990). Circulation in the Algerian Basin during June 1986. *J. Geophys. Res.* 95(C2): 1587–1598.

Pistek, P. (1987). Deep water mass circulation in the Alboran Basin: measurements—January to April '82, ALBORAN II. SACLANT ASW Research Centre Memorandum SM-195, September.

Pistek, P. (1984). Deep water mass circulation in the western Alboran Basin: measurements in July and September 1980 (ALBORAN I Experiment). SACLANT ASW Research Centre Report SR-81, July.

Robinson, A. R. et al. (1991). The eastern Mediterranean general circulation: features, structure, and variability. *Dyn. Atmos. and Oc.* 15: 215–240.

Salat, J. and J. Font (1987). Water mass structure near ond Offshore the Catalan coast during the winter of 1982 and 1983. *Ann. Geophys.* 5: 49–54.

Stanley, D. J. (1977). Post-Miocene depositional patterns and structural displacement in the Mediterranean. In *The Ocean Basins and Margins*, A. E. M. Narin, W. K. Kanes, and F. G. Stehli (eds.), New York: Plenum Press, v. 4A, pp. 77–150.

Stanley, D. J., ed. (1972). *The Mediterranean Sea: A Natural Sedimentation Laboratory.* Stroudsburg (Pennsylvania): Dowden, Hutchinson and Ross, 765 pp.

U.S. Naval Oceanographic Office (1970). Mine warfare pilot, Strait of Gibraltar-Rota approaches. Stennis Space Center, MS 39529-5004, SP 923, July

U.S. Naval Oceanographic Office (1978). Surface currents east central North Atlantic Ocean. Stennis Space Center, MS 39529-5004. SP 1400-NA7, 14 pp., April

U.S. Naval Oceanographic Office (1979). Data report, moored current meter measurements—Strait of Sicily, December, 1976. Stennis Space Center, MS 39529-5004, TN 7210-2-80, December.

Udias, A. (1985). Seismicity of the Mediterranean basin. In *Geological Evolution of the Mediterranean Basin*, D. J. Stanley and F. C. Wezel (eds.), New York: Springer-Verlag, pp. 55–63.

Wüst, G. (1961). On the vertical circulation of the Mediterranean Sea. *J. Geophys. Res.* 66: 3261–3272.

Distribution List

Amron
2001 Jefferson Davis Hwy.
Suite 610
Arlington, VA 22202

Applied Research Laboratory
University of Texas
P. O. Box 8029
Austin, TX 78713-8029
Attn: C. Penrod

AT&T Bell Laboratories
Room 15E317
Whippany, NJ 07981
Attn: A. Varma

AT&T Bell Labortories
Guilford Center
P. O. Box 20046
Greensboro, NC 27420
Attn: D. W. Ravenel

Naval Oceanographic Office
Stennis Space Center, MS 39529-5001
Attn: R. Merrifield (Code PE)
R. Christiansen

Naval Oceanography Command
Stennis Space Center, MS
Attn: CDR R. Hautman
C. Wilcox

Naval Postgraduate School
Monterey, CA 93943-5000
Attn: Library

Naval Research Laboratory
Washington, DC 20375-5000
Attn: H. Fleming

Naval Research Laboratory
Stennis Space Center, MS 39529-5004
Attn: Code 125P (1)
Code 125L (6)

Naval Warfare Systems Command
Washington, DC 20363-5100
Attn: D. Conlon (PD-80)

Office of Naval Research
AEAS
Stennis Space Center, MS 39529-5001

Office of the Chief of Naval Research
800 N. Quincy St.
Arlington, VA 22217-5000
Attn: Dr. M. Briscoe (Code 124)
Mr. R. Feden (Code 124A)
Mr. K. Dial (Code 124A1)

Resource Planning, Inc.
2300 Claredon Blvd.
Suite 400
Arlington, VA 22201
Attn: T. Clark

Space and Naval Warfare Systems Command
Washington, DC 20363-5100
Attn: CDR J. D. Liechty (PMW-184-3)

TRW Incorporated
7600 Colshire Drive
McLean, VA 22102
Attn: J. Frechette
L. Thorne

REPORT DOCUMENTATION PAGE

Form Approved
OBM No. 0704-0188

1. Agency Use Only *(Leave blank).*

2. Report Date. 1992

3. Report Type and Dates Covered. Final - AEAS

4. Title and Subtitle.
Environmental Assessment for Selected Regions in the Mediterranean Sea

5. Funding Numbers.

Contract	
Program Element No.	0603785N
Project No.	R0120
Task No.	806
Accession No.	DN251021
Work Unit No.	12221S

6. Author(s).
Mark J. Null, Paul J. Bucca, and Bruce R. Gomes

7. Performing Organization Name(s) and Address(es).
Naval Oceanographic and Atmospheric Research Laboratory
Ocean Acoustics and Technology Directorate
Stennis Space Center, MS 39529-5004

8. Performing Organization Report Number.
AEAS 92-004

9. Sponsoring/Monitoring Agency Name(s) and Address(es).
Naval Oceanographic and Atmospheric Research Laboratory
Ocean Acoustics and Technology Directorate
Stennis Space Center, MS 39529-5004

10. Sponsoring/Monitoring Agency Report Number.
AEAS 92-004

11. Supplementary Notes.

12a. Distribution/Availability Statement.
Approved for public release; distribution is unlimited.

12b. Distribution Code.

13. Abstract *(Maximum 200 words).*

This document contains a section of environmental parameters that is part of a larger Mediterranean Sea area acoustic assessment compiled under the auspices of the ASW Environmental Acoustics Support Project Office. Its contents reflect an environmental description of the geology, oceanography, sound speed variability, and currents in selected areas of the Mediterranean Sea. The geology section addresses the physiography, sediment thickness, despositional processes, volcanism, and seismicity of each region. In many areas, the oceanographic section represents a significant update, since it includes available documentation resulting from two large-scale multinational field investigations: the Physical Oceanography of the Eastern Mediterranean and the Western Mediterranean Circulation Experiment. The sound speed section, based on the Master Oceanographic Observation Data Set, is a tailored analysis of both temporal variability and profile gradient changes. This analysis results in the selection of the closest actual sound speed profiles to the arithmetic average. The section on currents focuses on the availability and description of abyssal current data and includes results from the Naval Oceanographic and Atmospheric Research Laboratory Layered Circulation Model.

14. Subject Terms.
Environmental/Acoustic Assessments, Oceanography

15. Number of Pages. 125

16. Price Code.

17. Security Classification of Report.	18. Security Classification of This Page.	19. Security Classification of Abstract.	20. Limitation of Abstract.
Unclassified	Unclassified	Unclassified	SAR